ANALYSIS AND DESIGN OF ELECTROMAGNETIC MOVING COIL VIBRATION GENERATORS

Ruben Jeevanasan Fair BSc.(Eng.)Hons. ACGI

Special Drives and Power Electronics Group
Department of Electrical Engineering
Imperial College of Science, Technology and Medicine
(University of London)
Exhibition Road, South Kensington
London
SW7 2BT

February 1986 - February 1989
(Submitted February 1991)

Project Supervisor
Professor H. R. Bolton

Sponsoring Company
Derritron Electronics International

Thesis submitted for the degree of Doctor of Philosophy

ABSTRACT

Shakers are used in the field of vibration testing to produce controlled vibrations of pre-determined force levels over a set frequency band. These machines can employ a wide variety of operating principles ranging from the magnetostrictive type, pneumatic type, and electromechanical type through to the electromagnetic type which forms the main body of this dissertation.

This thesis deals with the formulation of a mathematical model to predict the performance of certain types of electromagnetic moving coil shaker. The model was tested against measured results and then, together with a finite element modelling package, was used to design a 'C-Core' prototype shaker, according to specifications laid down by the sponsoring company.

The general field of Vibration Testing is outlined and the various ways of producing controlled vibrations are described. The composition of a typical vibration test system is described and details given of the basic components that make up the system. The construction of a typical unit is described in detail together with its mode of operation. The overall analysis technique is outlined and discussed, and the derivation of a set of equations and equivalent circuit parameters is dealt with. The nature of the frequency response of a typical moving coil shaker is discussed using an existing machine as an example. Predictions obtained using the model are compared with test data from several different machines.

A design methodology is then presented in detail together with the design flowchart. Comparisons are made between three magnetic circuit layouts using both electrical and mechanical criteria. The development of the prototype C-Core machine is then outlined and its performance discussed with the aid of test results and predictions. Conclusions relating to the prediction model and design methods used are discussed. Finally, the software package that resulted from the project is described and suggestions made for its further development.

ACKNOWLEDGEMENTS

The author would like to thank his project supervisor, Professor Hugh Bolton for his enthusiasm, drive and constant encouragement throughout the project. The sponsors Derritron Group Limited are also to be thanked for their financial and engineering support and the invaluable engineering expertise which was readily provided by the Mechanical Design and Development Department at Hastings. Thanks are due to Professor E. M. Freeman and Dr. Clive Bryant of the Electromagnetics Section at Imperial College for their assistance with the finite element software and various aspects of computer hardware. The author is also grateful to Dr. Richard Fletcher and Dr. Yahya Shakweh for their thoughts on switched mode power amplifiers.

Finally, the author would like to express his heartfelt gratitude to his parents and wife who have provided moral support and encouragement throughout the writing of this dissertation.

CONTENTS

Abstract *2*
Acknowledgements *3*
Symbol Table *6*

1. Introduction to Vibration Testing *8*
1.1. Types of Vibration Generator *9*
1.2. Other Types of Electromagnetic Oscillatory Drive *15*
1.3. Moving Coil Shakers - Background *20*
1.4. Project Objectives *21*
1.5. Chapter Contents *22*

2. Composition of a Typical Current Electromagnetic Vibration Test System *23*
2.1. The Vibration Generator ('Shaker') *23*
2.2. Power Supplies *29*
2.3. The Vibration Control System *30*
2.4. Photographs *32*

3. Analysis and Design - Overall Approach *35*
3.1. Project Path *35*
3.2. The A.C. Equivalent Circuit *39*
3.3. Equivalent Circuit Parameters *43*
3.3.1. *Primary Circuit 43*
3.3.2. *Secondary Circuit 50*
3.4. Mechanical Model *56*
3.4.1. *Two-Degree-of-Freedom Representation 56*
3.4.2. *System Equations 57*
3.5. Limitations of the Equivalent Circuit Approach *63*

4. Frequency Response of Moving Coil Shakers *65*
4.1. The A.C. Equivalent Circuit *65*
4.2. Typical Current, Voltage and KVA Variation with Frequency *66*
4.3. Explanation of Response Characteristics *69*
4.3.1. *Very Low Frequency 69*
4.3.2. *Constant Displacement - Constant Velocity Crossover Frequency 70*
4.3.3. *Mechanical Resonance 71*
4.3.4. *Constant Velocity Frequency Range 72*
4.3.5. *Constant Velocity - Constant Acceleration Crossover Frequency 73*
4.3.6. *Electromechanical Resonances 76*
4.3.7. *Maximum Shaker Impedance Frequency Point 78*
4.3.8. *High Frequency 79*
4.4. Comparison of Predictions with Test Data *80*
4.5. Further Comparisons Using the VP85 and VP30 Machines *85*

5. Electrical Design *98*
5.1. Design Procedure *98*
5.1.1. *Stage One - Required Specifications & Shaker Detail 99*
5.1.2. *Stage Two - Circuit Parameters 107*
5.1.3. *Stage Three - Frequency Response 107*
5.1.4. *Stage Four - Approximate Shaker Dimensions 108*
5.1.5. *Stage Five - Finite Element Modelling 112*
5.2. Comparison Between the Single-Ended, Double-Ended and C-Core Configurations *I*
5.2.1. *Electrical Aspects 125*
5.2.2. *Quantitative Mechanical Aspects 131*
5.2.3. *Qualitative Mechanical Features of the Three Configurations 134*
5.2.4. *Choice of Steel and A.C. Coil Construction 137*
5.2.5. *Effect of Changes in Design Parameters on Comparison 140*

6. The Prototype C-Core Machine *142*
6.1. Evolution of the New C-Core Magnetic Circuit *142*
6.2. Three-Degree-of-Freedom System Representation *149*
6.3. Comparison of Predictions and Test Data *156*
6.4. Further Work on the C-Core Machine *159*

7. Conclusions *161*

Appendix A - Derivation of Inductance Relations *163*
Appendix B - The Design Program *176*
References *180*
Bibliography *182*

SYMBOLS

a_c - Cross-sectional area of single turn of a.c. coil conductor
A - Pole face area
A'_{EL} - Annular area for secondaryright-hand leakage path
A'_{ER} - Annular area for secondary left-hand leakage path
A_s - D.C. slot cross sectional area
AT_{dc} - D.C. ampere turns

B_g - Airgap flux density (working value)
B_{mean} - Average value of flux density in airgap over a.c. coil height (usually = B_g)
B_z - Flux density at point z

C_{F1} - Correction factor for a.c. coil gap leakage flux
C_{F2} - Correction factor for copper plating gap leakage flux
C_j - D.C. current density in actual copper (d.c. winding)

D_{cp} - Diameter of iron centre pole
D_m - Mean diameter of moving element
D_{op} - Inner diameter of magnetic ring
D_z - Damping coefficient for link-arm suspension system

E_m - Motionally generated e.m.f.

F - Thrust

g - Radial length of air-gap
g'' - Radial clearances on either side of moving element

h - Axial height of pole face
h_{cpole} - Axial height of copper plating on centre-pole pole face
h_{cu} - Axial thickness of single turn of a.c. coil conductor (copper only)
h_{fac} - Axial height of fringe field due to a.c. flux
h_{fdc} - Axial height of fringe field due to d.c. flux
h_{magr} - Axial height of copper plating on magnetic ring pole face
h''' - Axial height of moving element

I_{rat} - Rated current of driving amplifier
I_1 - R.M.S. input current to a.c. coil
I_2 - R.M.S. current flowing in copper plating

k_{2CP} - Skin effect factor for centre pole copper plating layer
k_f - Ratio of iron circuit ampere turns to airgap ampere turns
k_{2MR} - Skin effect factor for magnetic ring copper plating layer
k_p - Packing factor (ratio of actual copper to d.c. slot area)
k_{SKIN1} - Skin effect factor for a.c. coil copper
k_{S1} - Stiffness of table/moving element joint
k_{S2} - Link-arm suspension stiffness (total)
k_{S3} - Axial stiffness of coil former between upper and lower coils in a C-Core machine
k_v - Thrust/Amp factor (unique to each shaker)
k_1 - Factor to allow for portion of a.c. coil actually within airgap
k'_1 - $(1 + k_1)/2$

L_{11} - Total primary inductance
L_{12} - Total magnetising inductance (also = L_m)
L_{22} - Total secondary inductance
L_{11AC} - Primary inductance due to internal flux
L_{2ACCP} - Secondary inductance due to internal flux within centre pole copper plating
L_{2ACMR} - Secondary inductance due to internal flux within magnetic ring copper plating
L_{11C} - Primary inductance due to main flux produced by a.c. coil

L_{12C} - Magnetising inductance due to main flux
L_{22C} - Secondary inductance due to main flux referred to primary
L_{OL1} - Primary inductance due to gap leakage flux
L_{EL} - Leakage inductance of righthand path
L_{ER} - Leakage inductance of left-hand path
L_{11F} - Primary inductance due to fringing flux
L_{12F} - Magnetising inductance due to fringing flux
L_{22F} - Secondary inductance due to fringing flux referred to primary
L_{L1} - Primary leakage inductance
L_{L2} - Secondary leakage inductance
L_{L2TOT} - Resultant secondary internal inductance referred to primary
L_{22L1} - Secondary inductance due to gap leakage flux referred to primary
L_m - Total magnetising inductance (also = L_{12})
L_{mt} - Length of mean turn of d.c. winding

m_1 - Moving element mass (a.c. coil + membrane)
m_2 - Table mass
m_3 - Mass of lower half of moving element in a C-Core machine

N & N_T - Number of turns in a.c. coil (per end for C-Core machine)

R_{1AC} - A.C. resistance of equivalent thin slab representing a.c. coils
R_{2ACCP} - A.C. resistance of equiv. thin slab representing copper plating on centre pole
R_{2ACMR} - A.C. resistance of equiv. thin slab representing copper plating on magnetic ring
R_{CMAG} - D.C. resistance of copper plating on magnetic ring
R_{CPOL} - D.C. resistance of copper plating on centre pole
R_{CUMAG} - Total resistance of copper plating on magnetic ring
R_{CUPOL} - Total resistance of copper plating on centre pole
R_{1DC} - D.C. resistance of a.c. coils
R_{DC1} - D.C. resistance of equiv. thin slab representing a.c. coils
R_{DC2CP} - D.C. resistance of equiv. thin slab representing copper plating on centre pole
R_{DC2MR} - D.C. resistance of equiv. thin slab representing copper plating on magnetic ring
R_{ET} - Total reluctance of primary leakage paths
R'_{EL} - Reluctance of secondary righthand path
R'_{ER} - Reluctance of secondary left-hand path
R_1 - Overall effective resistance of a.c. coil
R_2 - Overall effective resistance of copper plating referred to primary

t - Radial thickness of single turn of a.c. coil conductor (copper only)
t_a - Overall axial thickness of single turn of a.c. coil conductor (including insulation)
t_i - Thickness of one layer of insulation
t_{cpole} - Radial thickness of copper plating on centre pole
t_{magr} - Radial thickness of copper plating on magnetic ring
t_m - Radial thickness of moving element membrane

V_{ref} - Rated voltage of driving amplifier
V_1 - Voltage across a.c. coils
V_2 - Voltage across copper plating layers

x_1 - Displacement of moving element
$\dot{x}_1$ - Velocity of moving element
$\ddot{x}_1$ - Acceleration of moving element
x_2 - Displacement of table
$\dot{x}_2$ - Velocity of table
$\ddot{x}_2$ - Acceleration of table
X_1 - Amplitude of moving element displacement
$\dot{X}_1$ - Amplitude of moving element velocity
X_2 - Amplitude of table dispiacement

Z_m - Motional impedance

CHAPTER ONE
VIBRATION TESTING

1. Introduction to Vibration Testing

Vibration Testing is an important component in the successful design and production of modern equipment particularly when the equipment is likely to be subjected to difficult environmental conditions. The field of environmental engineering and testing includes consideration of and testing for the effects of high and low temperatures, high and low humidity levels, water and dust penetration, differences of pressure, etc.. The types of test chamber needed to investigate most of these factors are well known. The type of installation needed for vibration testing is perhaps less well known, and contains at its heart a vibration driver of some sort. In some cases, vibration testing is carried out in association with environmental chambers. The objective throughout is to ensure that industrial or consumer products are safe and will continue to function under different, and in some cases, extreme conditions. The products in question range from electronic amplifiers, radar equipment and missiles, which have to satisfy very stringent military standard specifications, to automobile chassis, television sets, aircraft fuselage, computers and a host of other products. So far as vibration testing is concerned, important application areas include the testing of defence and aerospace equipment and vehicles and earthquake simulation systems.

During vibration tests, the test object is subjected to either sinusoidal, random or shock tests, or a combination of all three, depending on the British Standard or other specification that needs to be satisfied. Vibration testing is particularly useful in the following specific ways ;

(i) At the product development stage, it can isolate troublesome resonances and identify potential vibration problem areas.

(ii) It can simulate the real vibration environment to see if the product will stand up to in-service use.

(iii) It provides the means of assessing performance and reliability during production control.

(iv) It enables test specifications to be established and applied.

(v) As mentioned above, coupled with an environmental chamber, temperature,

pressure, humidity and vibration forces can be altered and effects on the test object studied.

(vi) Shakers are often used in the calibration of various displacement/ velocity/acceleration transducers.

(vii) Determination of mechanical impedances and response of certain structures (e.g. building structure models) and test objects also require the use of a shaker. Shakers are much used in modal analysis work.

1.1. Types of Vibration Generator

There are a number of ways that controlled vibrations can be produced. The main categories are described in Reference 19. A short list of the various vibration machines and devices available would include :

(a) Direct Drive Mechanical Vibration Machines [19], (Fig. 1a)

These machines usually consist of a rotating eccentric or cam driving a table. This technique is good for low frequency operation where large displacements are required. On-line amplitude control needs complex mechanical features, and so the amplitude is normally preset. The top operating frequency is limited by the need to avoid excessive bearing loads. No variation of the vibration waveform is feasible and no shock or random vibration testing can be done. The waveform is not necessarily a pure sinewave and hence undesirable excitation of harmonic modes on the equipment being tested is a risk.

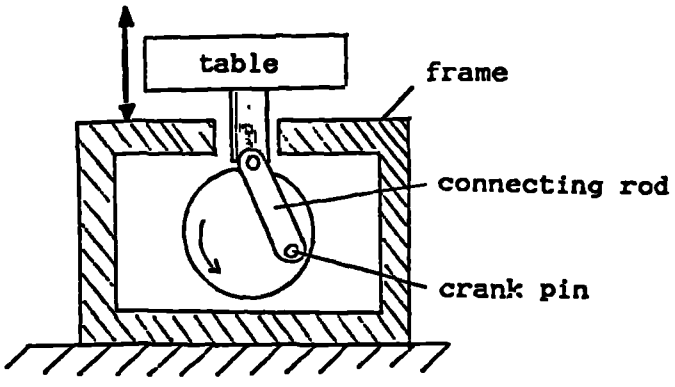


Fig. 1a Direct Drive Mechanical Vibration Machine

(b) Reaction Type Vibration Machines [19], (Fig. 1b)

This type uses rotating eccentrics. The attainable r.p.m. and load ratings on the machine bearings typically limit performance to approximately 60 to 70 Hz (120 Hz for smaller machines) and similar disadvantages to those mentioned under (a) occur.

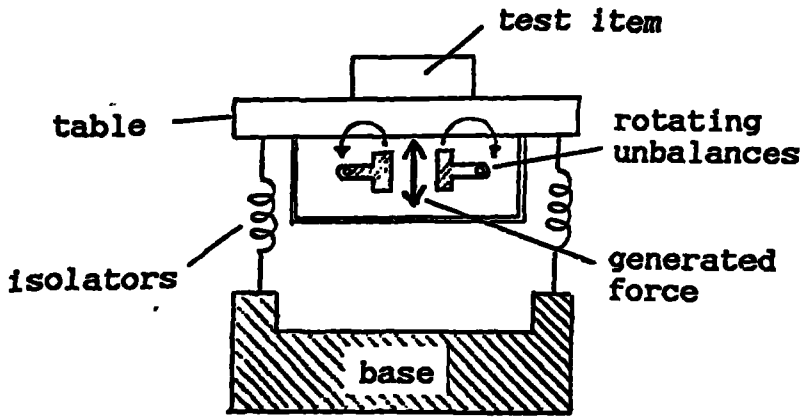


Fig. 1b Reaction Type Vibration Machine

(c) Hydraulic Vibration Machines [19], (Fig. 1c)

These machines transfer power in the form of a high-pressure flow of fluid from a pump to the motion of the table of the vibration machine. This type of machine requires a low power electromagnetic actuator of some sort to drive the first stage hydraulic valves. Here again high frequency operation in excess of 2 kHz is not possible due to various limitations of the hydraulic valves and the elasticity of the fluid. Hydraulic machines excel at low frequencies where large forces, strokes and power capacity are required. For even larger force or stroke requirements, more stages in the control valve systems can be used, or a number of valves used in parallel. These schemes however again tend to reduce high frequency performance.

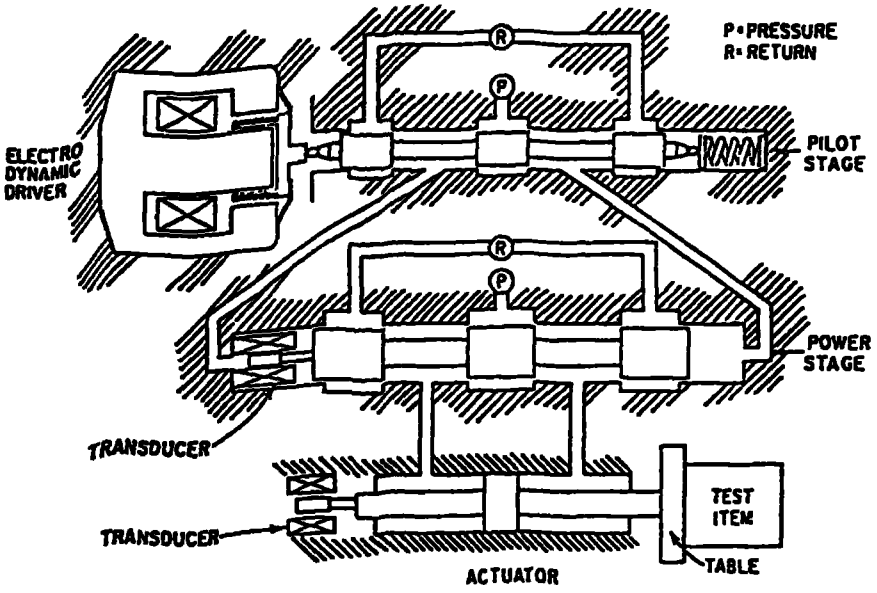


Fig. 1c Hydraulic Vibration Machine

(d) Ultrasonic Vibration Machines [3], (Figs. 1d & 1e)

The magnetostrictive transducer, which finds its use at both sonic and ultrasonic frequencies, depends for its action on the magnetostrictive properties of certain magnetic materials, such as nickel and nickel alloys. Rods of these materials change their physical length when magnetised along the length of the rod.

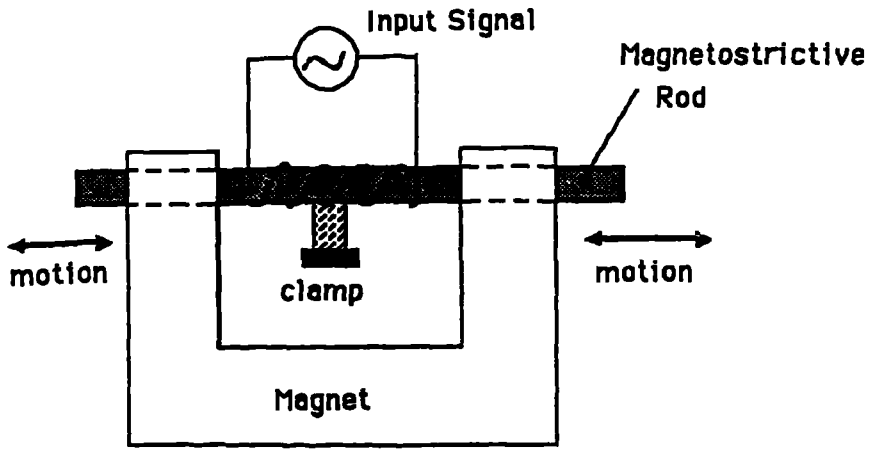


Fig. 1d Magnetostrictive Vibration Machine

The signal winding produces an alternating magnetic field along the length of the moveable magnetostrictive element which when superposed on the d.c. bias field produced by the bias winding or permanent magnet, results in a pulsating, unidirectional field which in turn produces movement of the faces of the rod at the signal frequency due to changes in current. Magnetostrictive effects are usually very small and hence these devices are used only for high frequency, small amplitude testing and are not used in large sizes. As mentioned in Reference 3, the magnetostrictive effect is temperature dependent, and the higher the operating temperature the lower the thermal stability. For example, in nickel-based transducers operating at a temperature of 100°C, a reduction in magnetic and magnetostrictive properties is observed. Upon further increase of temperature to the Curie point, (360°C for nickel), the magnetostrictive effect of nickel vanishes. The greatest stability is found in permendur-based transducers, which are capable of withstanding heat up to 600°C. The typical operating frequency range of magnetostrictive devices is approximately 5 kHz to 60 kHz.

Another type of ultrasonic vibration source generally used above 20 kHz is the piezoelectric (or electrostrictive) transducer. It is interesting that piezoelectric units can be used in the 'generating' mode, (i.e. producing an electrical output from a mechanical input), as accelerometers, microphones, stereo turntable cartridges, etc., or in the 'motoring' mode, whereby an input electrical signal produces the required limited mechanical motion. Examples of such materials are quartz and Rochelle salt.

When a voltage is applied to the electrodes of the piezoelectric stack, the amount of change in shape is dependent on the frequency of the applied voltage and the frequency response of the electromechanical system [3]. When the length of the piezoelectric element, in the direction of dimensional change, is a small fraction of a wavelength in the piezoelectric material at the highest operating frequency, the element acts as a spring having stiffness without appreciable mass. If the mass of the load carried by the piezoelectric element in combination with the stiffness of the element gives a resonant frequency well beyond the highest operating frequency, the system is spring controlled, providing a displacement proportional to the applied voltage and independent of frequency. For a mass load which results in a resonant frequency in or near the operating frequency range, a typical resonant magnification of force and displacement across the spring is obtained, corresponding to a system with small damping.

The machine shown in Figure 1e is intended to take advantage of operation at mechanical resonance, (i.e. over a very restricted frequency range only), generating

accelerations as high as 1000g at the upper operating frequencies.

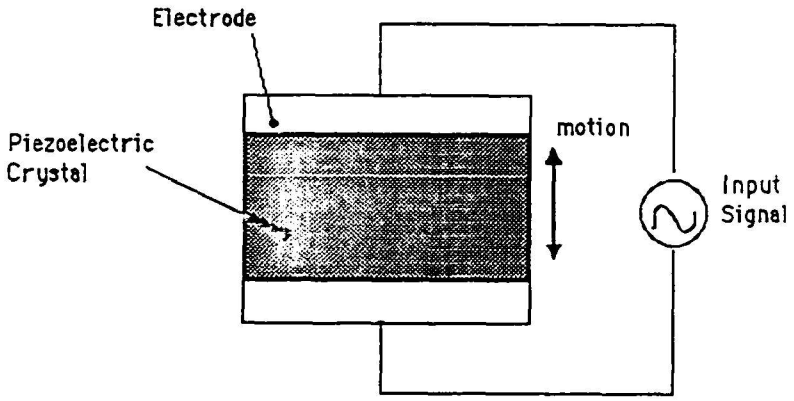


Fig. 1e Piezoelectric Vibration Machine

These small vibration devices are usually used for stressing items such as printed circuit boards, delicate measuring apparatus, microprocessor chips, etc.. Ultrasonic cleaning of devices, materials, etc. is another area of use of ultrasonic devices. Both the magnetostrictive and piezoelectric type of transducer have found important uses in the military and fishing industry, as SONAR devices, either in the 'passive' (listening) or 'active' (interrogating and listening) modes. They are usually used in 'array' form where large numbers of the devices are mounted on a suitable platform to provide a larger surface area, for improved sensitivity.

(e) Pneumatic Vibration Machines [19], (Fig. 1f)

Compressed air can be used to produce controlled vibrations. Figure 1f shows a rotating-disc modulator type pneumatic vibration machine.

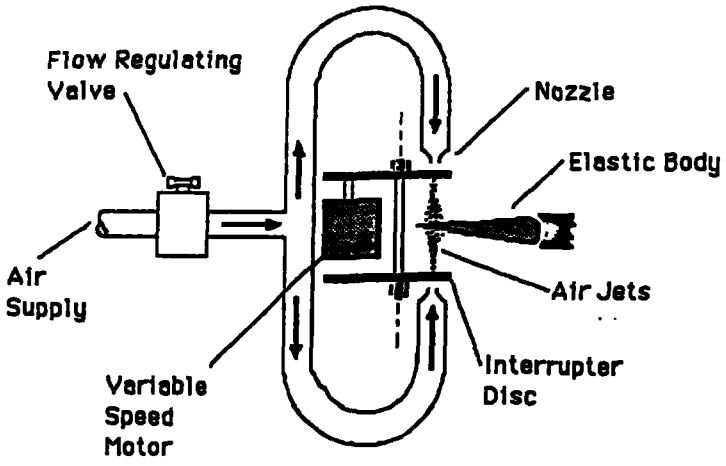


Fig. 1f Pneumatic Vibration Machine

The rotating discs, having notched edges, modulate, in an antiphase fashion, the two air jets impinging alternately on the moving element thereby causing side to side vibration. The air flow regulates the amplitude of the force while the rotational speed of the discs regulate the frequency.

The variation in the magnitude of the force with time can be made approximately sinusoidal by selection of the proper shape for the nozzle and the periphery of the rotating disc. Since the rotating disc simply deflects the stream of air, instead of changing the mass flow through the nozzle, and the velocity of the air is high compared to the velocity of the disc, the magnitude and waveform of the force are apparently independent of frequency up to at least 500 Hz.

(f) Electromagnetic Vibration Machines (Fig. 1g)

Of the many types of electromagnetic vibration machine that are feasible, it is the moving coil type that is used, almost to the complete exclusion of others. The working principle of this type of machine, the one that forms the subject of this thesis is shown here. Described in detail in Chapter Two, Figure 1g shows the electromagnetic vibration machine's , (also called a shaker), basic working principle, which relies

on the fact that a current carrying conductor, when placed in a magnetic field, will experience a force proportional to the strength of the magnetic field, the length of the conductor and the current through it.

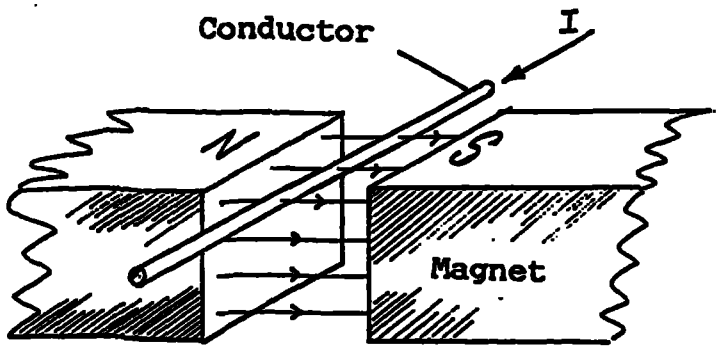


Fig. 1g Electromagnetic Moving Coil Principle

1.2. Other Types of Electromagnetic Oscillatory Drive

Several different types of electromagnetic oscillatory drive are described below. Obviously some designs may have similar operating principles but for clarity they have been given suitable type labels.

(a) Moving Coil - Type 1 [9]

As mentioned in Reference 9, a moving coil electromagnetic vibrator was developed and built as a design exercise in the Philips Research Laboratories, to drive the compressor in a domestic refrigerator, replacing the single phase induction motor which is normally used, (see Figure 1h). The vibrator compressor takes the coolant in at its inlet as gas and compresses it, by moving a plunger to and fro in a cylinder. The vibrator proved to be a suitable power source, providing efficiencies of about 60% for a 120 litre domestic refrigerator as opposed to about 50 to 55% found with conven refrigerator compressors, but was apparently not cost-competitive with conventional rotary motor driven units.

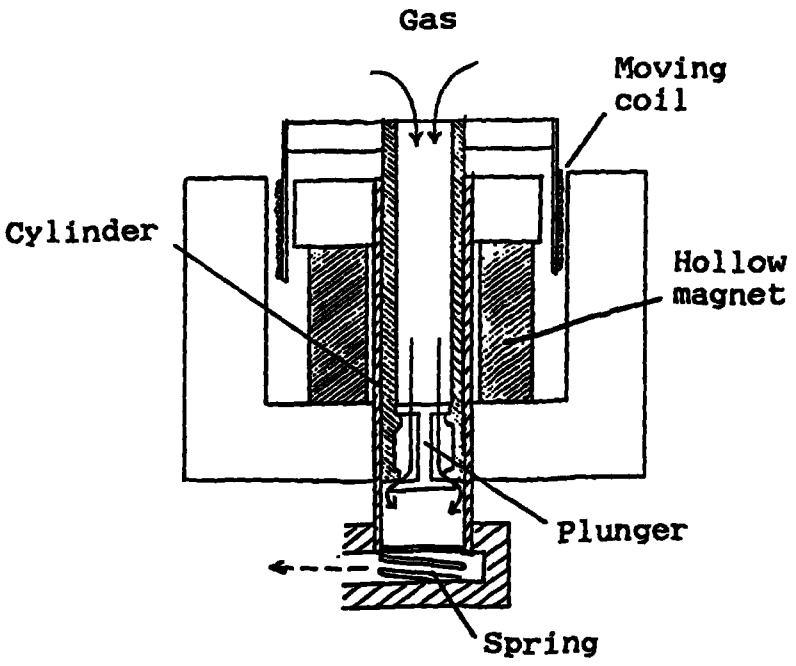


Fig. 1h Vibrator Compressor

(b) Moving Coil - Type 2 [17 & 18]

The same principle as used in shaker operation was utilised in work done by Freris and Carvalho on an electromechanical (e.m.) filter. The e.m. filter was developed to provide an alternative to conventional static filters for both the suppression of harmonics and supply of reactive power on the a.c. side of d.c. link convertors. This type of device is shown schematically below :

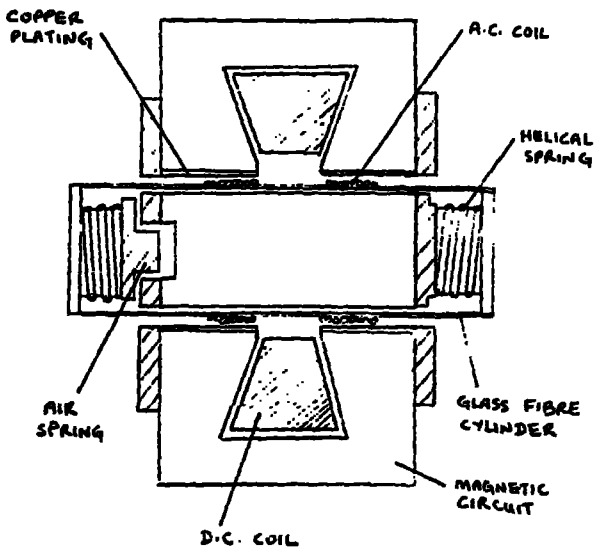


Fig. 1i Electromechanical Filter

As in shaker operation, this is a mass-spring system driven by the force produced

by the interaction of the a.c. coil current and the d.c. flux. The natural resonance frequency of the system is given approximately by :

$$\omega_n = \sqrt{k_s/m}$$

where,

k_s = suspension stiffness

m = moving mass

As for moving coil shakers, at the natural resonance point the input impedance, Z is high and resistive. For $\omega > \omega_n$, Z is mainly capacitive, and, for $\omega < \omega_n$, it is mainly inductive. The resonance frequency can be shifted by changes to the suspension stiffness, accomplished by incorporating an air-spring as shown. By the appropriate choice of parameters, the filter impedance can be made to be low at all harmonics except the first. Similarly, changes in suspension stiffness can compensate, (to an extent), for variations in the capacitive impedance due to changes in the a.c. system frequency. The characteristics of the e.m. filter were found to be superior to those of static filters, but due to the inherent, (relatively long), time constant, fast control of the filter is not possible. Also, the properties of the materials which were studied for springs required a complex mechanical system.

*

(c) Reluctance Type (Ref. 9)

The same research laboratories designed a smaller vibrator employing a different electromagnetic principle for electric shaver units (Figure 1j).

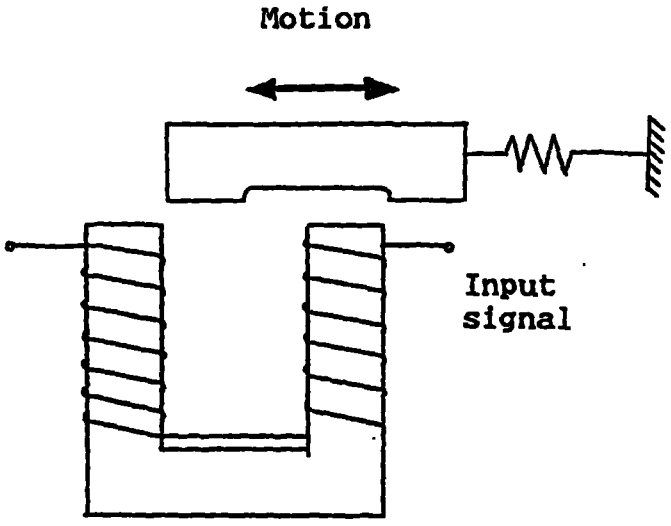


Fig. 1j *Electric Shaver Vibrator*

The electric shaver vibrator has a soft laminated iron yoke, (provided with a winding), which forms a closed magnetic circuit together with a moveable armature. When the current flows in the winding, the armature whose 'zero position' is asymmetric with respect to the yoke, will be drawn to a position above the poles of the yoke. With an a.c. supply, this happens twice in each period; the armature will thus vibrate at a frequency equal to twice that of the supply current. The mechanical system is tuned to this frequency in order to produce maximum vibration amplitude.

(d) Induction Type (Ref. 12)

In a 1956 IEE paper Laithwaite and Lawrenson demonstrated how an oscillatory drive based on induction forces could be engineered. The drive, developed for textile shuttle drive applications, was based on two linear induction motors (LIMs) with inward directed fields placed end to end. With these LIMs supplied directly from the 3-phase mains, the authors were able to demonstrate that self-oscillation of a short induction rotor occurred if the X_m/R_2 of the rotor was high enough (appreciably above unity). With this X_m/R_2 condition, the forward thrust exceeds the braking thrust leading to an oscillation amplitude that increases about the machine's centre until the peak velocity exceeds the speed for 'pull-out'. A stable oscillation could hence be finally attained. With end springs, efficiency was reasonably good but since control of amplitude, frequency and waveform is very restricted, this type of induction machine is not suitable for today's vibration testing requirements. Induction based shakers having other configurations from this are feasible, and some attention was devoted to them within the sponsored program of work. However, partly for company confidentiality reasons, it was decided to exclude description of them from the thesis.

(e) Moving Magnet Type (Ref. 13)

A moving magnet linear actuator was built and studied using the finite element technique as part of a PhD project by A.C. Smith and L.C. Appel of Imperial College. A cross-section through one half of the complete actuator is shown below.

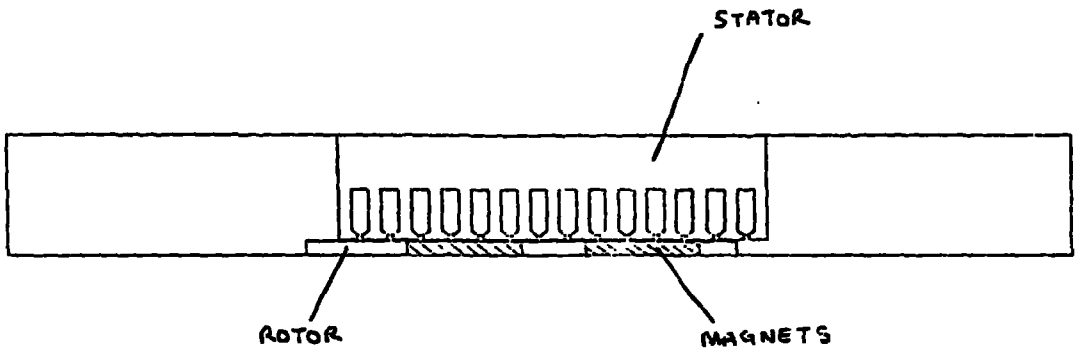


Fig. 1k *Cross-Sectional View of Actuator*

The stator is constructed from standard laminations and the magnets (Nd-Fe-B rare earth or Sm-Co) are mounted in an aluminium holder to reduce the overall inertia of the rotor. For oscillatory drive applications, alternating current would be fed to the distributed a.c. winding in the stator and the resulting mmf would react with the d.c. flux from the magnets to produce an alternating thrust. It was demonstrated that permanent magnet d.c. actuators using the latest Nd-Fe-B rare earth magnets are capable of maintaining a much greater thrust over a limited range than was previously possible using conventional magnets. The maximum thrust obtained using the above mentioned magnets was approximately 620N compared with about 310N when using Sm-Co magnets. However the maximum continuous thrust available is limited by possible demagnetisation effects resulting from excessive ultimate temperature rise at high currents. This form of actuator would be worth assessing for use in the vibration testing field.

(f) Polarised Reluctance Type (Ref. 14)

Roubicek and Pejsek of the Research Institute of Electrical Engineering, Czechoslovakia, have developed over many years a type of permanent-magnet-excited linear oscillatory motor, intended for driving resonance mechanisms.

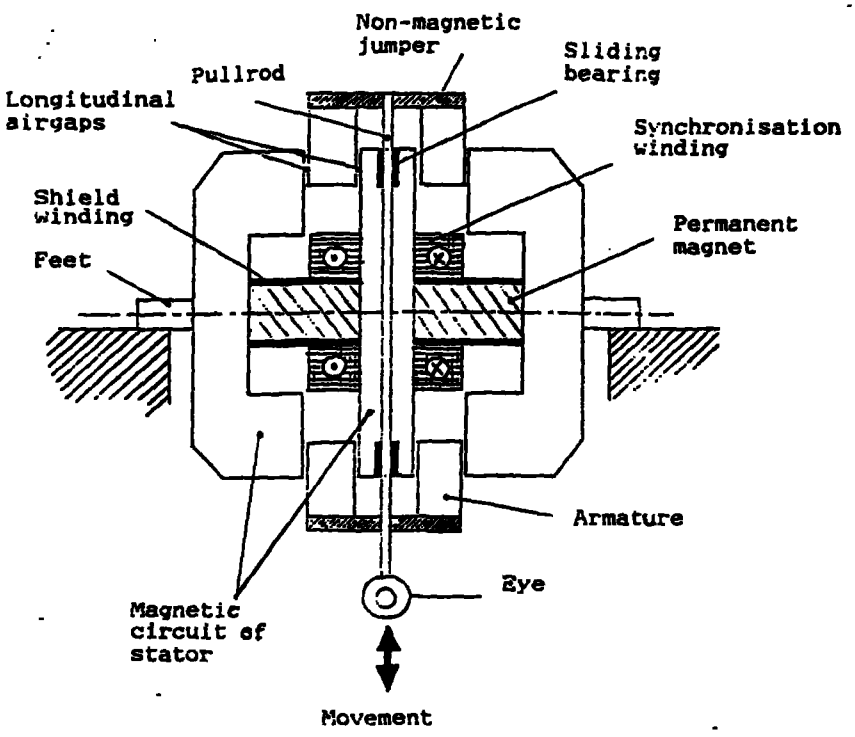


Fig. 11 *Construction of Motor*

The magnetic circuit of the motor consists of a laminated iron column , two laminated iron pole pieces and two cross-mounted permanent magnets. The armature is formed by laminated iron sections carried by a non-magnetic frame fixed to a pushrod. The armature is guided with respect to the stator by sliding bearings. The central column of the armature carries two series-connected a.c. windings. The permanent magnets are shielded by a winding which can also be used for magnetisation/demagnetisation purposes. The alternating current interacts with the field from the magnets to produce oscillatory motion.

The force output, length of stroke and operating frequency range are still limiting factors for this type of drive. Typical figures quoted in Roubicek's paper are 33N per 1kg of weight, a 5cm stroke and a frequency range of 6 to 70 Hz which do not satisfy the wide operational requirements desired for vibration testing.

1.3. Moving Coil Shakers - Background

There appears to be very little written about the origins and development of shaker systems although this information quite possibly exists within confidential company

literature. The moving coil electromagnetic shaker has many similarities with the moving coil loudspeaker (Ref. 4) in that they both employ the same operating principles. In fact, P. Grootenhuis, (now in the Mechanical Engineering Department at Imperial College), developed probably the first industrial moving coil shaker from a large Goodmans loudspeaker driver. The equivalent circuits found in standard texts incorporating descriptions of loudspeakers have features in common with those evolved during this project. However, shakers are generally larger and certain size effects become prominent, the application demands are different and the input VA requirements are often critical. Also, the speaker's air-load is different from the shaker's mainly inertial loads. Hence, the equivalent circuits, design constraints and probably the design process differ in many respects.

1.4. Project Objectives

The main and subsidiary objectives were :

(i) to draw up an analysis for an electromagnetic shaker and to use this as a basis for a mathematical model and prediction code.

(ii) to find an optimum design of a 'C-Core' electromagnetic shaker to meet specified performance requirements. In achieving this a number of important tasks needed undertaking,

- *comparison of two different types of a.c. coil construction*
- *assessment of heating levels in the copper plating and a.c. coils*
- *adjustment of magnetic circuit dimensions and proportions to attain correct weight/performance trade-offs*
- *examination of several different C-Core magnetic circuit layouts for different a.c. coil axial lengths*
- *alteration of detailed a.c. coil design to optimise either thrust or velocity requirements, or to increase operating frequency bandwidth subject to specified supply voltage and current constraints*
- *derivation of model for the mechanical system represented by the shaker's moving element, suspension and table.*

(iii) It was also necessary to verify the prediction techniques established, via test data, to allow continual improvement of the prediction formulae through further extensions to the electrical equivalent circuit, and establishing and verifying several different starting points for design flow.

(iv) to contrast and compare the final design with existing shaker designs and suggest possible improvements to the latter, (e.g. alterations to the magnetic circuit in order to reduce the amount of machining required)

(v) to draw up a design rationale to enable new designs for given specifications to be carried out quickly. The final version of the software package had to be easy to understand and to use, and it had to be written so as to allow changes and additions to the code to be made easily if the necessity arose.

1.4. Chapter Contents

In this thesis an attempt as been made, not only to deal with analytic factors, but also to cover the important design (synthesis) aspects of the shaker manufacturing task.

In Chapter one the reader has been led briefly through the field of Vibration Testing and the various methods of obtaining controlled vibrations. A typical vibration test system setup is described in Chapter two together with the constructional details and operating principle of a typical electromagnetic moving coil shaker. The equivalent circuits evolved for the project are introduced in Chapter three which also includes an exposition of the overall approach used in the analysis and design of a shaker, based on the various sets of system equations and equivalent circuit parameters. Chapter four uses the equivalent circuits to explain the nature of the frequency response of the moving coil shaker, and, in this chapter, model predictions are compared with test results.

The actual design procedures used are described in Chapter five together with a typical design example. The three principal magnetic circuit configurations are compared, and their electrical and mechanical advantages and disadvantages discussed. Chapter six outlines the development of the prototype C-Core shaker from its early beginnings to its final state, and its performance is discussed using test results and predictions. Conclusions relating to the prediction model, the design methods used and the software package resulting from this work are discussed in Chapter seven.

CHAPTER TWO

COMPOSITION OF A TYPICAL CURRENT ELECTROMAGNETIC VIBRATION TEST SYSTEM

2. The Vibration Test System

The basic components of a typical vibration test system are shown schematically in Figure 2a. At the heart of the system is the vibration generator, (from here on referred to as a 'shaker'), which produces the mechanical motion required to vibrate the test object. For a constant input signal, the vibration amplitude produced by the shaker will change markedly with frequency, so the power amplifier used to drive the shaker is usually governed by a control system. This monitors the mechanical motion, (usually via transducers mounted either on the table top or on the test object itself), and corrects for amplitude variations as the drive frequency is changed. Refer to the photographs in Figures 2f, 2g, 2h and 2i.

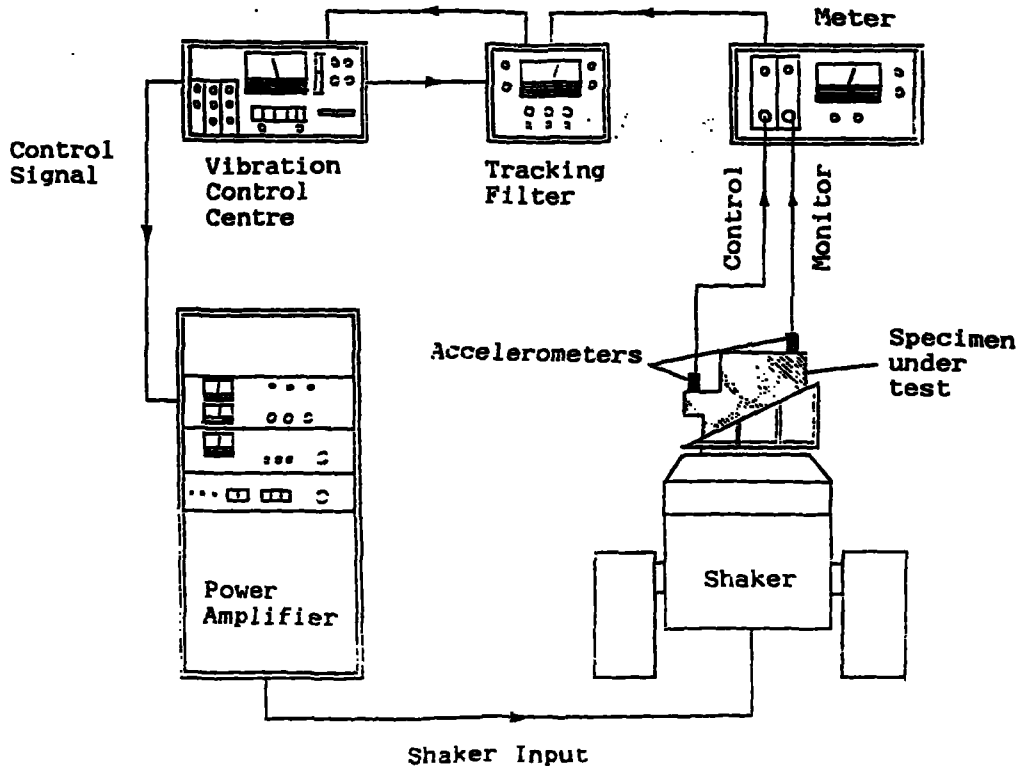


Fig. 2a Basic Components of a Vibration Test System

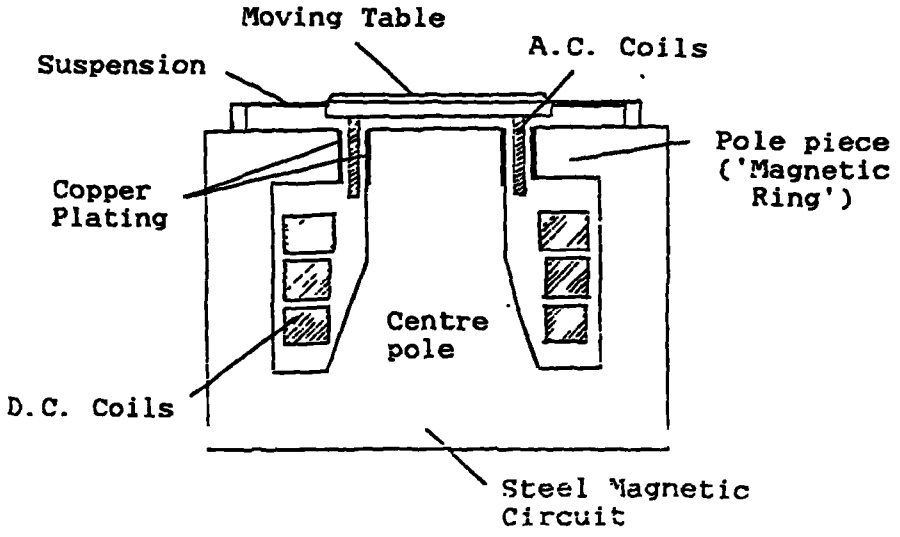
2.1. The Vibration Generator ('Shaker')

As stated in chapter one, electromagnetic shakers are almost exclusively of the moving coil type. Figures 2b(ii) & 2b(iii)), show a typical 'single-ended' magnetic circuit as used in louspeaker units.

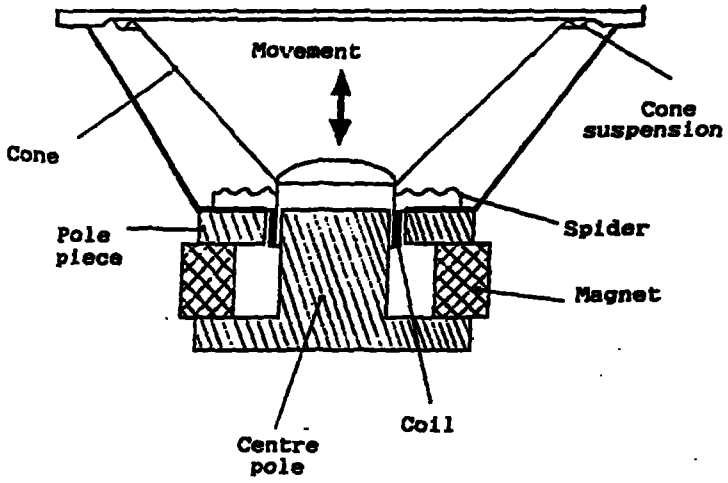
As shown in Figure 2b(i), the force generating coil takes a circular form of several turns and is situated in the annular air-gap. This coil is usually attached to a working surface called a table, (both together termed the 'armature'). The magnetic circuit is made of soft iron and also forms the body of the vibration machine. The body is magnetically energised, usually by field coils, generating a radially directed field in the air-gap, which is perpendicular to the direction of current flow in the moving coil. Alternatively, in small shakers, the magnetic field is generated by permanent magnets. The force produced is of course axial in direction, perpendicular to the table surface and also at right angles to the armature current direction and to the air-gap field direction.

The pole faces are generally plated with copper, and these 'shorted-turns' or 'kellog-rings' [7] act similarly to compensating windings in d.c. machines to counteract the mmf produced by the armature coil. This is dealt with in greater detail later.

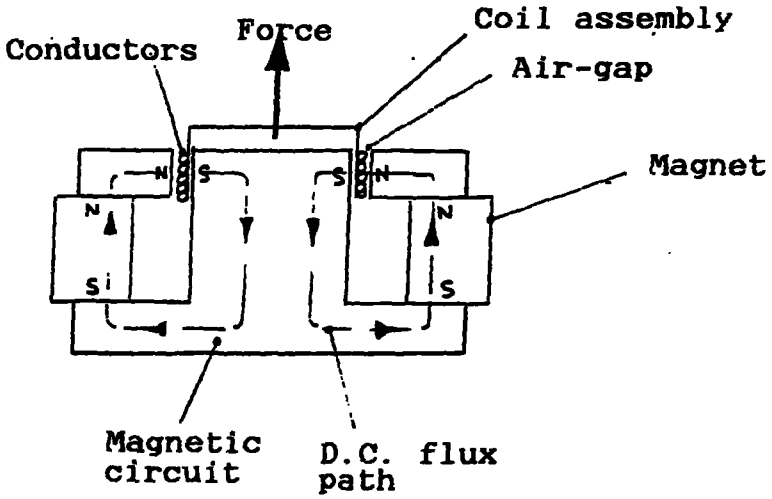
The shaker often needs to be isolated from the floor of the test facility, otherwise undesirable and even harmful vibration modes may be set up in the building structure, (resonance frequencies usually between 10 - 30 Hz). Where it is desired to eliminate a high proportion of the vibration being transmitted, the shaker may be mounted on a concrete block and the block supported on damped spring isolators. Another more flexible method is to mount the shaker on an isolation trunnion having an air-spring suspension of very low natural frequency [7].



(i) Construction of a Simple Shaker



(ii) Loudspeaker Unit



(iii) Internal Construction

Fig. 2b Conventional Loudspeaker

Table and A.C. Coil

Support for the test object is supplied by the table which must be light in weight but sufficiently stiff to ensure that the complete armature assembly acts as a solid piston over the frequency range of interest. For this reason the table is usually constructed from a magnesium based alloy containing threaded inserts for mounting the test object on the working plane, whilst remaining areas are ribbed and hollowed [5,7].

The a.c. coil is usually wound from rectangular copper strip on a glass fibre reinforced former giving high strength with minimum weight penalty. The force produced can also be harnessed by using a 'Force Take-Off' unit, (Figure 2c(i)), to provide a small active area, or by using the shaker to drive another larger test-table, (Figure 2c (ii)).

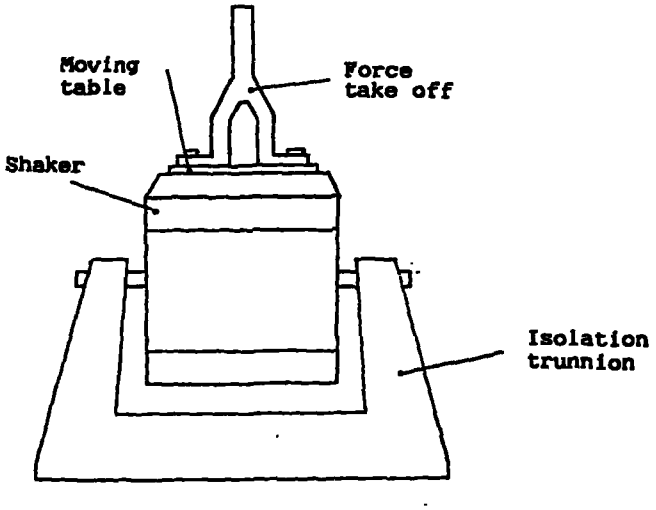


Fig. 2c(i) Shaker with 'Force Take-Off' Unit

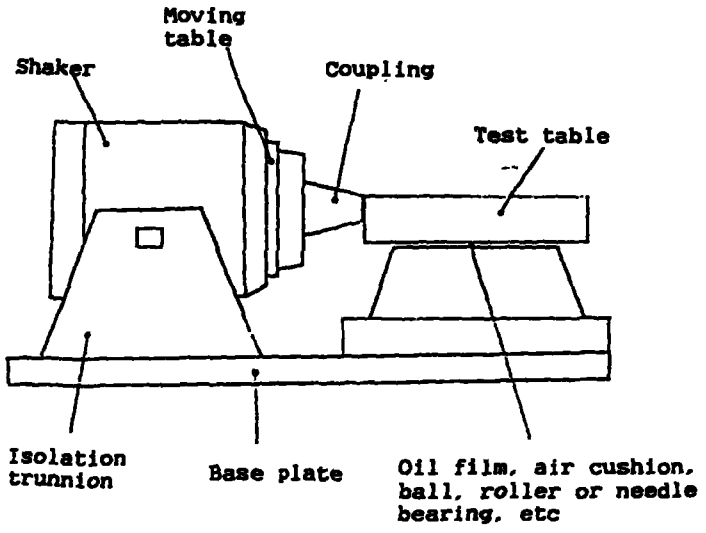


Fig. 2c(ii) Shaker with Auxiliary Table

Suspension

The armature assembly and test object must be supported by a suitable suspension system capable of restricting cross-axis movement to an absolute minimum whilst permitting only axial vibration. In addition the table must be capable of supporting the static load exerted by the object under test. Suspension systems having linear force/deflection characteristics are ideally what is required but in practice, most systems are somewhat non-linear. Suspension designs tend to be based on three-arm hinged links or on rolling elements.

Degaussing

Magnetic field strengths at the table surface must be kept to a minimum, as certain test objects, (e.g. sensitive electronic equipment), may be affected permanently by high flux levels. In order to reduce stray flux densities in the table region, a 'degaussing coil' located between the air-gap and table is used. The degaussing coil MMF counteracts the stray flux produced by the d.c. field coils and hence carries direct current. Degaussing is normally fitted as standard in most commercial machines. In some cases where even exceptionally low levels of flux at the table top are undesirable, iron and/or copper screens are inserted, usually below the table. The iron reduces the d.c. stray flux while the copper damps out the a.c. stray flux from the a.c. coil.

Cooling

The thrust capability of a given shaker is primarily limited by temperature rises due to internally generated heat, (from the armature coil, the d.c. field coils, the degaussing coils and the shorted turns). In order to obtain high thrust per shaker size strong cooling measures are employed in all except very small shakers. Forced air cooling is used typically for shakers with force outputs in the range 10 - 20 kN. Oil spray and even direct liquid cooling is used in larger units with the liquid circulating in hollow conductors. The coolant may be air, distilled water or oil, and, depending on the severity of the problem, may require associated pumps, heat exchangers and even chiller plants.

Acceleration Response

The acceleration response of a typical electromagnetic shaker over a typical

frequency range when fed with a constant voltage is shown in Figure 2d.

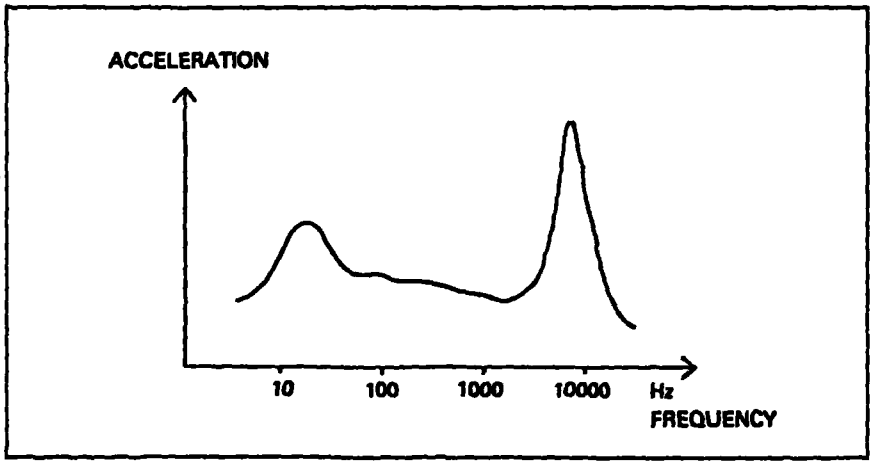


Fig. 2d Acceleration Response of a Typical Electromagnetic Shaker

Two regions of the response curve are dominated by resonances :

(i) The lower frequency peak is a result of the resonance of the armature mass on its spring suspension system. This resonance frequency is determined by the axial stiffness of the suspension system, (usually a set of suspension link arms), and the total mass of the armature assembly and test object.

(ii) The higher frequency peak corresponds to the first major axial resonance of the armature assembly itself. This frequency point can be determined approximately if the axial stiffness of the a.c. coil/table joint is known. It is usually advisable to operate the shaker at frequencies below this resonance to avoid possibility of damage to the shaker and the test object. In practice, advantage is taken of this second resonance point to maintain a constant level of acceleration, (via the control system), over part of the high frequency range where the amplifier voltage and current usually limits.

(iii) Further resonance peaks may be present if the test object itself possesses dynamic characteristics. Also, if the joint between the test object and the table is insufficiently stiff, (axially), another mechanical resonance may occur.

Hence the dynamics of the load being tested can have quite an effect on the overall

performance of the shaker, even though the amplitude control system employed may try its best to compensate.

Performance Chart

It is common practice to illustrate the maximum performance of a given shaker and amplifier system using a performance chart of the type shown in Figure 2e.

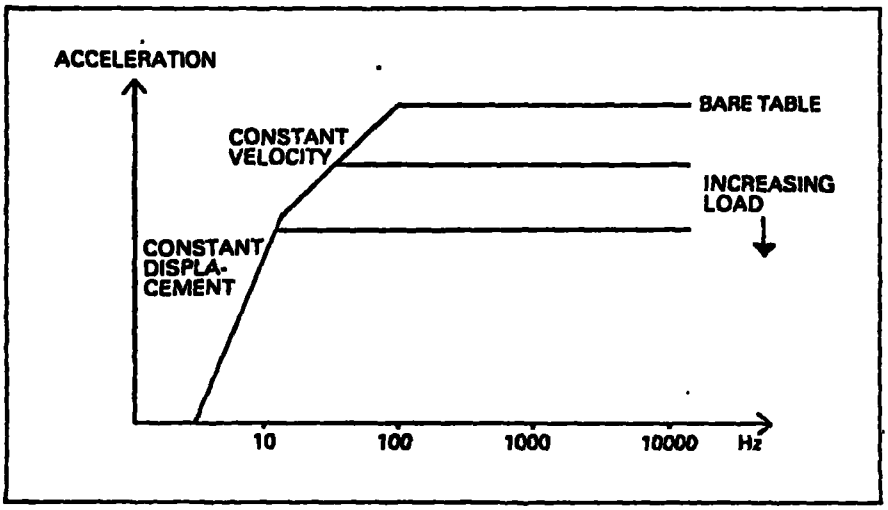


Fig. 2e Electromagnetic Shaker Performance Chart

This provides information on the maximum feasible displacement and velocity limits at low frequencies, and on the maximum acceleration capability for various test loads. These charts usually accompany any sales literature that a shaker manufacturer produces to comply with the British Standards Specifications set down.

2.2. Power Supplies

The electromagnetic shaker requires a suitable power amplifier to convert the controlling input signal to a level necessary to drive the shaker. In addition, the field coils used by many larger shakers require a d.c. supply and this may be

derived from the amplifier power supply.

The electrical impedance of an electromagnetic shaker varies with frequency and the choice of power amplifier capabilities is hence not easy. The voltage required to drive sufficient current through the shaker at maximum shaker impedance is not required at other frequencies where the impedance is less. The high ratings of shaker amplifier output stages mean that considerable dissipation levels will occur particularly if linear rather than switch mode operation is used. Below typically 24 kilowatts, linear amplifier output stages are generally air cooled, oil cooling being frequently used above 24 kW [7].

Switch mode power amplifiers, (SMPA), are now being widely introduced, resulting in amplifier units which are not only compact but more efficient and reliable. The high efficiency, (usually about 90%), gives of course lower running costs and involves less heat dissipated to the surrounding environment. The d.c. field power supply and shaker cooling control are included in the same supply cabinet for convenience. Switch mode feeds produce radio-frequency interference, and hence must be adequately shielded. They also tend to feed harmonic currents and voltages back into the supply network and this means that adequate filtering must be used.

Because the driving amplifiers for shakers are designed to very strict specifications, (e.g. providing output with less than 1% harmonic distortion over the operating frequency range), they sometimes find uses as variable frequency single phase power supplies, public address and music amplifiers.

2.3. The Vibration Control System

The complex nature of the variation in shaker impedance with frequency means that no simple relationship exists between power amplifier current and voltage and shaker table amplitude. Hence as stated before some form of amplitude control on the amplifier output must be used. The form of this control varies according to the type of test technique being employed, that is, sinusoidal vibration testing, random vibration testing, shock testing or some combination of all three. A feedback signal is usually obtained via accelerometers attached either to the table or the test object, and is fed into a tracking filter of some sort which filters out all noise, distortion, harmonics, etc. thus enabling measurements and control to be made using the fundamental frequency component only. This filtered feedback signal is then used to provide automatic

control of the output signal level from the amplifier via a unit called a 'Vibration Control Centre'. This control unit has the facility of allowing the user to specify the type of test programme to be used, thus allowing the displacement, velocity and acceleration profiles to be built up, stored and checked before actual testing begins [7].

Electromagnetic vibration test systems have proven to be extremely versatile within the vibration testing field especially in the frequency band 1Hz to approximately 5kHz, and will probably continue to be so for some time to come yet.

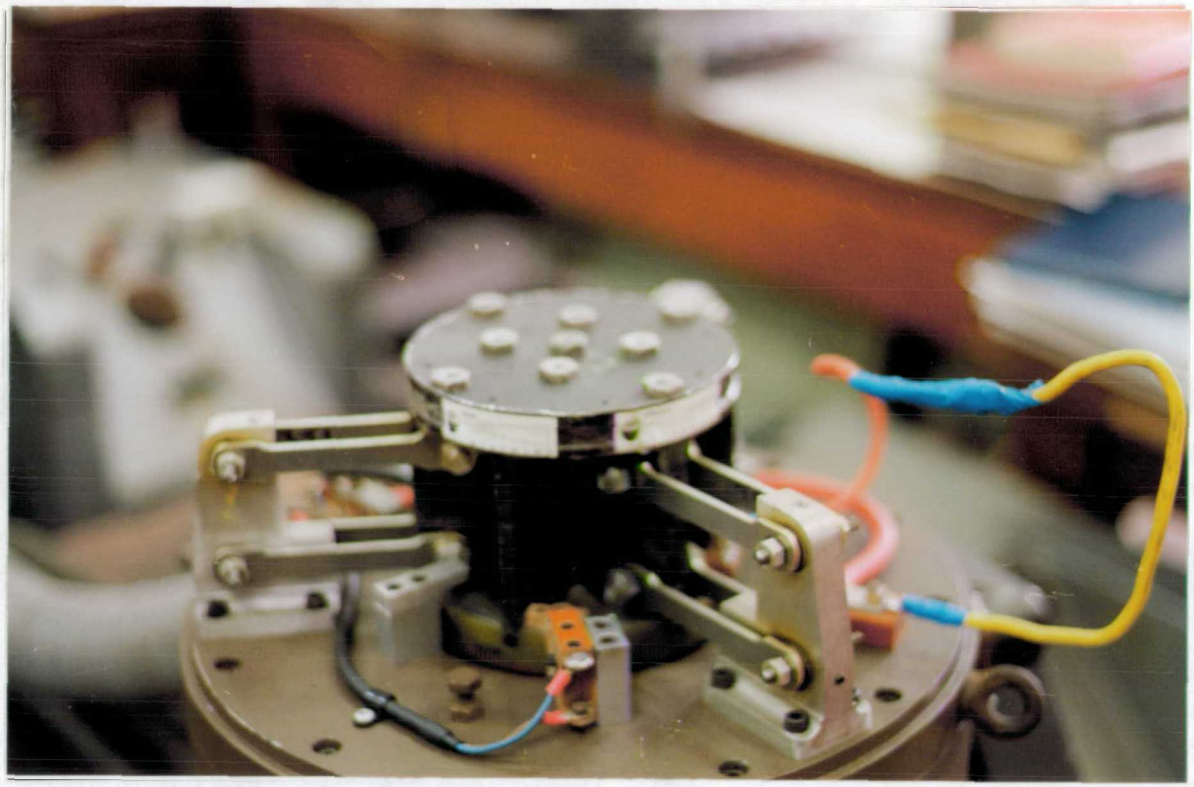


Fig. 2g VP30 Shaker - view of Travel Limiter Contacts

Figure 2g shows a closer view of the moving table and suspension. The 'travel limiter contacts' can be clearly seen. These operate during very large displacements of the table and disconnect the a.c. coil current supply to prevent damage to the moving element. On the edge of the table can be seen 'displacement triangle' stickers which are used for the calibration of table displacement prior to the setting up of test programmes on the Vibration Control Centre. The yellow coloured cable shown has merely been added to facilitate easier monitoring of the a.c. coil current via a clip-on current transformer.

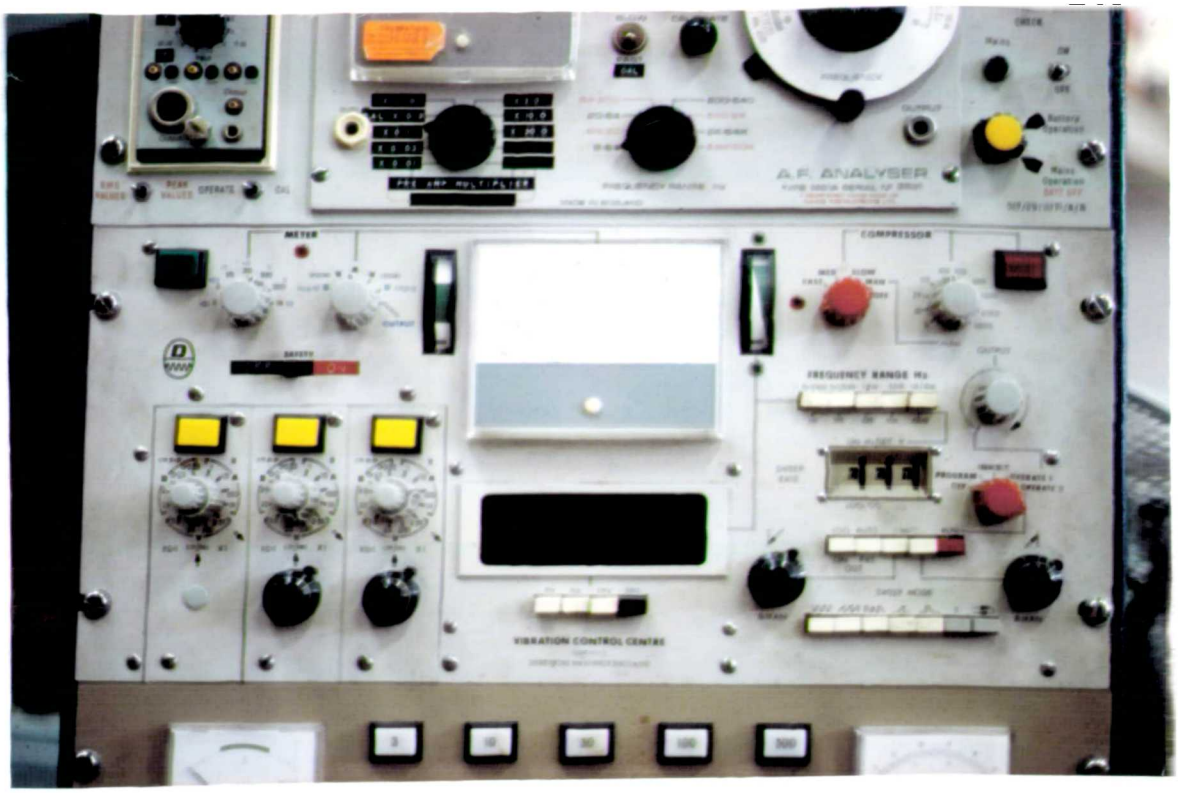


Fig. 2h Vibration Control Centre

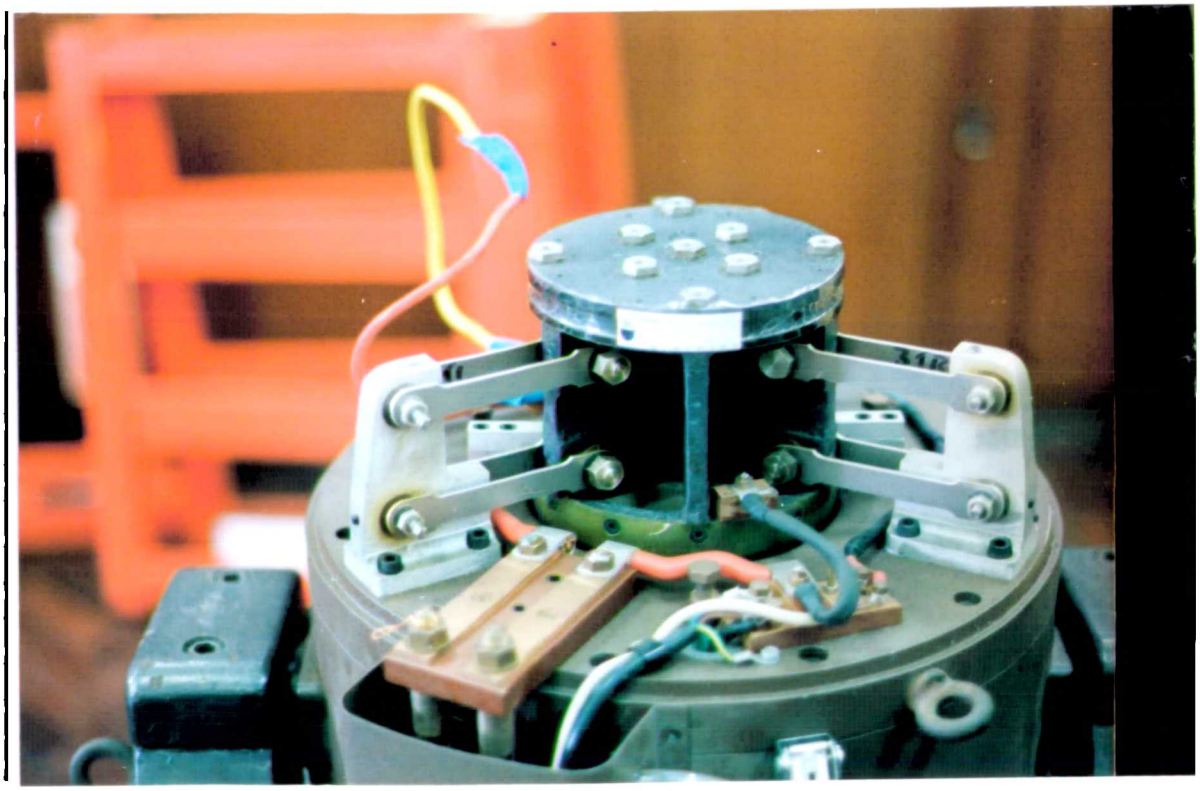


Fig. 2i VP30 Shaker - A.C. Coil Cable Connections

This view shows the a.c. coil cable connections from the amplifier to the connection block on the shaker body.

CHAPTER THREE
ANALYSIS AND DESIGN

3. Analysis and Design - Overall Approach

The analysis and design procedure processes were split into two major parts; one dealing with d.c. (magnetostatic) flux conditions in the steel magnetic circuit and the other with the phenomena in the a.c. moving coil and copper plating. A 2D field analysis using a finite element modelling package was used for the former while a lumped parameter equivalent circuit approach was used for the a.c. coil and copper plating.

The equivalent circuit employed to model the electrical characteristics of the moving coil shaker was coupled to a mechanical equivalent circuit, to take account of the shaker's mechanical characteristics.

Throughout the first two years of the project, emphasis was placed mainly on producing a prototype design of a moving coil shaker, as the sponsoring company was quite keen on re-establishing itself in the vibration testing field with a new range of shakers. At the same time, in parallel with this project, the company was also backing the development of switch mode power amplifiers to drive their new shakers. They previously employed linear amplifiers which were not only large physically but were also very lossy. The need to complete the shaker development project in approximately the same time scale as the amplifier project prompted the adoption of a simple and easy-to-use design tool.

This design tool would finally take the form of a FORTRAN-77 program running on an IBM compatible personal computer. Using the program together with a commercially available 'off-the-shelf' finite element CAD package, the shaker manufacturer's design engineers are now able conveniently to predict quantitatively how changes to the shaker system will affect overall shaker performance. They are also able to experiment with different and novel magnetic circuit configurations and literally design shakers from 'scratch', if they so desire.

3.1. Project Path

The flow chart below provides a guide to the work format that was adopted.

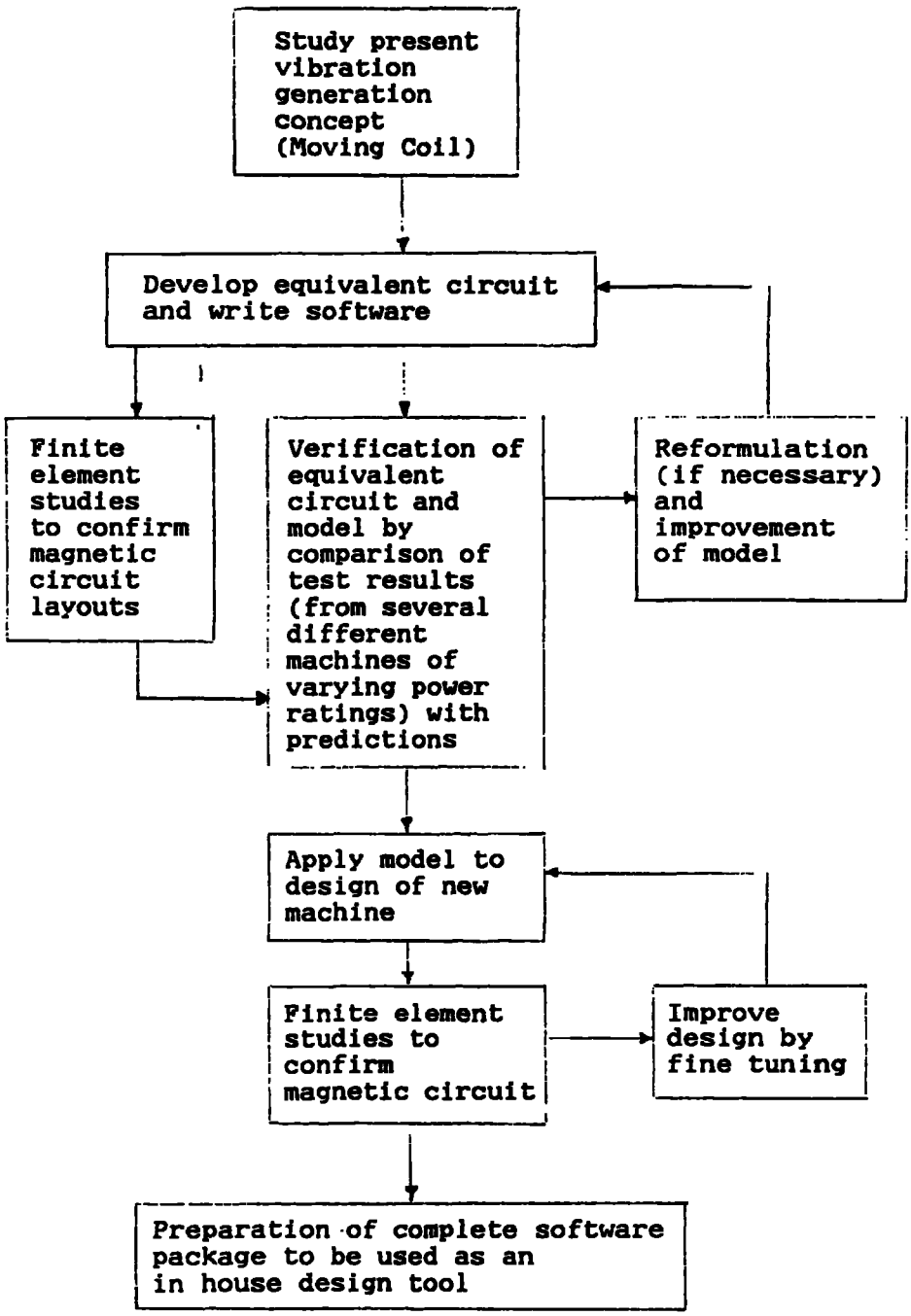


Fig. 3a Flowchart of Project Path

Because the sponsor produces shakers of different sizes, each one satisfying different force requirements, it was decided that initially consideration would be given to one of the more popular shakers in the range. A 6 kVA shaker was considered first, the 'VP85' (manufacturer's designation), to see if shaker performance could be improved either by using a new magnetic circuit configuration or by redesigning the a.c. coil or both. The work on the VP85 machine enabled the mathematical model to be developed and verified by comparing test data with predictions.

The VP85 shaker used the 'single-ended', (loudspeaker-like), magnetic circuit and a double-layered a.c. coil to produce the thrust. Although the coil was wound in-house, the winding and curing processes were rather tedious and time consuming, taking up to several days to prepare a single coil. Proper curing and very careful quality control, particularly of the coil-support to table joint assembly, was necessary to ensure good reliability in service and high axial stiffness. The double-layered coil construction also seemed prone to over-heating and occasionally the a.c. coils became deformed and broke up under prolonged operation of the shaker. One of the priorities in the project was to assess the feasibility of replacing the usual double-layered winding designs with ones incorporating a single-layered a.c. coil.

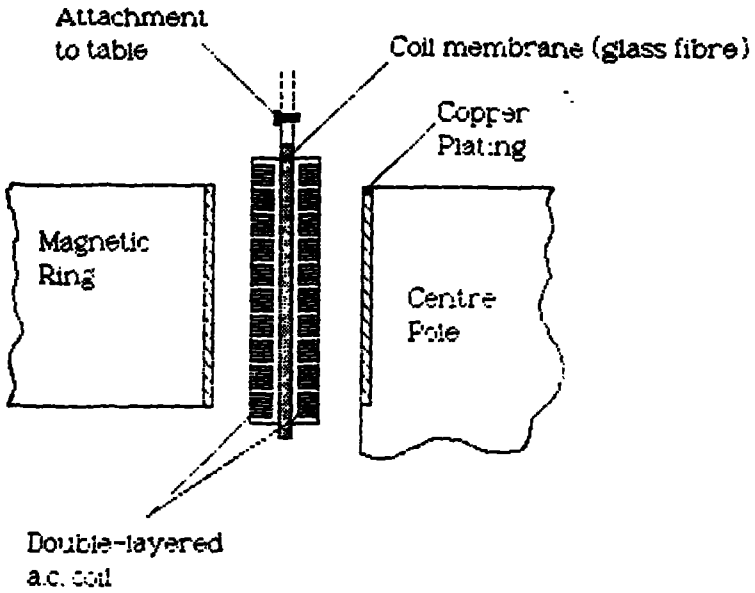


Fig. 3b Double Layered A.C. Coil

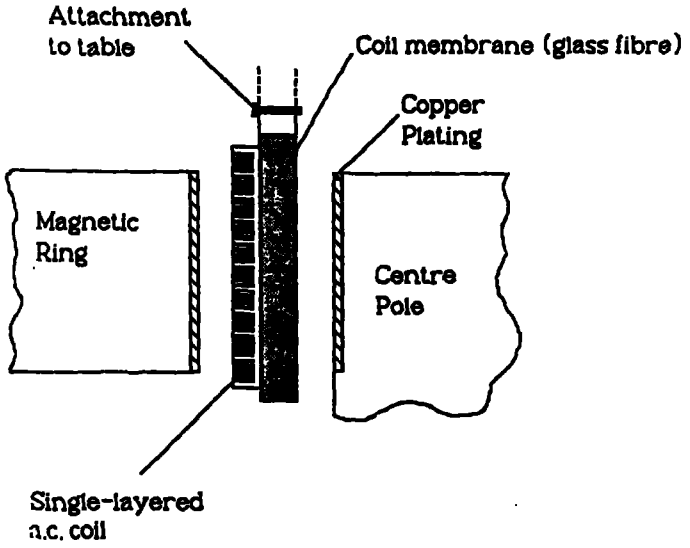


Fig. 3c Single Layered A.C. Coil

This would hopefully make the winding and curing processes less time consuming and possibly ease the over-heating problem.

It was also decided to investigate whether alternatives to the single ended magnetic circuit configuration, (viz. the double ended and c-core configurations), would provide shaker designs with reduced magnetic circuit weight and/or improved performance. There was finally the question of whether shaker designs based on the induction principle would be viable and competitive with those based on the moving coil principle.

The various options were thus :

- *1 layer v 2 layer a.c. coil*
- *single ended v double ended v c-core*
- *moving coil v induction*

In reaching conclusions on preferred options, it was of course necessary to have obtained 'good', i.e. near-optimised, designs of each option combination, obtained by careful tuning of each design. The tuning process, heavily influenced by company policy on weight/performance/cost trade-offs, involved step by step development of the magnetic circuit and winding dimensions and specifications, and was necessarily lengthy and involved a considerable number of discussions with company

personnel. To avoid excessive length, it was decided for this thesis to present only a small part of this design development work, and to omit entirely the investigation of induction shakers, the theory of which has been evolved largely by the author's supervisor.

3.2. The A.C. Equivalent Circuit

A schematic of a moving coil shaker possessing a single-ended magnetic circuit is shown in Figure 3d.

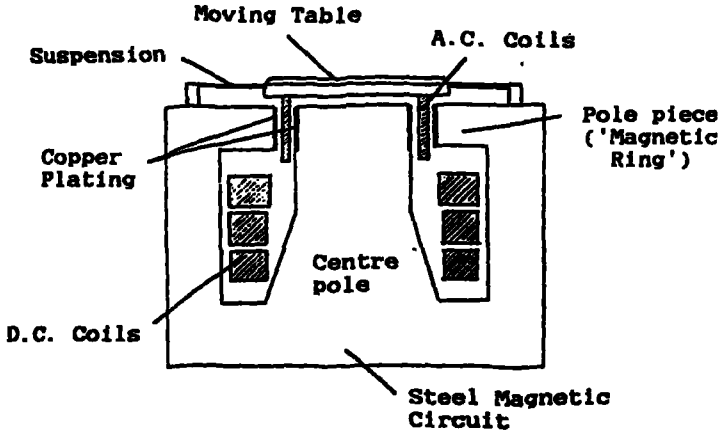


Fig. 3d Single Ended Moving Coil Shaker

The a.c. coil will have resistance and self-inductance associated with it. Also, the various a.c. flux paths, (fringing, leakage, etc.), give rise to several components of inductance, of which four are considered here. This gives us the initial circuit in Figure 3e(i).

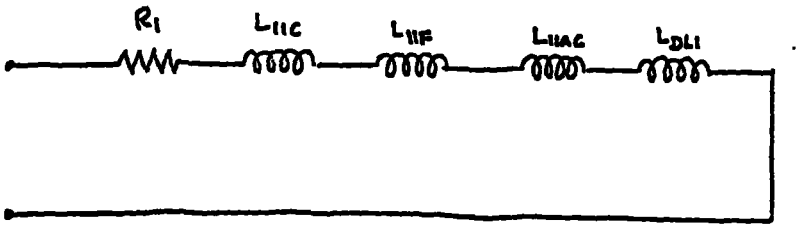


Fig. 3e(i) Stationary A.C. Coil

An e.m.f. will be induced in the a.c. coil as a result of its motion through the d.c. flux. This e.m.f. is velocity dependent and is particularly noticeable for the larger coil sizes where larger coil displacements are present. Since, for linear loads the velocity and hence e.m.f. at a given frequency varies linearly with the current, this 'motional e.m.f.' can be interpreted as the voltage across a motional impedance and is represented in the primary circuit as shown in Figure 3e(ii).

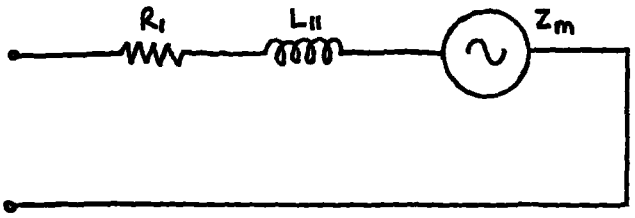


Fig. 3e(ii) Circuit with Motional E.M.F. Generator

The motional e.m.f. generator can be thought of as the element where the electrical to mechanical energy conversion process takes place. As will be shown later, this can also be considered as the place where the mechanical equivalent circuit links the electrical circuit.

Since early in the development of modern shakers, the pole faces, (magnetic ring and centre pole), have been plated with copper. These plating layers act as shields to the a.c. flux produced by the a.c. coil, reducing iron losses in the pole faces and reducing the a.c. fluxes and effective inductance of the winding. Current flowing in the a.c. coil induces currents in the copper plating by transformer action. The plating can be regarded as a transformer secondary circuit. Like the a.c. coil, the plating has resistance and inductance components associated with it, and these can be incorporated into the circuit as indicated in Figure 3e (iii).

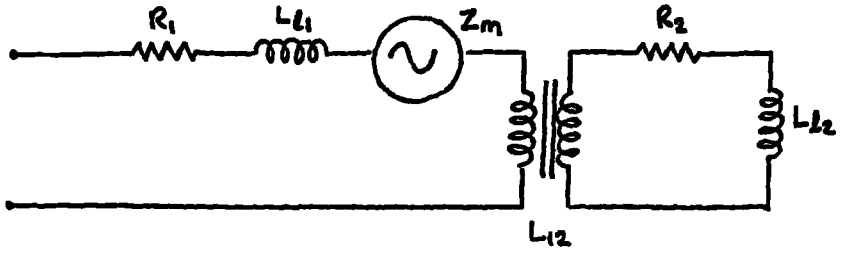


Fig. 3e(iii) A.C. Coil and Copper Plating Layers (showing idealised transformer)

The circuit used here is quite similar to that adopted for short circuited transformers or locked rotor induction machines with the difference that a motional e.m.f. generator is added to the primary circuit, on account of the motion of the primary in the d.c. field.

To be able to solve the full equivalent circuit using normal circuit techniques, the idealised transformer can be replaced by a T-equivalent circuit with a magnetising inductance branch as follows

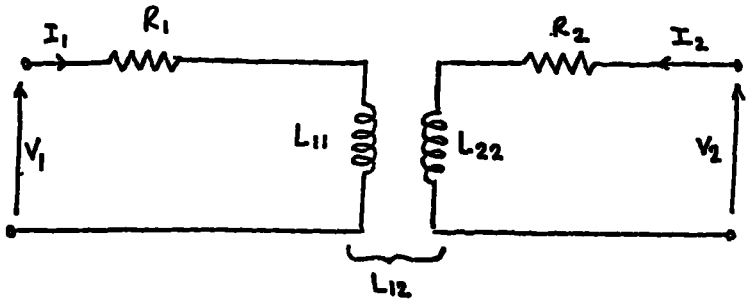


Fig. 3e(iv) Circuit with Idealised Transformer

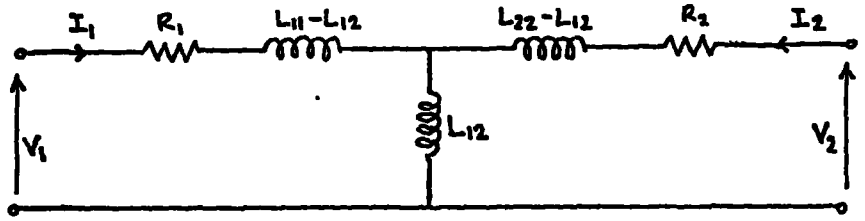


Fig. 3e(v) Without Idealised Transformer

From Figure 3e(iv),

$$V_1 = I_1.L_{11} - I_2.L_{12}$$

$$V_2 = I_1.L_{12} - I_2.L_{22}$$

And, from Figure 3e(v),

$$V_1 = I_1.(L_{L1} + L_m) - I_2.L_m$$

$$V_2 = I_1.L_m - I_2.(L_{L2} + L_m)$$

Then, equating coefficients for the two sets of circuit equations,

$$L_{11} = L_{L1} + L_m$$

$$L_{22} = L_{L2} + L_m$$

$$L_m = L_{12}$$

Thus,

$$L_{L1} = L_{11} - L_{12}$$

$$L_{L2} = L_{22} - L_{12}$$

$$L_m = L_{12}$$

And, this gives the reduced T-equivalent circuit of Figure 3f.

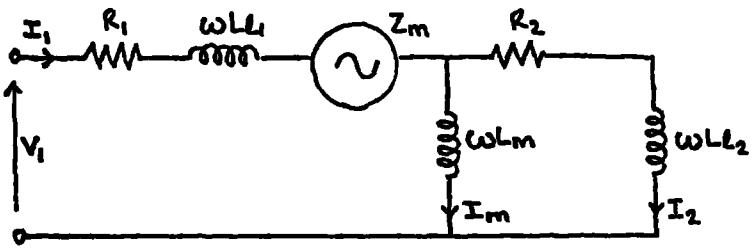


Fig. 3f A.C. T-Equivalent Circuit

Note that whereas iron-core transformers generally have a high value of magnetising inductance and low leakage inductance due to the very closely coupled primary and secondary circuits, in the case of the electromagnetic moving coil shaker, (as in the induction machine), the presence of an air-gap means that the machine possesses a lower magnetising inductance and high leakage inductance.

3.3. Equivalent Circuit Parameters

In deriving the parameter prediction relations, simplifying assumptions are made as usual about the relevant current and flux distributions.

3.3.1. Primary Circuit

The primary circuit consists of the a.c. moving coil and is made up of resistance and inductance components. Both the resistance and inductance parameters are subject to skin effect factoring since skin effect is quite significant in the a.c. coils, (typical thickness of about 8mm), of large shakers at higher frequencies.

(a) Resistance

The primary resistance is given by;

$$R_1 = K_{SKIN1} . R_{1DC} \qquad \text{..... (3.1)}$$

where the skin effect factor is,

$$K_{SKIN1} = \frac{R_{1AC}}{R_{DC1}} \qquad \ldots\ldots\ldots\ldots (3.2)$$

The d.c. resistance is straightforward, given simply by;

$$R_{1DC} = \frac{\rho_1 . \pi . D_m . N}{a_c} \qquad \ldots\ldots\ldots\ldots (3.3)$$

The skin effect factor is obtained by assuming that the multi-turn a.c. coils resemble in electromagnetic terms a single turn conductor in the form of a long thin slab h''' metres high, (axially), 1 metre long, (circumferentially), and t metres thick. The a.c. resistance of such a slab [6] is ;

$$R_{1AC} = \frac{\rho_1}{2.h''' . \delta_1} \cdot \left\{ \frac{\sinh(t/\delta_1) + \sin(t/\delta_1)}{\cosh(t/\delta_1) - \cos(t/\delta_1)} \right\} \qquad \ldots\ldots\ldots\ldots (3.4)$$

where,

$$\delta_1 = \sqrt{\frac{2.\rho_1}{\omega . \mu_o}}$$

is the skin depth, (depth of current penetration into conductor). Since the d.c. resistance of the slab is,

$$R_{DC1} = \frac{\rho_1}{t.h'''} \qquad \ldots\ldots\ldots\ldots (3.5)$$

Hence,

$$K_{SKIN1} = \frac{t}{2}\sqrt{\frac{\omega \cdot \mu_o}{2 \cdot \rho_1}} \cdot \left\{ \frac{\sinh(t/\delta_1) + \sin(t/\delta_1)}{\cosh(t/\delta_1) - \cos(t/\delta_1)} \right\}$$

(b) Inductance (See Appendix A for derivations of inductance relations)

There are considered to be four components of flux that give rise to the total inductance associated with the a.c. coil. Each is considered to give rise to a corresponding component of inductance.

(i) Main Flux

The main flux produced by the current flowing in the a.c. coils links both the coils themselves and the copper plating, (see Figure 3g).

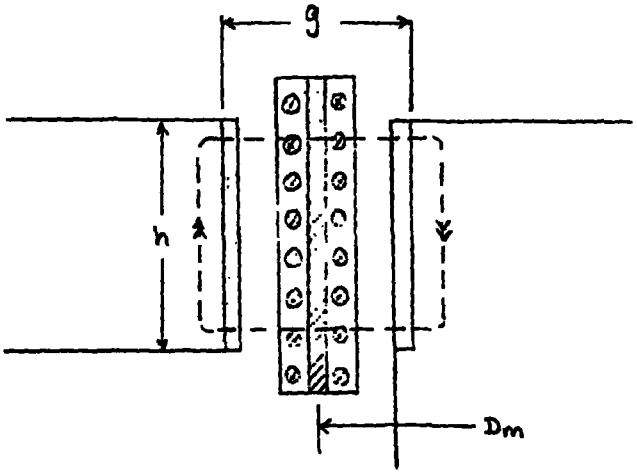


Fig. 3g Main A.C. Flux Path

The main inductance is :

$$L_{11C} = \frac{\mu_o . \pi . D_m . h . (k_1 . N)^2}{12 . g} \qquad \ldots\ldots\ldots\ldots (3.6)$$

where,

$$k_1 = h/h'''$$

k_1 allows for the fact that since the a.c. coil is usually axially longer than the pole face height, only a part of the a.c. coils will be totally within the air-gap at any time during shaker operation.

(ii) Fringing Flux

The inductance due to fringing flux is :

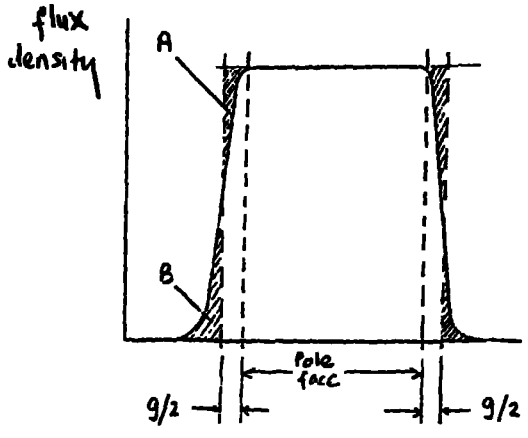
$$L_{11F} = \frac{\mu_o . \pi . D_m . h_{frac} . (k'_1 . N)^2}{2 . g} \qquad \ldots\ldots\ldots\ldots (3.7)$$

where,

$$k'_1 = \frac{(1 + k_1)}{2} = \frac{1 + (h/h''')}{2}$$

$$h_{frac} = g/2$$

Referring to the diagram below, it is found that A ≈ B. Hence the total flux including fringing corresponds to the pole extension of g/2 at each end.



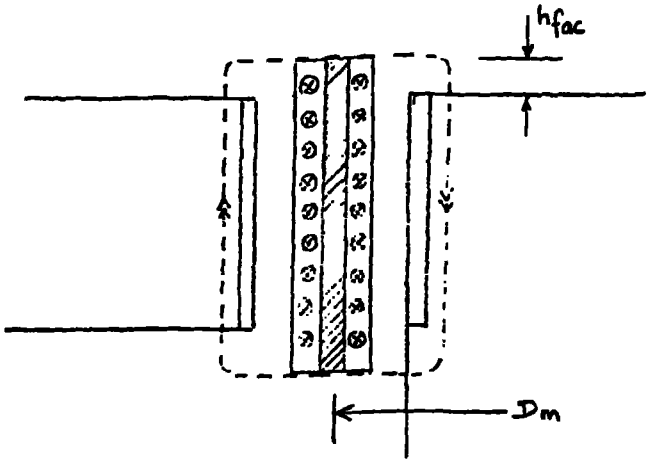


Fig. 3h Primary Fringing Flux Path

(iii) Internal Flux

This is the flux circulating within the a.c. coil itself. Treating the a.c. coil again as a thin slab of conductor, (this can be done whether it is of the single-layered or double-layered construction), enables a standard relation for the inductance of a slab subject to skin effect to be used. The Reference 6 relation is :

$$L_{11AC} = \frac{\rho_1}{2.\delta_1.\omega.h'''} \cdot \left\{ \frac{\sinh(t/\delta_1) - \sin(t/\delta_1)}{\cosh(t/\delta_1) - \cos(t/\delta_1)} \right\} \quad \ldots\ldots\ldots (3.8)$$

Hence, for the N turn coil, (πD_m) in circumferential length, the skin effect adjusted internal inductance is :

$$L_{11AC} = \frac{\rho_1.\pi.D_m.N^2}{2.\delta_1.\omega.h'''} \cdot \left\{ \frac{\sinh(t/\delta_1) - \sin(t/\delta_1)}{\cosh(t/\delta_1) - \cos(t/\delta_1)} \right\} \quad \ldots\ldots\ldots (3.9)$$

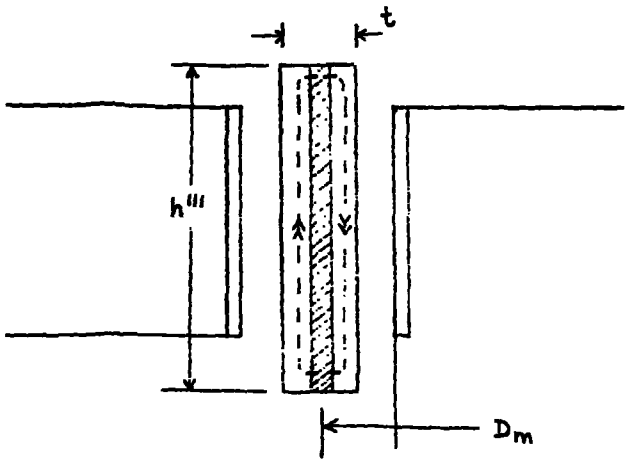
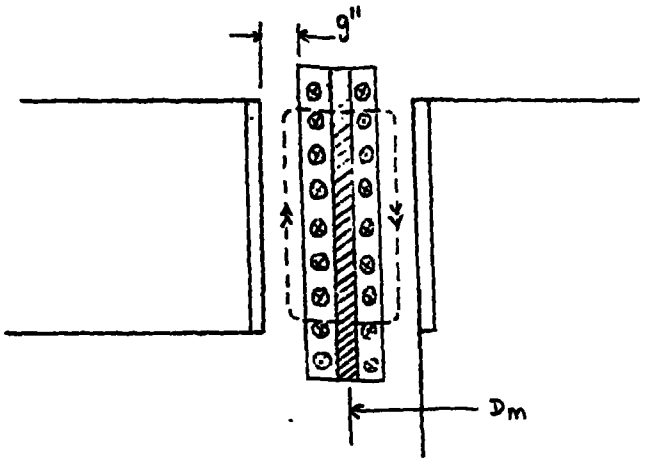


Fig. 3i Primary Internal Flux Path

(iv) Gap Leakage Flux

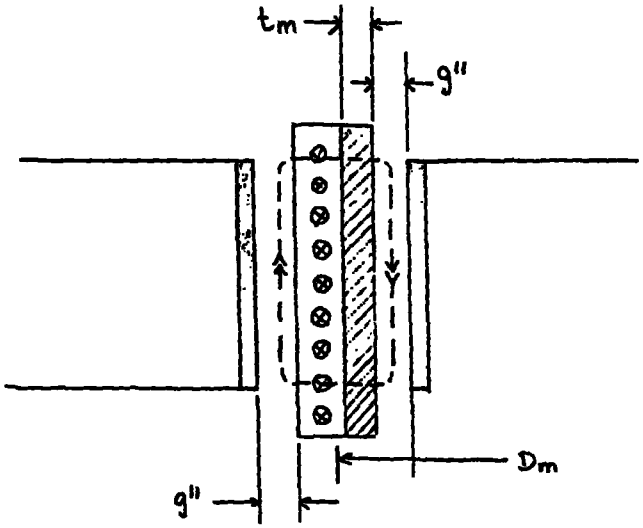
An important component of the flux set up by the a.c. coil mmf but not linking the plating is the flux which passes axially in the two clearances between coil surface and pole face. The corresponding inductance relation is formulated in a way similar to that used for slot leakage inductance in conventional rotating machinery. The reluctance of these paths differs depending on whether a single or double layered coil is used due to the difference in thickness of the coil membrane used. This is dealt with separately using 'correction-factors' (C_{Fx}).

$$L_{DL1} = \frac{\mu_o . \pi . D_m . g'' . N^2}{4 . h'''} \cdot C_{F1} \qquad \ldots\ldots\ldots\ldots (3.10)$$



$$C_{F1} = 1$$

Fig. 3j(i) Standard Double Layered Coil



$$C_{F1} = \left[\frac{2\left[1 + (t_m/g'')\right]}{2 + (t_m/g'')} \right]$$

Fig. 3j(ii) Single Layered Coil

Hence, the total a.c. coil inductance, L_{11} , is ;

$$L_{11} = L_{11C} + L_{11F} + L_{DL1} + L_{11AC}$$

..... (3.11)

3.3.2. Secondary Circuit

The secondary circuit is assumed to comprise just the copper plating layers present on the pole faces. These are considered as single turn coils in parallel. They act as a.c. screens for the a.c. flux produced by the a.c. coils, and thus help to flatten the impedance curve over the operating frequency range. The conductivity of the solid iron poles is taken as negligible, an assumption which gives rise to less error than would otherwise be the case, due to the high conductivity ratio between the copper of the plating and the iron, and by the deliberately high effectiveness, (in minimising a.c. flux in the iron), of the plating as an a.c. flux screen.

(a) Resistance

The resistance for the two plating layers, (on the centre pole and on the magnetic ring respectively), are dealt with separately.

Centre-pole,

$$R_{CUPOL} = k_{2CP}.R_{CPOL} \qquad R_{CPOL} = \frac{\rho_2.\pi.D_{cp}}{t_{cpole}.h_{cpole}} \qquad \ldots\ldots\ldots\ (3.12)$$

and, magnetic ring,

$$R_{CUMAG} = k_{2MR}.R_{CMAG} \qquad R_{CMAG} = \frac{\rho_2.\pi.D_{cp}}{t_{magr}.h_{magr}} \qquad \ldots\ldots\ldots\ (3.13)$$

where, k_{2CP} and k_{2MR} , the skin efect factors for the centre pole and magnetic ring, are found from standard results for slab conductors as before :

Centre Pole

$$R_{2ACCP} = \frac{\rho_2}{2.h_{cpole}.\delta_2}.\left\{\frac{\sinh(t_{cpole}/\delta_2) + \sin(t_{cpole}/\delta_2)}{\cosh(t_{cpole}/\delta_2) - \cos(t_{cpole}/\delta_2)}\right\} \qquad \ldots\ldots\ldots\ (3.14)$$

where, skin depth is,

$$\delta_2 = \sqrt{\frac{2.\rho_2}{\omega.\mu_o}}$$

D.C. resistance of the thin slab ;

$$R_{DC2CP} = \frac{\rho_2}{t_{cpole}.h_{cpole}} \qquad \text{..... (3.15)}$$

Giving the secondary skin effect factor for the centre pole as,

$$k_{2CP} = \frac{R_{2ACCP}}{R_{DC2CP}} = \frac{t_{cpole}}{2.\delta_2}\left\{\frac{\sinh(t_{cpole}/\delta_2) + \sin(t_{cpole}/\delta_2)}{\cosh(t_{cpole}/\delta_2) - \cos(t_{cpole}/\delta_2)}\right\} \qquad \text{..... (3.16)}$$

Magnetic Ring

Similarly, for the plating on the magnetic ring pole face ;

$$k_{2MR} = \frac{t_{magr}}{2.\delta_2}\left\{\frac{\sinh(t_{magr}/\delta_2) + \sin(t_{magr}/\delta_2)}{\cosh(t_{magr}/\delta_2) - \cos(t_{magr}/\delta_2)}\right\} \qquad \text{..... (3.17)}$$

Thus, the overall effective secondary resistance, (referred to the primary), will be ;

$$R_2 = \left[\frac{R_{CUPOL}.R_{CUMAG}}{R_{CUPOL} + R_{CUMAG}}\right].(k_1.N)^2 \qquad \text{..... (3.18)}$$

where the factor k_1 again allows for the fact that only a fraction k_1 of the coil turns are actually in the gap at any instant.

(b) Inductance (Secondary inductances are all referred to the primary)

As for the primary circuit, there are again four components to be taken into account.

(i) Main Inductance

$$L_{22c} = \frac{\mu_o . \pi . D_m . h . (k_1 . N)^2}{12 . g} \qquad \ldots\ldots\ldots\ldots (3.19)$$

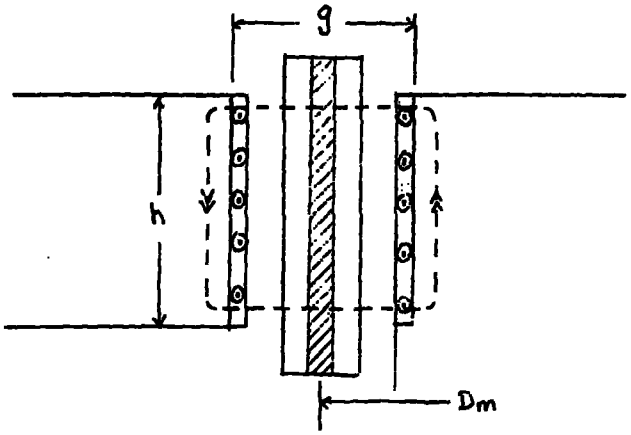


Fig. 3k Main Secondary Flux Path

(ii) Inductance due to Fringing Flux

$$L_{22F} = \frac{\mu_o . \pi . D_m . h_{fac} . (k'_1 . N)^2}{2 . g} \qquad \ldots\ldots\ldots\ldots (3.20)$$

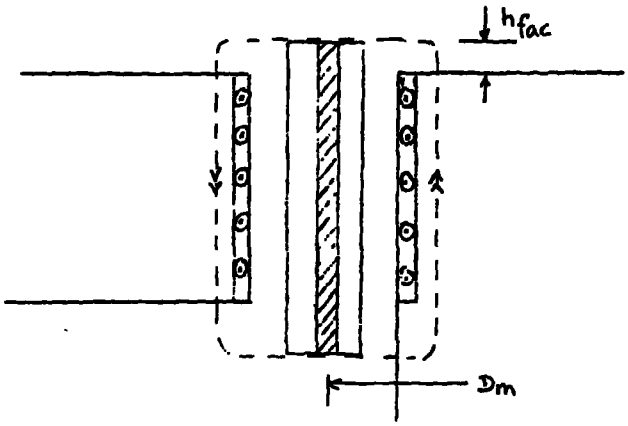


Fig. 3l Secondary Fringing Flux Path

(iii) Internal Inductance

The internal inductance associated with internal flux is dealt with separately for the plating layers on the centre pole and magnetic ring. They are very small in view of the thinness of the layers but are considered to be just worth taking into account.

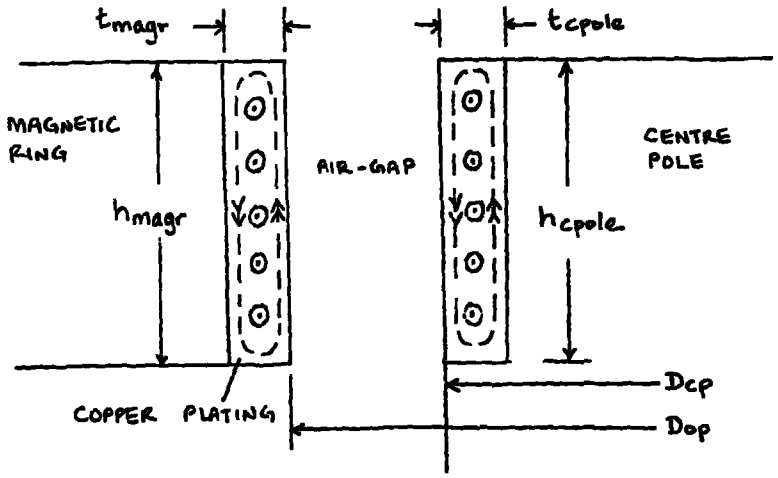


Fig. 3m Secondary Internal Flux Paths

Centre Pole

$$L_{ZACCP} = \frac{\rho_2 . \pi . D_{cp}}{2 . \delta_2 . \omega . h_{cpole}} \left\{ \frac{\sinh(t_{cpole}/\delta_2) - \sin(t_{cpole}/\delta_2)}{\cosh(t_{cpole}/\delta_2) - \cos(t_{cpole}/\delta_2)} \right\} \quad \ldots\ldots\ldots (3.21)$$

Magnetic Ring

$$L_{ZACMR} = \frac{\rho_2 . \pi . D_{op}}{2 . \delta_2 . \omega . h_{magr}} \left\{ \frac{\sinh(t_{magr}/\delta_2) - \sin(t_{magr}/\delta_2)}{\cosh(t_{magr}/\delta_2) - \cos(t_{magr}/\delta_2)} \right\} \quad \ldots\ldots\ldots (3.22)$$

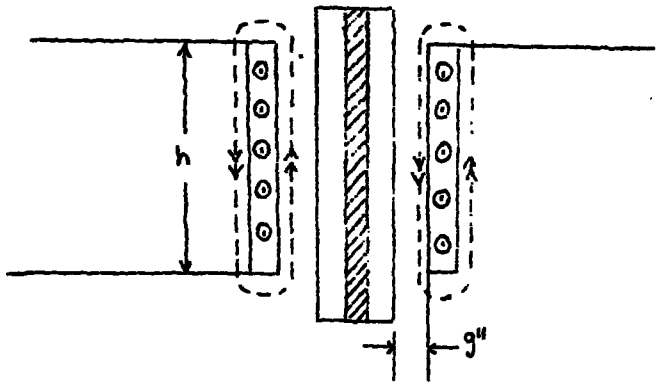
As the inductances of the two plating layers are effectively in parallel, the resultant internal inductance is thus given by ;

$$L_{L2TOT} = \left[\frac{L_{2ACCP} . L_{2ACMR}}{L_{2ACCP} + L_{2ACMR}} \right] \cdot (k_1 . N)^2 \qquad \ldots\ldots\ldots\ldots (3.23)$$

(iv) Gap Leakage Flux

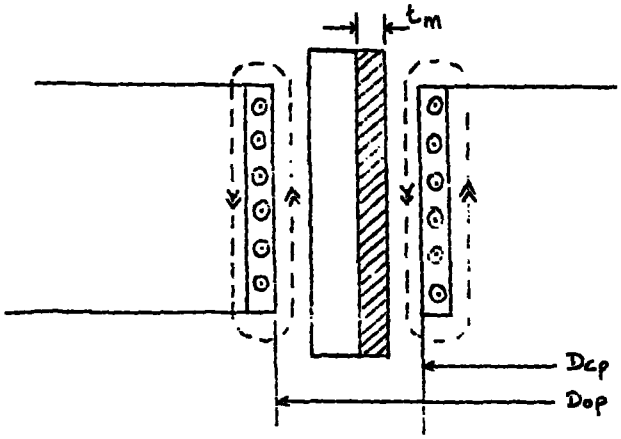
Correction factors to allow for differing a.c. coils are used in this case too.

$$L_{22L1} = \frac{\mu_o . \pi . D_{op} . D_{cp} . g'' . (k_1 . N)^2}{2 . h . (D_{op} + D_{cp})} \cdot C_{F2} \qquad \ldots\ldots\ldots\ldots (3.24)$$



$$C_{F2} = 1$$

Fig. 3n(i) Secondary Leakage Flux Path - Standard Double Layered Coil



$$C_{F2} = \left[\frac{(g'' + t_m) . (D_{op} + D_{cp})}{D_{cp} . (g'' + t_m) + D_{op} . g''} \right]$$

Fig. 3n(ii) Secondary Leakage Flux Path - Single Layered Coil

The total secondary inductance L_{22} is hence,

$$L_{22} = L_{22C} + L_{22L1} + L_{L2TOT} + L_{22F}$$

..... (3.25)

3.3.3. Magnetising Inductance

In the T-equivalent circuit, the magnetising inductance, (L_m or L_{12}), corresponds to flux linking both the primary and secondary. Both the 'main flux' and 'fringing flux' do this so L_{12} is given by :

$$L_{12} = L_m = L_{12C} + L_{12F}$$

..... (3.26)

where, L_{12C}, due to main flux is,

$$L_{12C} = \frac{\mu_o . \pi . D_m . h . (k_1 . N)^2}{12 . g}$$

..... (3.27)

and, L_{12F}, due to fringing flux is,

$$L_{12F} = \frac{\mu_o . \pi . D_m . h_{rec} . (k'_1 . N)^2}{2 . g}$$

..... (3.28)

The primary and secondary leakage inductances L_{L1} and L_{L2} in the T-equivalent circuit are found by subtracting the magnetising inductance from the primary and secondary total inductances derived earlier, (i.e. L_{11} and L_{22}),

$$L_{L1} = (L_{11} - L_{12})$$

$$L_{L2} = (L_{22} - L_{12})$$

..... (3.29)

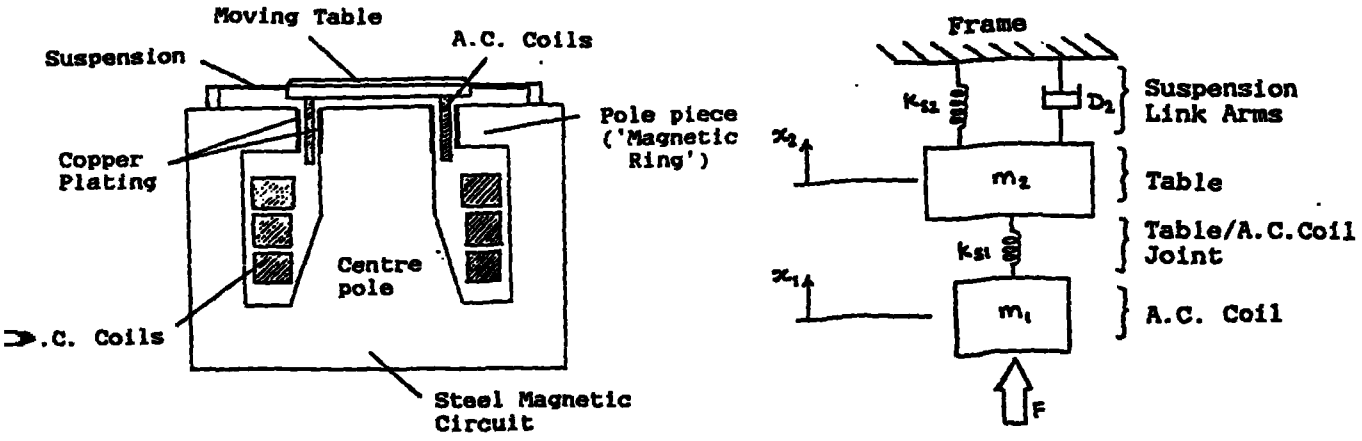
The next stage in the analysis and design procedure is suitably to model the mechanical aspects of the shaker and to link this with the electrical equivalent circuit.

3.4. Mechanical Model

3.4.1. Two-Degree-of-Freedom Representation

The simple mass/spring lumped approach is used to model the mechanical aspects of each shaker layout, be it of the single-ended, double-ended or c-core variety. Single-ended and double-ended shakers can be suitably represented by using a two mass/spring system while a three mass/spring system is adopted for the c-core system, since the two moving coils present in such shakers are mounted at different axial locations on a tube of some axial compliance. The two mass/spring system will be dealt with here and linked with the electrical circuit; the c-core system is dealt with in Chapter six.

Figure 3o shows how the two mass/spring system is developed using the single-ended shaker as an example.



(i) Single Ended Shaker *(ii) Two Mass/Spring System*

Fig. 3o Two-Degree-of-Freedom Representation

Only motion in the vertical axis is of interest here and any displacement in the horizontal plane is assumed to be very small and to have no influence on the vertical motion. This assumption is quite valid as the suspension systems employed by shakers are almost always designed with extremely high lateral stiffness figures, when compared with the figure for the axial stiffness.

3.4.2. System Equations

Referring to Figure 3o and applying Newton's Second Law of Motion to both masses;

Mass m_1 ,

$$F = m_1.\ddot{x}_1 + k_{s1}.(x_1 - x_2) \qquad \text{..... (3.30)}$$

Mass m_2 ,

$$0 = m_2.\ddot{x}_2 + D_2.\dot{x}_2 + k_{s2}.x_2 + k_{s1}.(x_2 - x_1) \qquad \text{..... (3.31)}$$

where,

m_1 - *total mass of a.c. coil copper, coil former and bonding materials.*
m_2 - *total table mass including any fixtures*
k_{s1} - *armature/table joint stiffness. The joint between the table and the armature, (which consists of bolts and bonding agent), is slightly flexible in the axial direction at certain frequencies.*
k_{s2} - *suspension stiffness.*
D_2 - *damping coefficient for suspension arms.*

This pair of linear ordinary differential equations are assumed to possess only constant coefficients and can thus be solved by a 'standard' procedure. In reality, the coefficients, k_{s1} , k_{s2} and D_2 are not quite constant; in fact, the suspension stiffness factor k_{s2} may often possess two values of stiffness, one for positive x_2 , (i.e. upward travel of the table), another for negative x_2 , (i.e. downward travel). But this variation is only slight and, for first order approximations, can be ignored.

Assuming sinusoidal motion, let,

$$F = F.e^{j\omega t}$$

$$x_1 = X_1.e^{j\omega t} \; ; \; \ddot{x}_1 = -\omega^2.X_1.e^{j\omega t}$$

$$x_2 = X_2.e^{j\omega t} \; ; \; \dot{x}_2 = j\omega.X_2.e^{j\omega t} \; ; \; \ddot{x}_2 = -\omega^2.X_2.e^{j\omega t}$$

Because the performance specifications of displacement, velocity and acceleration for a particular shaker relate to the motion of the table, (picked up by an accelerometer on the table surface), the system equations should be derived in terms of table displacement x_2 .

Force, **F**

Substituting into equations (3.30) and (3.31);
Equation (3.30) gives;

$$F.e^{j\omega t} = -m_1.\omega^2.X_1.e^{j\omega t} + k_{s1}.(X_1.e^{j\omega t} - X_2.e^{j\omega t})$$

$$F = (k_{s1} - m_1.\omega^2).X_1 - k_{s1}.X_2 \qquad \ldots\ldots\ldots\ldots (3.32)$$

and equation (3.31) gives;

$$0 = -k_{s1}.X_1 + (k_{s1} + k_{s2} - m_2.\omega^2 + j.\omega.D_2).X_2 \qquad \ldots\ldots\ldots\ldots (3.33)$$

Solving equation (3.33) for X_1 ;

$$X_1 = \frac{(k_{s1} + k_{s2} - m_2.\omega^2 + j.\omega.D_2).X_2}{k_{s1}} \qquad \ldots\ldots\ldots\ldots (3.34)$$

From equations (3.32) and (3.34), the force expression is given by;

$$F = \frac{(k_{s1} - m_1.\omega^2).(k_{s1} + k_{s2} - m_2.\omega^2 + j.\omega.D_2).X_2 - k^2_{s1}.X_2}{k_{s1}} \quad \ldots\ldots\ldots\ldots (3.35)$$

Input Current, I_1

The electrical force generated by the shaker is given by;

$$F = k_v.I_1$$

This gives us;

$$I_1 = \frac{F}{k_v}$$

which in turn provides an expression for the input current in terms of X_2 , (displacement of the table) :

$$I_1 = \frac{X_2}{k_v.k_{s1}} \left\{ (k_{s1} - m_1.\omega^2).(k_{s1} + k_{s2} - m_2.\omega^2) - k^2_{s1} + j.\omega.D_2.(k_{s1} - m_1.\omega^2 \right. \quad \ldots\ldots\ldots\ldots (3.36)$$

Equivalent expressions for the current in terms of the peak to peak displacement, peak velocity and peak acceleration can be obtained by substituting,

$$X_2 = \frac{\hat{\hat{x}}_2}{2\sqrt{2}} \qquad X_2 = j.\frac{\hat{\dot{x}}_2}{\sqrt{2}\omega} \qquad X_2 = \frac{-9.81\ \hat{\ddot{x}}_2}{\omega^2\sqrt{2}}$$

where, the units of $\ddot{x}_2$ are 'g'. The following resultant expressions are used for calculations in the displacement-limited, velocity-limited and acceleration-limited frequency bands respectively.

$$I_1 = \frac{\hat{\hat{x}}_2}{2.\sqrt{2}.k_v.k_{s1}} \left\{ (k_{s1} - m_1.\omega^2).(k_{s1} + k_{s2} - m_2.\omega^2) - k^2_{s1} + j.\omega.D_2.(k_{s1} - m_1.\omega^2 \right. \quad \ldots\ldots\ldots\ldots (3.37)$$

$$I_1 = \frac{\hat{\dot{x}}_2}{\sqrt{2}.\omega.k_v.k_{s1}}\left\{\omega D_2.(k_{s1} - m_1.\omega^2) - j\left[(k_{s1} - m_1.\omega^2).(k_{s1} + k_{s2} - m_2.\omega^2) - k^2_{s1}\right.\right.$$

..... (3.38)

$$I_1 = \frac{9.81\,\hat{\ddot{x}}_2}{-\omega^2.\sqrt{2}.k_v.k_{s1}}\left\{(k_{s1} - m_1.\omega^2).(k_{s1} + k_{s2} - m_2.\omega^2) - k^2_{s1} + j.\omega.D_2.(k_{s1} - m_1.\omega^2)\right.$$

..... (3.39)

***Motional E.M.F.*, E_m**

The motional e.m.f. is generated as a result of the motion of the moving coil through the d.c. flux and, assuming constant mean d.c. flux density, is proportional to the instantaneous velocity of the moving coil. Thus, the motional e.m.f. should be derived in terms of the velocity of the armature, (moving coil + membrane), rather than the table velocity which will have its own somewhat different motion characteristics, due to the finite stiffness k_{s1} between them.

From equation (3.34);

$$X_2 = \frac{k_{s1}.X_1}{(k_{s1} + k_{s2} - m_2.\omega^2 + j.\omega.D_2)}$$

..... (3.40)

and substituting into equation (3.32);

$$F = \frac{(k_{s1} - m_1.\omega^2).(k_{s1} + k_{s2} - m_2.\omega^2 + j.\omega.D_2).X_1 - k^2_{s1}.X_1}{(k_{s1} + k_{s2} - m_2.\omega^2 + j.\omega.D_2)}$$

..... (3.41)

and using,

$$F = k_v.I_1$$

the displacement x_1 of the armature is,

$$X_1 = \frac{k_v.I_1.(k_{s1} + k_{s2} - m_2.\omega^2 + j.\omega.D_2)}{(k_{s1} - m_1.\omega^2).(k_{s1} + k_{s2} - m_2.\omega^2 + j.\omega.D_2) - k^2_{s1}}$$

..... (3.42)

The motional e.m.f. is given by,

$$E_m = k_v.\dot{X}_1$$

$$E_m = j.\omega.k_v.X_1 \qquad \ldots\ldots\ldots\ldots (3.43)$$

$$E_m = \frac{j.\omega.k^2_v.I_1.(k_{s1} + k_{s2} - m_2.\omega^2 + j.\omega.D_2)}{(k_{s1} - m_1.\omega^2).(k_{s1} + k_{s2} - m_2.\omega^2 + j.\omega.D_2) - k^2_{s1}} \qquad \ldots\ldots\ldots\ldots (3.44)$$

Hence, E_m , on the basis of the linear system behaviour assumed, is found to be proportional to the a.c. coil current I_1.

Motional Impedance, Z_m

The statement above means that the ratio of E_m/I_1 is constant at a given frequency, whatever the amplitude. The concept of a 'motional impedance' is hence feasible.

$$Z_m = \frac{E_m}{I_1}$$

$$Z_m = \frac{j.\omega.k_v.X_1}{I_1} \qquad \ldots\ldots\ldots\ldots (3.45)$$

$$Z_m = \frac{j.\omega.k^2_v.(k_{s1} + k_{s2} - m_2.\omega^2 + j.\omega.D_2)}{(k_{s1} - m_1.\omega^2).(k_{s1} + k_{s2} - m_2.\omega^2 + j.\omega.D_2) - k^2_{s1}} \qquad \ldots\ldots\ldots\ldots (3.46)$$

The motional impedance parameter is where the electrical to mechanical energy conversion takes place, and the relationship between the VA absorbtion in Z_m and the product of the r.m.s. force and velocity can be found as follows,

$$E_m.I = k_v.\dot{X}_1 \times \frac{F}{k_v} = F.\dot{X}_1$$

Hence, one can think of I^2Z_m as converted complex power. This is thus the link between the mechanical model, (lumped mass/spring system), and the electrical circuit. Put another way, since $F = m\ddot{x} = \omega m\dot{x}$ neglecting suspension forces, therefore $\dot{x}/F = 1/\omega m$ which is directly proportional to $1/\omega$.

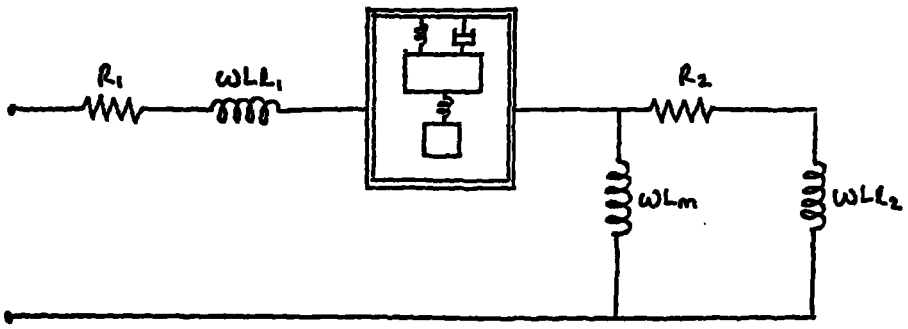


Fig. 3p Electrical/Mechanical Model of Shaker

Because the motional impedance is proportional to the velocity divided by the thrust of the moving coil, it is especially high at low to medium frequencies, where the shaker is operating in its velocity limited phase, thus dominating the overall impedance presented by the shaker to the driving amplifier. Dealing with a one-degree-of-freedom system for purposes of clarity, and now including the suspension force term, the motional impedance is,

$$Z_m = \frac{j.\omega.k^2_v}{(k_s - m.\omega^2)} \qquad \ldots\ldots\ldots\ (3.47)$$

Examination of eqn. (3.47) shows that this impedance is inductive at low frequencies,

(below the spring, that is, suspension, resonance), due to the +j term in the numerator. At the spring resonance, Z_m tends to infinity, this resonance frequency being given by,

$$\omega = \sqrt{\frac{k_s}{m}}$$

for a one-degree-of-freedom mass/spring system, or by,

$$\omega_1 = \left\{ \frac{1}{2} \left[\frac{k_{s1}}{m_1} + \frac{k_{s1} + k_{s2}}{m_2} \right] + \sqrt{\left[\frac{k_{s1}}{m_1} + \frac{k_{s1} + k_{s2}}{m_2} \right]^2 - \frac{4.k_{s1}.k_{s2}}{m_1.m_2}} \right\}^{1/2}$$

..... (3.48)

for a two-degree-of-freedom mass/spring system without damping, (to make solution easier). Above the spring resonance frequency, it is capacitive, and partially cancels the leakage inductances, (i.e. go into partial electrical resonance), lowering the net inductance seen at the a.c. coil terminals. In fact, in the mid to high frequency band, the capacitive Z_m exceeds the net inductance and a higher inductance would then be beneficial in reducing the coil overall impedance. To achieve this in practice, it may be possible to add a fixed inductor in series with the primary circuit which could be switched in, in the mid to high frequency band where it is needed, and then switched out at the higher frequencies where the Z_m becomes smaller than ωL. This would be possible if the shaker were to be used only for very slow sinusoidal sweep tests, thus permitting easy and error-free frequency detection for the switching system to work properly. But, unfortunately, most test specifications very rarely call for such tests. The usual tests used are rapid sinusoidal sweeps and random and pulse tests, and the switching system would not be able to cope adequately under such test conditions.

As detailed later, the variation in a.c. coil Z due to the large changes in Z_m has to be taken into account in the design of the moving coil and copper plating layers on the pole faces.

3.5. Limitations of the Equivalent Circuit Approach

The electrical/mechanical equivalent circuit described above can only be used

for predicting the steady state sinusoidal performance of a shaker system, and is not valid for transient conditions. This is not thought to present undue problems since sine-wave conditions are always used as a basis for design. Further work into shock or random test prediction techniques would perhaps be worthwhile.

Because an equivalent circuit approach has been adopted for ease and clarity of design, certain assumptions have had to be made. Note that for sine-wave operation, the input signal being fed to the a.c. coil is in practice very close to a pure sine-wave, possessing extremely little distortion or harmonic content, since the power supplies and amplifiers employed for driving electromagnetic shakers are designed and constructed with this as a mandatory requirement.

Another assumption is to regard all leakage inductances and the k_v factor as independent of the a.c. coil position. In reality these parameters will change as the a.c. coil moves up and down, because the a.c. flux set up by and linking the a.c. coil and copper plating will be affected somewhat by the coil position relative to the pole upper and lower surfaces. Because the coil moves only a very short distance however, (typically equivalent to about 14% of the coil height), the variation in these factors are likely to be relatively small. (Note that a constant or near constant k_v is essential if shaker behaviour is to be linear, and this must hence be assured at the design stage by assessing B_{max} v displacement x).

Thirdly, iron losses in the solid iron due to a.c. fluxes set up by coil and plating currents have not been allowed for. Fourth, leakage paths have been idealised and iron reluctance neglected. Fifth, eddy current effects at high frequencies in the a.c. coil and copper plating have been modelled by considering current flow in finite thickness sheets of infinite extent. This does not take into account any axial non-uniformities in the currents, particularly the plating current. At high frequencies this is likely to cause significant errors since axial redistribution effects could be severe.

Finally, suspension stiffnesses and damping coefficients have been assumed to be constant, when in reality they are dependent upon the forces and particularly the motion executed. High amplitude displacements occur at the low end of the operating frequency range and hence changes in the mechanical coefficients are likely to have only slight influence over the general performance of the shaker.

CHAPTER FOUR
FREQUENCY RESPONSE OF MOVING COIL SHAKERS

It should be noted that some of the material in this chapter is based on a report [16] prepared for the sponsor during the project.

The a.c. equivalent circuit of a moving coil shaker, already dealt with, can be used to explain its frequency response when operating with a sprung, inertial load, with an amplifier having specified voltage and current capabilities, and with a fixed value of d.c. flux. Simple relations are derived relating table motion to voltage and current, and the shapes of the voltage, current and kVA characteristics are shown to be the result of the shaker's inherent operating features. Numerical values from the performance of the single-ended VP700 shaker, are used to exemplify the trends.

4.1. A.C. Equivalent Circuit

The a.c. equivalent circuit is shown here again for convenience and will be referred to throughout this chapter as the discussion proceeds.

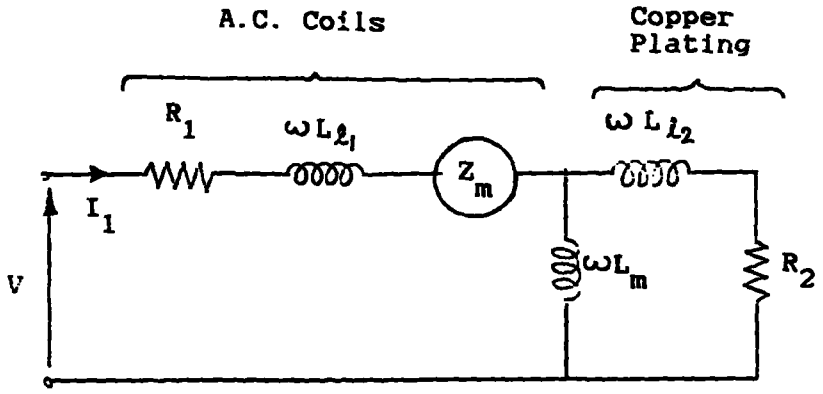


Fig. 4a Moving Coil Shaker A.C. Equivalent Circuit

Like a d.c. machine, the electrical to mechanical energy conversion process takes place at the motional e.m.f. generator indicated above. The other parts of the equivalent circuit can be regarded as being essentially parasitic components. The product of the instantaneous motional e.m.f. and the armature current, (i.e. current flowing in the a.c. coil), is equal to the instantaneous output mechanical power. With a loss-free inertial load, (assumed throughout this discussion), the mean mechanical power oscillates about zero. Under sinusoidal conditions, the thrust $F = k_v.I_1$ is in phase

with the current. Except at frequencies near or below the spring resonance where spring forces are important, $F = m\ddot{x}$ so that $\ddot{x}$ is also in phase with the current. The velocity $\dot{x} = \int \ddot{x}.dt$ hence lags the acceleration, the thrust and the current by 90°. Since the motional e.m.f., $E_{em} = k_v\dot{x}$, is in phase with the velocity, the e.m.f. lags the current by 90°. Since $E_{em} \propto \dot{x} \propto \ddot{x} \propto F \propto I_1$, the ratio of E_{em}/I_1 is fixed at a given frequency as pointed out in chapter 3 and can be thought of as an impedance - the motional impedance Z_{em}. Since E_{em} lags I_1, the impedance is capacitive. At frequencies below the spring resonance where spring forces are dominant and inertial forces small, the impedance is inductive, (since then $F = k_s . x$ rather than $m\ddot{x}$).

4.2. Typical Current, Voltage and KVA Variation With Frequency

Figure 4b shows the supply current, voltage and kVA predictions for the single-ended moving coil shaker, the VP700, together with the corresponding peak acceleration and velocity data for the table. This shaker makes use of the standard double-layer a.c. coil construction and is driven here by a 24 kVA amplifier. The predictions assume a suspension stiffness of 930 kN/m and a total moving mass of 35 kg. Table 4a below summarises the essential data items relating to this shaker.

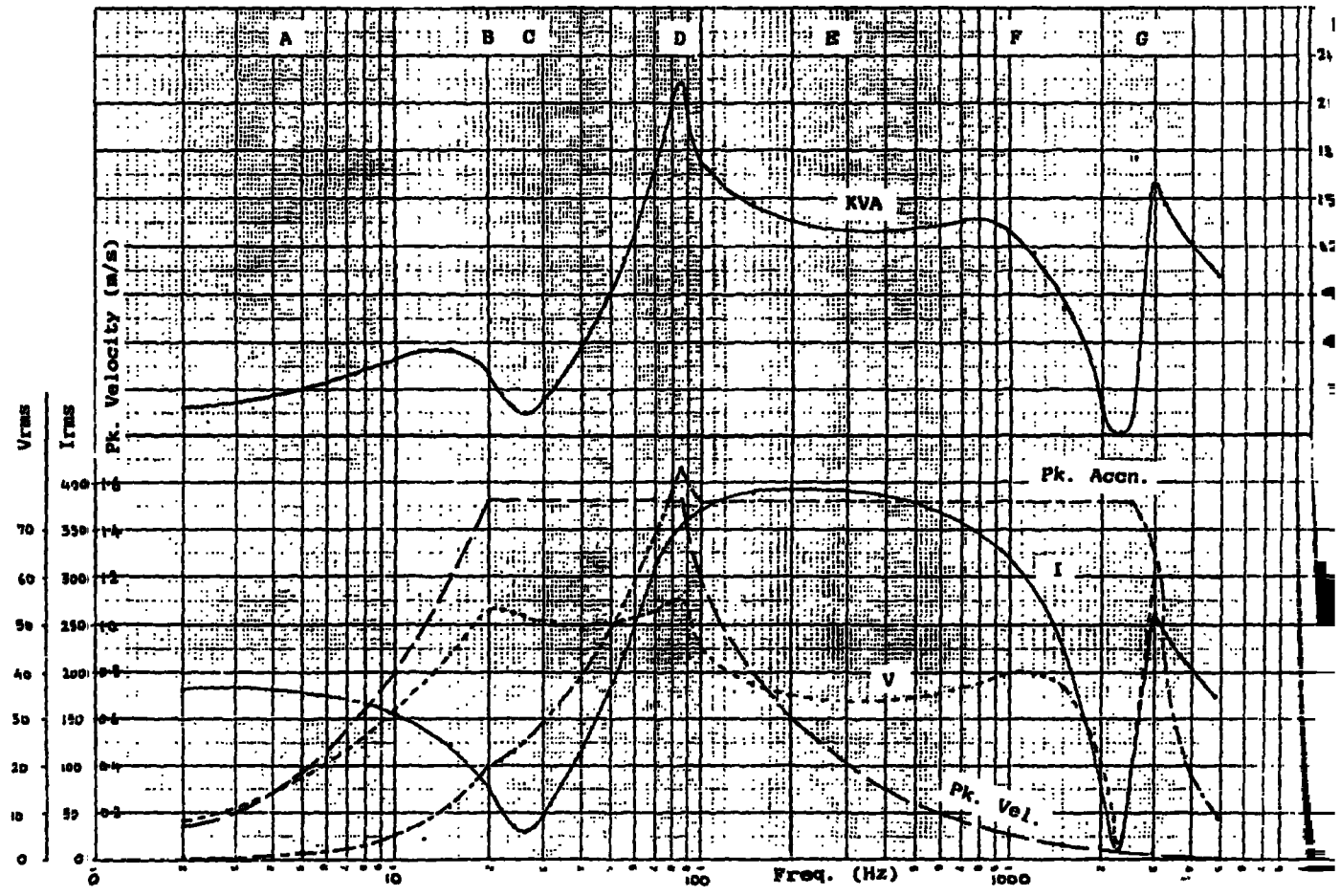


Fig. 4b Current, Voltage and kVA Variation with Frequency

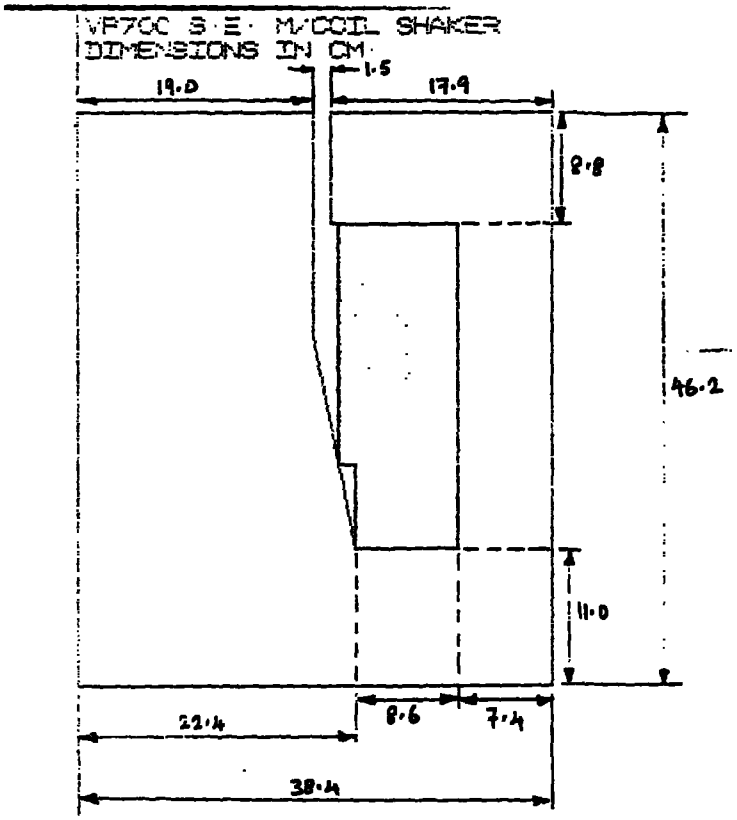


Fig. 4c VP700 Single-Ended Shaker - Essential Dimensions

Coil height	h'''	= 98 mm
Conductor radial thickness	t	= 3.55 mm
Conductor axial thickness	h_{cu}	= 7.10 mm
Conductor cross sectional area	a_c	= 25.2 mm²
Total number of a.c. coil turns	N_T	= 25.5
Coil former thickness	t_m	= 1.87 mm
Armature mass	M_1	= 8.5 kg
Table mass	M_2	= 26.5 kg
Armature/Table stiffness	k_{s1}	= 1.3 x 10⁹ N/m
Suspension stiffness	k_{s2}	= 9.34 x 10⁵ N/m
Damping coefficient	D_2	= 1275 Ns/m

Table 4a VP700 Single-Ended Shaker - Essential Data

The required response specifications are:

Peak to peak displacement = 2.54 cm (1 to 19 Hz)

Peak velocity = 1.52 m/s (20 Hz to 85 Hz)

Peak acceleration = 76g (85 Hz upwards)

In order that the 24 kVA amplifier limit was not exceeded, the shaker's design performance was finally set at somewhat lower levels in respect of maximum velocity and high frequency acceleration roll-off.

The kVA characteristic has the double maximum shape typical of moving coil shakers. The shapes and approximate key values of the kVA, input current and input voltage characteristics can all be explained using the shaker's basic relations and equivalent circuit. The derived relations can be of considerable help in establishing 'best feasible performance levels' and in clarifying design trade-offs when fixing shaker and amplifier specifications. Except for the motional impedance, relations for the equivalent circuit parameters are not discussed again.

The motional impedance is derived from the equation of motion for the table mass :

$$m.\ddot{x} = F - (k_{s2}.x)$$

Putting,

$$x = X.e^{j\omega t} \quad and \quad F = F.e^{j\omega t},$$

$$-m.X\omega^2 = F - (k_{s2}.X)$$

Hence,

$$X = \frac{-F}{m\omega^2 - k_{s2}}$$

Since,

$$\dot{X} = j.\omega.x \; ; \; E_m = k_v.\dot{X} \text{ and } F = k_v.I_1$$

Hence,

$$Z = E_m / I_1 = \frac{-j.\omega(k_v)^2}{m\omega^2 - k_{s2}}$$

where,

$\omega = 2\pi f$

k_{s2} = suspension stiffness

m = total moving mass

k_v = ratio of thrust to a.c. current = ratio of motional e.m.f. to coil velocity

i.e.

$$k_v = |E/\dot{x}| \quad \text{and} \quad k_v = |F/I_1|$$

The symbols x, $\dot{x}$, $\ddot{x}$, V, I and F all refer to r.m.s. values. Hence,

$$\text{peak to peak displacement} = \hat{\hat{x}} = 2\sqrt{2}\,x$$
$$\text{peak velocity} = \hat{\dot{x}} = \sqrt{2}\,.\,\dot{x}$$
$$\text{peak acceleration in 'g'} = (\sqrt{2}\,\ddot{x}) / 9.81$$
$$\text{peak thrust} = \hat{F} = \sqrt{2}\,F$$

4.3. Explanation of Response Characteristics

Considerable parts of the current and voltage characteristics can be explained quite simply. Except at low frequencies where suspension forces are important, the required input current is simply that needed to generate the $m\ddot{x}$ accelerating thrust on the total moving mass. Since thrust is given by : $F = k_m I_1$, the shape of the current versus frequency characteristic simply follows the acceleration characteristic. This is very apparent in Figure 4b. (Note that internal table resonance phenomena have been allowed for in the high frequency predictions here).

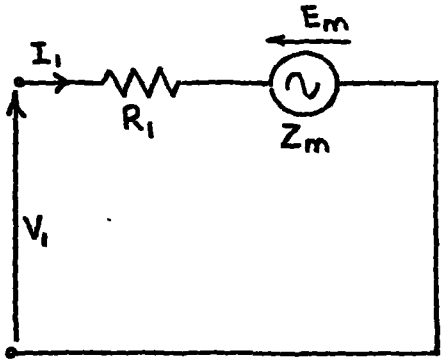
Similarly, since the motional e.m.f. is directly proportional to the coil velocity, (i.e. $E_m = k_v.\dot{x}$), and except at frequencies beyond about 200 Hz or so, the dominant voltage in the equivalent circuit is the motional e.m.f., the shape of the supply voltage characteristic will simply follow the velocity characteristic. As the frequency increases through 150 to 800 Hz and beyond, the motional e.m.f.'s dominance fades due to the continual decrease in velocity, ($\dot{x} = \ddot{x}/\omega$), at constant acceleration, and to the ever increasing total leakage reactance and resistance drops : $I_1.(L_{11} + L_{12})$ and $I_1.(R_1 + R_2)$. These drops finally become so important due to the ω term in the reactance, to the maintenance of I_1 at the maximum value in order to keep acceleration at the maximum value, and possibly to the influence of skin effect in increasing resistance values, that they reach maximum supply voltage levels. From then on, the amplifier voltage is unable to maintain input current and, assuming table resonances are absent, maximum accelerations will gradually reduce. In reality table resonances are present at high frequencies and the control system makes use of these resonance peaks to maintain maximum acceleration.

Reference should be made to Figure 4b for the following sections. The frequency response characteristics have been divided into several regions of interest and each region will now be dealt with separately.

4.3.1. Very Low Frequency (Region A - 0 to 10 Hz)

At these frequencies, the inductances have a negligible effect and the $m\ddot{x}$ inertial

thrust requirement is negligible compared to the maximum suspension force, $k_{sz}x$. The equivalent circuit becomes :



Since $F = k_{sz}\,x$ and $F = k_v I_1$, $I_1 = (k_{sz}/k_v)\,x$, and is constant for a given maximum displacement. The supply voltage is :

$$V_1 = I_1 \cdot \sqrt{R_1^2 + Z_m^2}$$
$$= (k_{sz}/k_v).x.\sqrt{R_1^2 + (\omega k_v^2/k_{sz})^2}$$

Except at 1 or 2 Hz, $R_1 < Z_m$ and hence,

$V_1 = jk_v.\omega x$ or $k_v \dot{x}$ and hence builds linearly with ω at constant x.

The input kVA are negligible in view of the low current requirement, (maximum spring thrust $k_{sz}\hat{x}$ << maximum shaker thrust $m\hat{\ddot{x}}$), and the relatively low velocity. Note that I_1 lags V_1, (at approximately 90°), in this frequency range.

4.3.2. Constant Displacement - Constant Velocity Crossover Frequency (Point B - 20 Hz)

Even without the resonating effect of the suspension, the motional impedance Z_m is still relatively high at this frequency because of the term in the denominator of the Z_m relation, and because of the still low value of ω. In typical designs, Z_m will completely dominate the equivalent circuit :

$$Z_m >> | R_1 + j\omega L_{11} |$$ and,

$$Z_m >> j\omega L_m$$ in parallel with $(R_2 + j\omega L_{12})$

The equivalent circuit can hence still be approximated to just the motional

impedance. The required supply voltage, (usually at or near the amplifier's maximum, since x, the displacement, is maximum), will be :

$$V_1 = k_v.\dot{x}$$

where $\dot{x}$ is the r.m.s. specified velocity, and the supply current will be :

$$I_1 = V_1/Z_m$$

So long as the ω_{mech} is not within 7 Hz or so of the crossover frequency,

$$Z_m = -j.k_v^2/\omega m$$

Hence,

$$I_1 = j.k_v.\dot{x}.\omega.m / k_v^2$$

Thus,

$$I_1 = j.m.\omega.\dot{x} / k_v$$

Note that at ω_{mech} the phase of the current changes from approximately 90° lagging, (inductive), to approximately 90° leading, (capacitive), and is still leading at the x / $\dot{x}$ crossover frequency. The input VA is :

$$I_1.V_1 = m.\omega.\dot{x}^2$$

4.3.3. Mechanical Resonance (Point C - 26 Hz)

When the moving mass resonates with the suspension, very little thrust is needed.

$$Z_m \longrightarrow \infty \qquad \text{and} \quad I_1 \longrightarrow 0$$

The resonant frequency is :

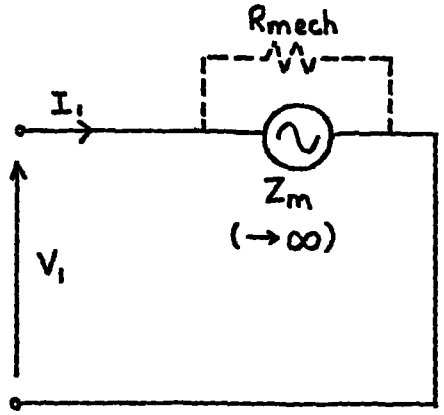
$$\omega_{mech} = \sqrt{k_{s2}/m}$$

Substituting k_{s2} and m values for the VP700 design gives us an ω_{mech} of 26 Hz.

Although the current will be very small, a voltage is needed to overcome the velocity-induced motional e.m.f.. At this frequency :

$$V_1 = E_m = k_v \cdot \omega_{mech} \cdot X$$

and the equivalent circuit can be approximated to :



In practice, mechanical windage and suspension hysteresis losses will occur, their effects being virtually equivalent to the addition of a high-value resistor R_{mech} as shown. Since I_1 is very small, the input kVA is virtually zero.

4.3.4. Constant Velocity Frequency Range (Points C to D - 26 to 85 Hz)

Because the thrust requirement grows with frequency, ($F = m\ddot{x} = m\omega\dot{x}$), the input supply current must also steadily increase if velocity is to be maintained. The supply voltage must stay at or near its maximum value in order to maintain E_m, ($\dot{x} = E_m / k_v$). The velocity in practice tends to increase a little with frequency if V_1 is maintained at maximum value. This is caused by the improving balance between the decreasing capacitive, but still large Z_m, and the increasing, but still small combined inductive impedance of L_{11} and L_{12}. A very slight cancellation can sometimes occur between the oppositely-phased voltage drops, ($V_1 = I_1.(Z_m - X_L)$), enabling the motional voltage E_m to increase to slightly above the supply voltage V_1. This in turn allows a slightly raised velocity, perhaps even beyond the 'theoretical' maximum V_1 / k_v. However, in the case of the VP700 machine here, an $\hat{\dot{x}}$ of 1.52 m/s is predicted at 85 Hz as opposed to the 1.85 m/s calculated from $\sqrt{2}\ V_{1max} / k_v = \sqrt{2} \cdot 60 / 45.962$, a difference of some 18 %.

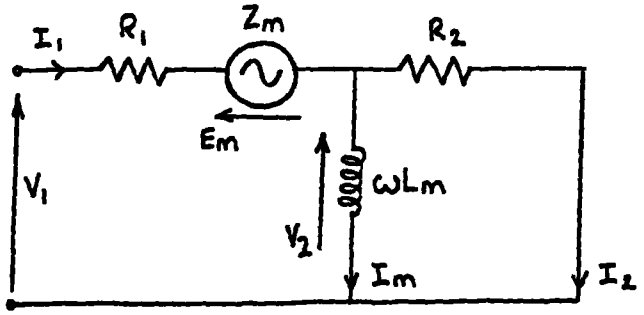
Also within this frequency range, the reactance of the ωL_m branch increases to become comparable with Z_m, so that the shunting effect of the ($R_2 + j.\omega.L_{12}$) branch becomes vital in avoiding drastic increases in supply voltage requirement. In physical terms, this is tantamount to saying that the secondary, (eddy), currents in the plating become vital in reducing the a.c. flux created by the a.c. coil

currents, that would otherwise be giving rise to increasingly troublesome inductive e.m.f.s, (e.m.f. per flux and hence per current increases with frequency : $E \propto \omega \phi_m$).

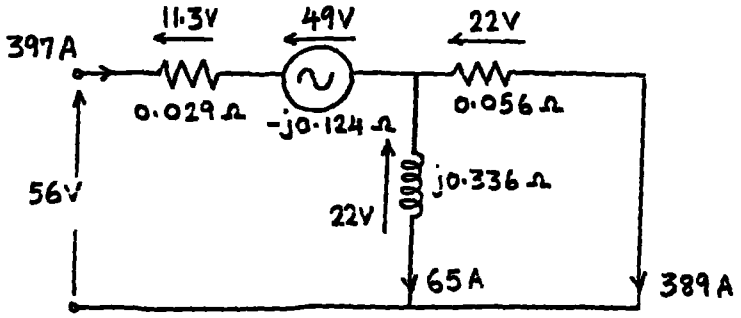
4.3.5. Constant Velocity - Constant Acceleration Crossover Frequency (Point D - 85 Hz)

At this frequency, the specification requires the shaker to be producing both its maximum velocity and its maximum thrust. These requirements lead directly to a need for both maximum voltage, ($V_1 = k_v \dot{x}$), and maximum current, ($I_1 = F/k_v$), and the input kVA is hence bound to be at or very near a maximum. The $V_1 = k_v \dot{x}$ approximation is undesirable when estimating V_1 at this critical frequency, so conditions are now looked at in somewhat more detail.

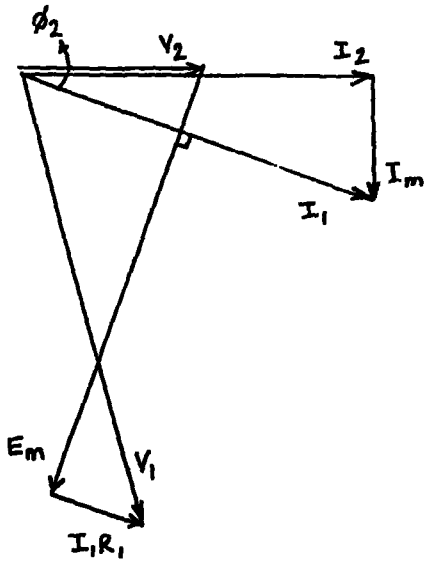
Leakage reactances are still negligible, so the equivalent circuit is, to a good approximation :



Numerical values for the VP700 machine at this frequency and at full thrust are :



The corresponding phasor diagram is :



The input current I_1 is given by :

$$I_1 = F / k_v$$
$$= m.\ddot{x} / k_v$$

This simple expression enables estimates of I_1 and/or k_v to be made for specified figures of m and $\ddot{x}$.

The input voltage expression is more complicated since, (except for those due to leakage reactances), there are no voltage drops of negligible size in the equivalent circuit at this frequency. Resolving voltages in phase and in quadrature with V on the phasor diagram gives :

$$V_1 = \sqrt{(V_2 - E_m \sin \phi_2 + I_1R_1 \cos \phi_2)^2 + (E_m \cos \phi_2 + I_1R_1 \sin \phi_2)^2}$$

where ϕ_2 is the phase angle of the parallel L_m, R_2 branches, given by,

$$\phi_2 = \tan^{-1} (R_2 / \omega L_m)$$

Substituting :

$$V_2 = I_1.(\cos \phi_2).R_2$$
$$= (m.\ddot{x} / k_v).(\cos \phi_2).R_2$$

$$E_m = k_v.\dot{x}$$
$$= k_v.\ddot{x} / \omega$$

$$I_1 = m.\ddot{x} / k_v$$

gives :

$$V_1 = \frac{k_v.\ddot{x}}{\omega} \sqrt{(\sin \phi_2 - \frac{m\omega}{k_v^2}(R_1 + R_2) \cos \phi_2 + (\cos \phi_2 + \frac{m\omega}{k_v^2} R_1 \sin \phi_2)^2}$$

This expression, valid at all frequencies up to those where leakage drops become significant, enables V_1 to be estimated for a specified $\ddot{x}$ and m when the shaker's design k_v, R_1, R_2 and L_m are known. The only approximation possible at the $\dot{x}$ to $\ddot{x}$ crossover frequency involves the last term,

$$(m\omega / k_v^2).R_1.\sin \phi_2$$

corresponding to,

$$I_1 R_1.\sin \phi_2$$

This will be negligible so long as ϕ_2 is small, (i.e. $R_2 < \omega L_m$, i.e. most of the current is flowing in the R_2, plating branch, as opposed to through the L_m branch).

The V_1 expression can be written as :

$$V_1 = (k_v.\ddot{x} / \omega)\, k_c$$
$$= (k_v.\dot{x}).k_c$$
$$= E_m.k_c$$

where k_c, assuming the above approximation holds, is :

$$k_c = \sqrt{(\sin \phi_2 - (m\omega / k_v^2).(R_1 + R_2).\cos \phi_2)^2 + \cos^2 \phi_2}$$

k_c is the factor by which V_1 differs from the motional e.m.f., E_m. The minus sign in the k_c expression confirms that k_c can be less than unity. How much less k_c can be made by skilful design has not been properly investigated. At first sight the room for manoeuvre seems rather limited.

4.3.6. Electromechanical Resonances (Region E)

With moving coil shakers electromechanical resonances occur between the capacitive Z_m and (a) the magnetising inductance, L_m and (b) the total leakage reactance, $\omega(L_{11} + L_{12})$. The frequencies at which these occur are given by :

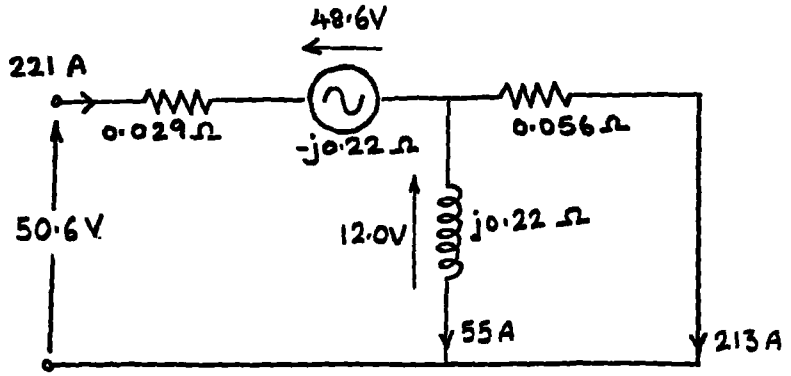
$$Z_m = k_v^2 / \omega m = \omega L_m \quad , \text{ giving,}$$
$$\omega_{em} = k_v / \sqrt{m.L_m}$$

and,

$$Z_m = k_v^2 / \omega m = \omega(L_{11} + L_{12}) \quad , \text{ giving,}$$
$$\omega_{emhf} = k_v / \sqrt{m.(L_{11} + L_{12})}$$

These relations give the frequencies at which the capacitive reactance of the motional impedance becomes equal and opposite to the inductive reactance of (a) the magnetising inductance and (b) the total leakage inductance. However, the location of the Z_m component in the equivalent circuit reduces the benefit to the shaker's terminal properties. The reasons for this can be seen by examining conditions in the equivalent circuit at ω_{em} and ω_{emhf}. For the VP700 shaker, $\omega_{em}/2\pi$ is 55 Hz and $\omega_{emhf}/2\pi$ is 333 Hz.

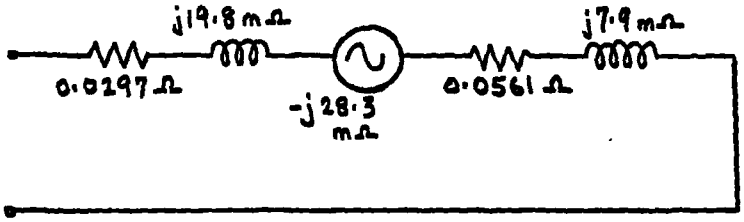
At ω_{em} (55 Hz) :

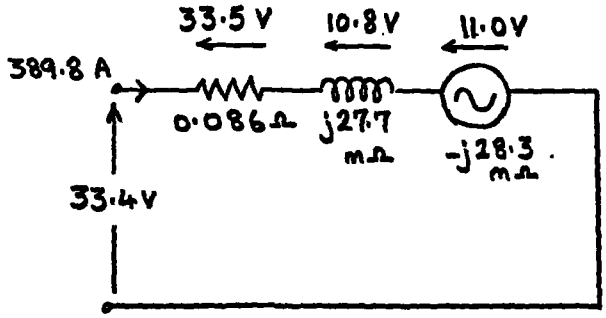


The ωL_m can be seen to be heavily shunted by the plating resistance so that the voltage, $I_m \omega L_m$ across L_m is very much less than $I_1 Z_m = E_m$ in spite of the equality between Z_m and ωL_m. There is hence relatively little cancellation of E_m by the magnetising branch voltage. The phasor diagram also shows that in any case E_m and $I_m \omega L_m$ are nearer 90° out of phase with each other than 180°. And in any case, here this electromechanical resonance would be swamped by the increasing kVA demand as the constant velocity-constant acceleration point is approached.

Similar remarks will apply to any moving coil shaker whose ω_{em} lies beyond the frequency at which the plating current becomes a substantial fraction of the primary current (ampere-turns). This would always seem to be the case at ω_{em}, except possibly in small shakers where ω_{em} is reduced by the lower k_v, (though L_{em} is also lower in small shakers), and where size effect, (or even an absence of plating), gives a higher R_2 and hence less shunting of L_{em}.

At ω_{emhf} (333 Hz) :





The ωL_{em} branch at ω_{emhf} is of high impedance compared with the plating branch and can hence be omitted, (approximates to an open circuit). It can be seen that the series resonance reduces the voltage from :

$$V_1 = I_1 . \sqrt{(R_1 + R_2)^2 + Z_m^2}$$

(V_1 is 35.3V for the VP700 shaker at maximum current), to :

$$V_1 = I_1 . (R_1 + R_2)$$

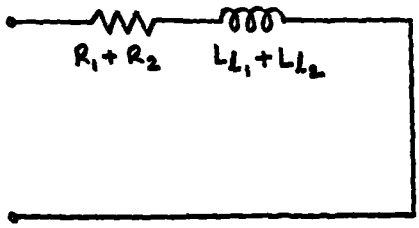
(which gives 33.4V for the VP700).

The reduction tends to be only modest because the Q factor is rather low due to the significant value of $(R_1 + R_2)$ and the low values of Z_{em} and $\omega(L_{11} + L_{12})$ at ω_{emhf}. It may be noted that the main reason for the fall in V_1 between points D and E in Figure 4b is not this high frequency resonance, but the reduction in motional

e.m.f. $k_v.\dot{x}$ due in turn to the reducing velocity $\ddot{x}/\omega$ at constant acceleration as ω increases.

4.3.7. Maximum Shaker Impedance Frequency Point (Point F - 1000 Hz)

As the frequency increases beyond ω_{emf}, the motional e.m.f. becomes less and less significant alongside the resistance and leakage reactance drops. The leakage reactance drops, $I_1.\omega.(L_{l1} + L_{l2})$, increase due to the constant current, $\ddot{x}/k_v$ and the increasing ω and this leads to an increasing voltage requirement. The equivalent circuit approximates to :



When

$$\sqrt{(R_1 + R_2)^2 + \omega^2(L_{l1} + L_{l2})^2}$$

attains V_{max}/I_{max}, the shaker's input impedance exactly matches the amplifier's capability. Since both V_1 and I_1 are hence at or close to maximum values at this frequency, a kVA maximum occurs. The frequency is given by :

$$f_m = \frac{1}{2\pi} \cdot \frac{\sqrt{(V_{max}/I_{max})^2 - (R_1 + R_2)^2}}{L_{l1} + L_{l2}}$$

With a 60V, 400A amplifier, V_{max}/I_{max} = 0.15 ohms and f_m for the VP700 shaker, based on the d.c. values of R and L_1, is estimated to be approximately 1000 Hz. (Skin effect increases in R_1 and decreases in L_{l1} are beginning to occur beyond 1 kHz but only change this frequency estimate by 3 Hz or so). Note that in practice table resonances are being relied on to maintain table acceleration beyond 1000 Hz in the VP700 machine. The maximum impedance point in practice has been shifted to approximately 2200 Hz due to the resonance between the table and armature.

4.3.8. High Frequency (Region G - 2000 Hz and above)

Beyond f_m the amplifier cannot maintain I_{max} in the face of the shaker's increasing impedance, and predicted electrical thrust gradually decreases. The equivalent circuit can still be approximated to the one shown in section 4.3.7., and the maximum current and thrust capability at any frequency in this range are given by :

$$I_1 = V_{1max} / \sqrt{(R_1 + R_2)^2 + \omega^2(L_{11} + L_{12})^2}$$

$$F = k_v . I_1$$

hence,

$$\ddot{x} = \frac{k_v . V_{1max}}{m\sqrt{(R_1 + R_2)^2 + \omega^2(L_{11} + L_{12})^2}}$$

In the VP700 shaker, and probably other designs having a double layer moving coil, (L_{11} + L_{12}) is relatively high due to the significant radial winding thickness, (giving larger leakage flux within the conductors). The highish (L_{11} + L_{12}) leads to the input impedance of the shaker being approximately equal to $\omega(L_{11} + L_{12})$ for all frequencies in this range, in spite of skin effect increases in R. The maximum theoretical acceleration, (table resonance effects neglected), at a frequency $\omega/2\pi$ is thus approximately :

$$\ddot{x} = F/m = \frac{k_v V_{max}}{m\omega(L_{11} + L_{12})}$$

Depending on a shaker's design, skin effect may give rise to a useful reduction in L_{11}, (though present estimates for the VP700 suggest that the reduction for this design is fairly modest : 6.6 μH at 4.9 kHz compared with approximately 10 μH at low frequencies), and to an appreciable increase in R_1, (0.09Ω at 4.9 kHz compared with 0.057Ω at 2kHz and 0.029Ω at low frequencies for the VP700). L_{12} and R_2 are very little affected by skin effect because even at 5 kHz, the plating thicknesses, are less than the copper skin depth at 5 kHz. Figure 4d below indicates the variation of the main equivalent circuit parameters with frequency.

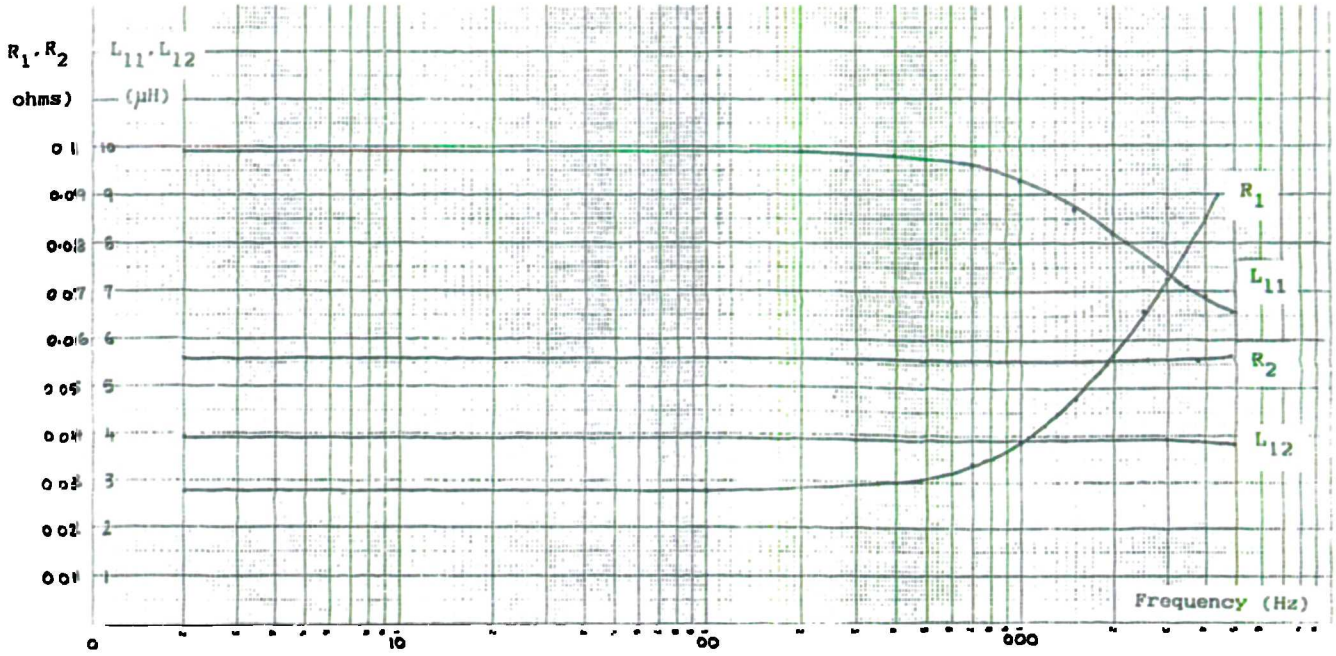


Fig. 4d Variation of Equivalent Circuit Parameters with Skin Effect

4.4. Comparison of Predictions with Test Data

The VP700, (sponsor's designation), single-ended moving coil shaker driven by a 24 kVA amplifier will be used for the comparisons. The performance profile specification is shown graphically below.

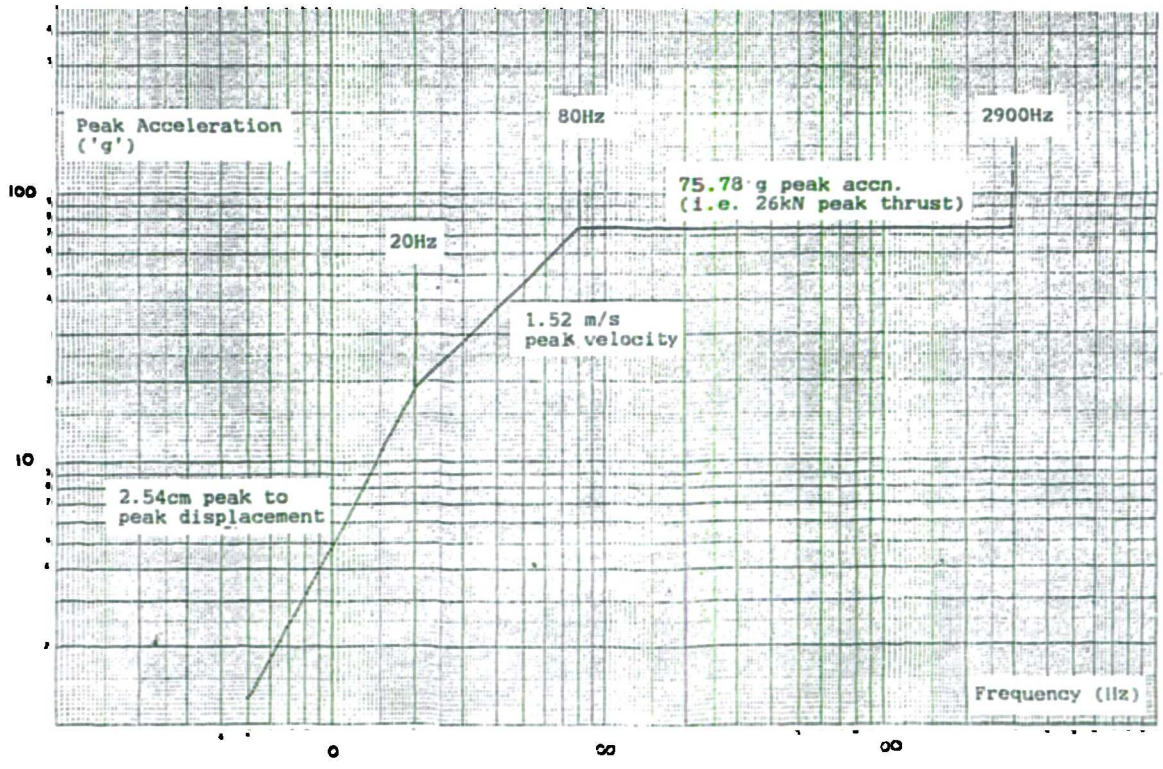


Fig. 4e VP700 Perf rmance Profile

The curr nt versus frequency curve shown below indicates quite a go d tie-up between predicted and test re ults although there appears to be a discrepancy at low frequencies. Although this could stem from the imperfect nature of the prediction model, there are thought to be two possible sources of error associated with the table suspension and the measuring techniques respectively. During low frequency operation, the shaker table suspension system forces are of first order importance due to the high displacements that occur. The discrepancy could therefore be attributed to suspension stiffness changes, (i.e. non- linear suspension). The test curve suggests that this suspension becomes quite stiff at low frequencies thus requiring more input current to produce the required displacement or velocity. The shaker a.c. current measuring system employed by the sponsor during tests incorporated current transformers whose low frequency performance had not been calibrated or checked. Significant errors in low frequency current measurement are hence quite likely to have occured.

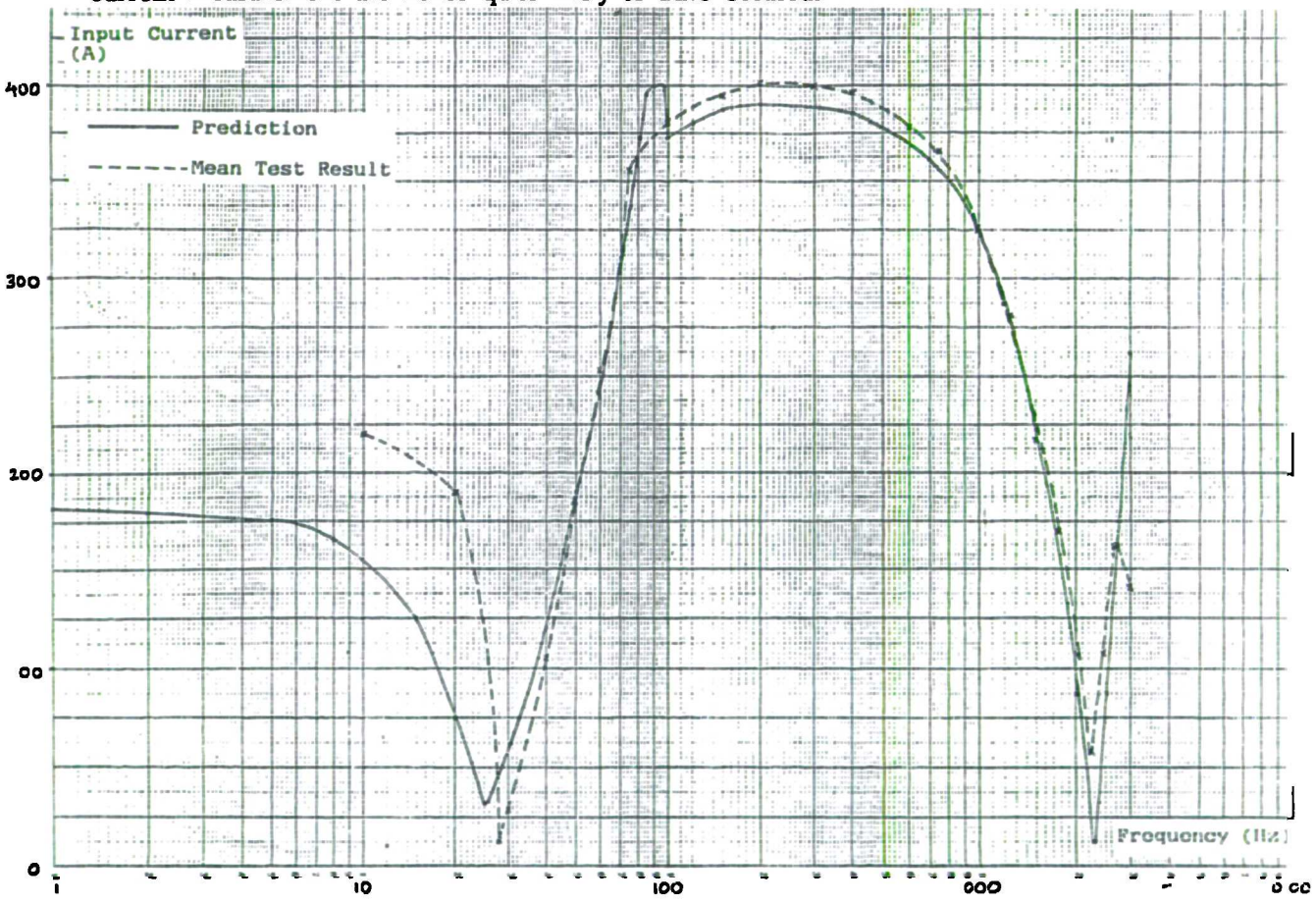


Fig. 4f VP700 - Current v Frequency

The equivalent circuit indicates the respective component values and current flows f r the frequency point in question. Almost all the current at thi point is used to provide the magnetising flux, with very little current flow in the copper plating.

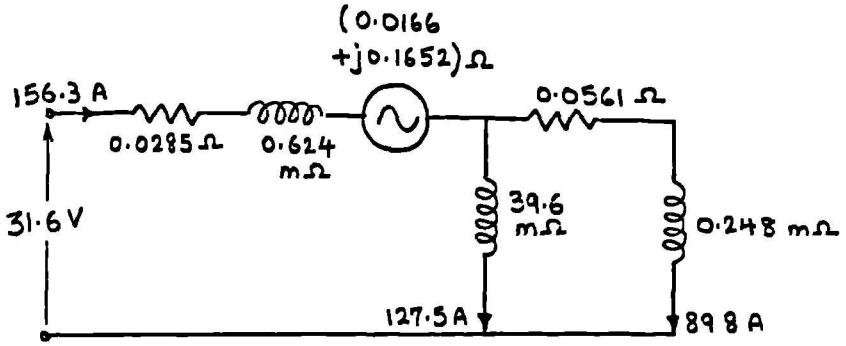


Fig. 4g VP700 - Equivalent Circuit at 10 Hz

Referring to Figs. 4f and 4h, the mechanical resonance point is clearly indicated by the sharp dip in the input current requirement and a slight fall in the voltage curve.

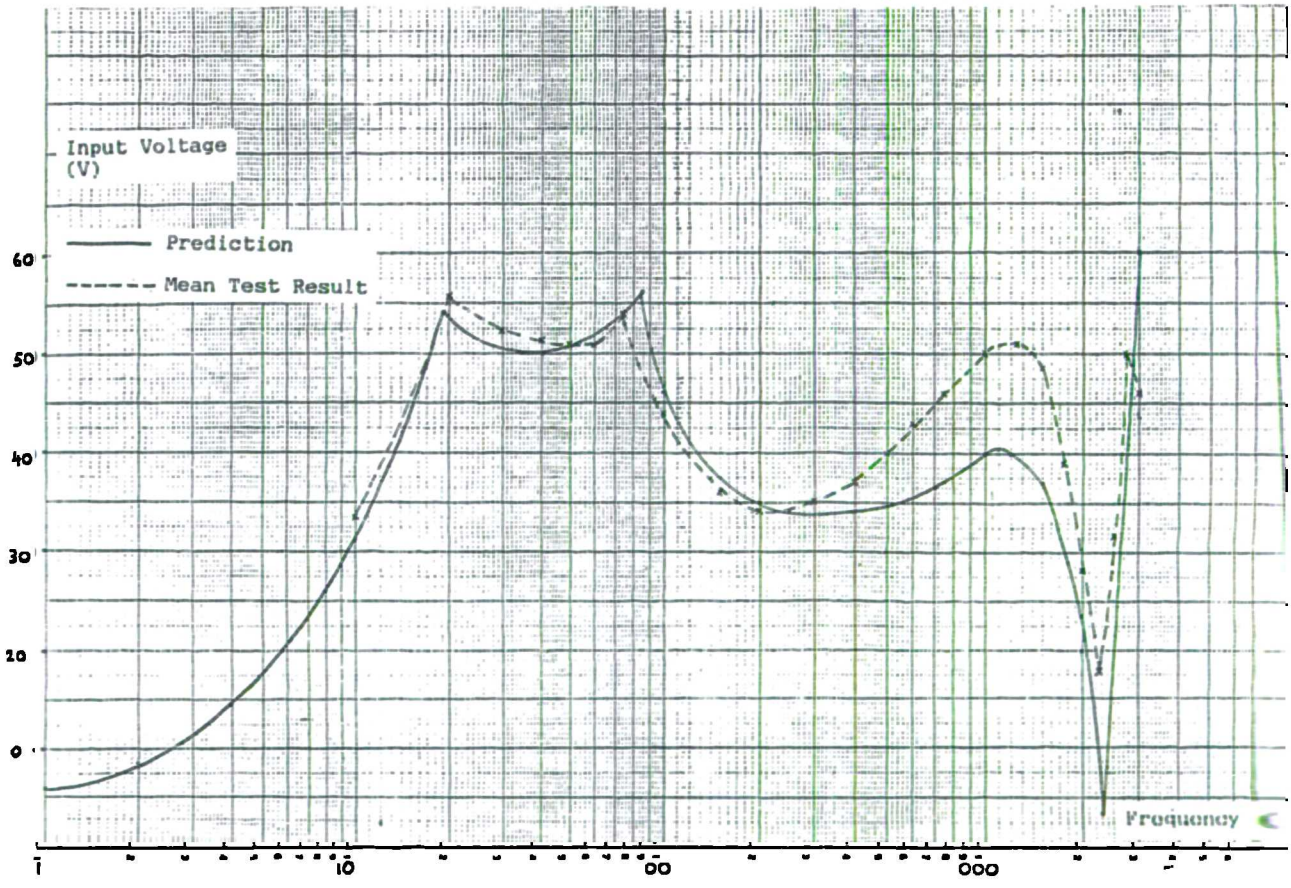


Fig. 4h VP700 - Voltage v Frequency

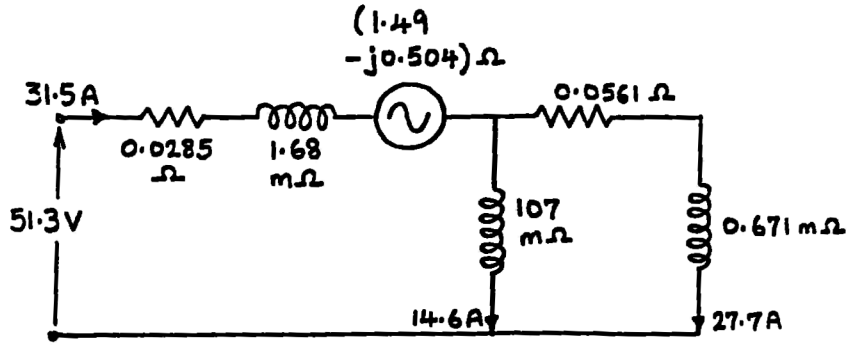


Fig. 4i VP700 - Equivalent Circuit at 26 Hz

The motional impedance becomes capacitive and is quite high at this point due to the large displacement of the moving coil. The copper plating begins to carry more and more current from this frequency point onwards.

As the requirements switch from the velocity-limited phase to the acceleration-limited phase, the model predicts an 'overshoot' in the input current as the amplifier attempts to supply both maximum voltage and current, at the point where both peak velocity and peak acceleration are required.

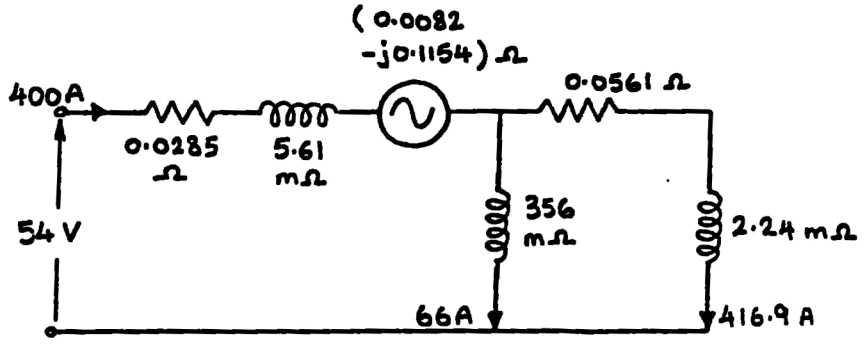


Fig. 4j VP700 - Equivalent Circuit at 85 Hz

At this point the copper plating is already shunting the magnetising branch quite well and thus providing effective shielding of the a.c. flux.

As the frequency increases and the next resonance point is approached, (table/armature resonance), the current demand drops and an increase in the voltage across the shaker terminals occurs. The voltage curves at this point show a discrepancy between test and prediction and this possibly indicates predicted leakage inductance values somewhat

lower than in reality. The impedance curves seem to confirm this effect.

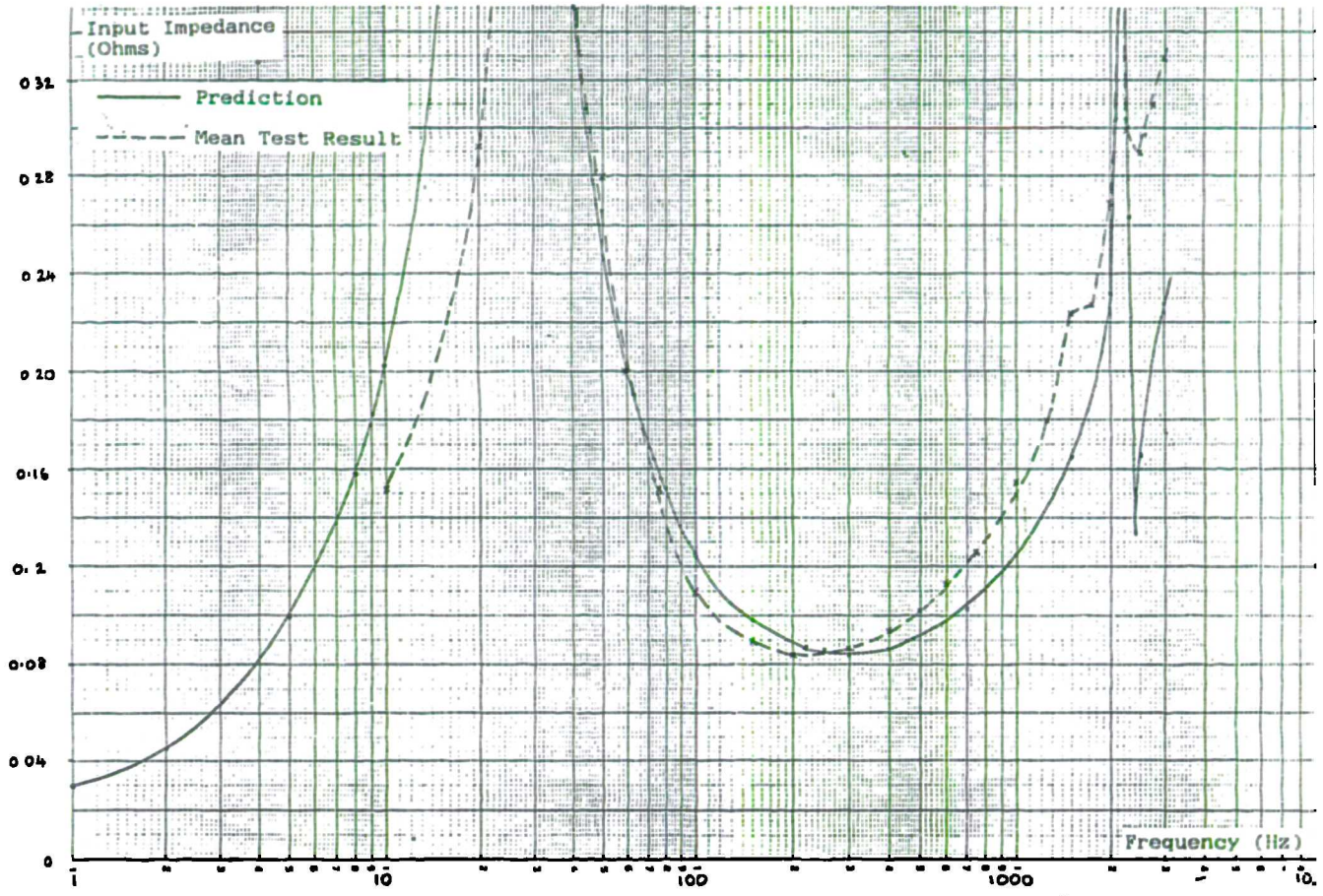


Fig. 4k VP700 - Impedance versus Frequency

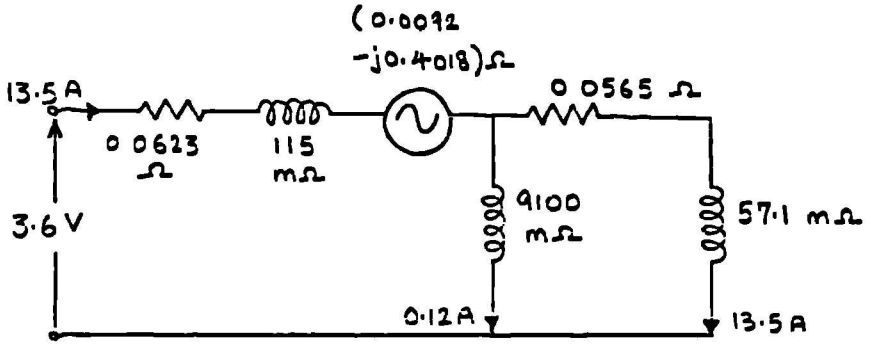


Fig. 4l VP700 - Equivalent Circuit at 2300 Hz

The following set of curves indicates the levels of heating present in the copper plating layers on the magnetic ring as well as on the centre pole. As expected these curves follow the current curves closely and indicate levels of heating which are well within the experience of the sponsors. These heat levels suggest that air-cooling is still feasible. The curves shown are for model predictions only, but since the current versus frequency test and predicted curves show a reasonable tie-up, especially at mid to high frequencies, it would be safe to assume that the predicted heat flux densities are not too far off the mark. Obviously at the lower frequencies, where the current predictions are less accurate, heating levels in the plating may be appreciably higher in practice.

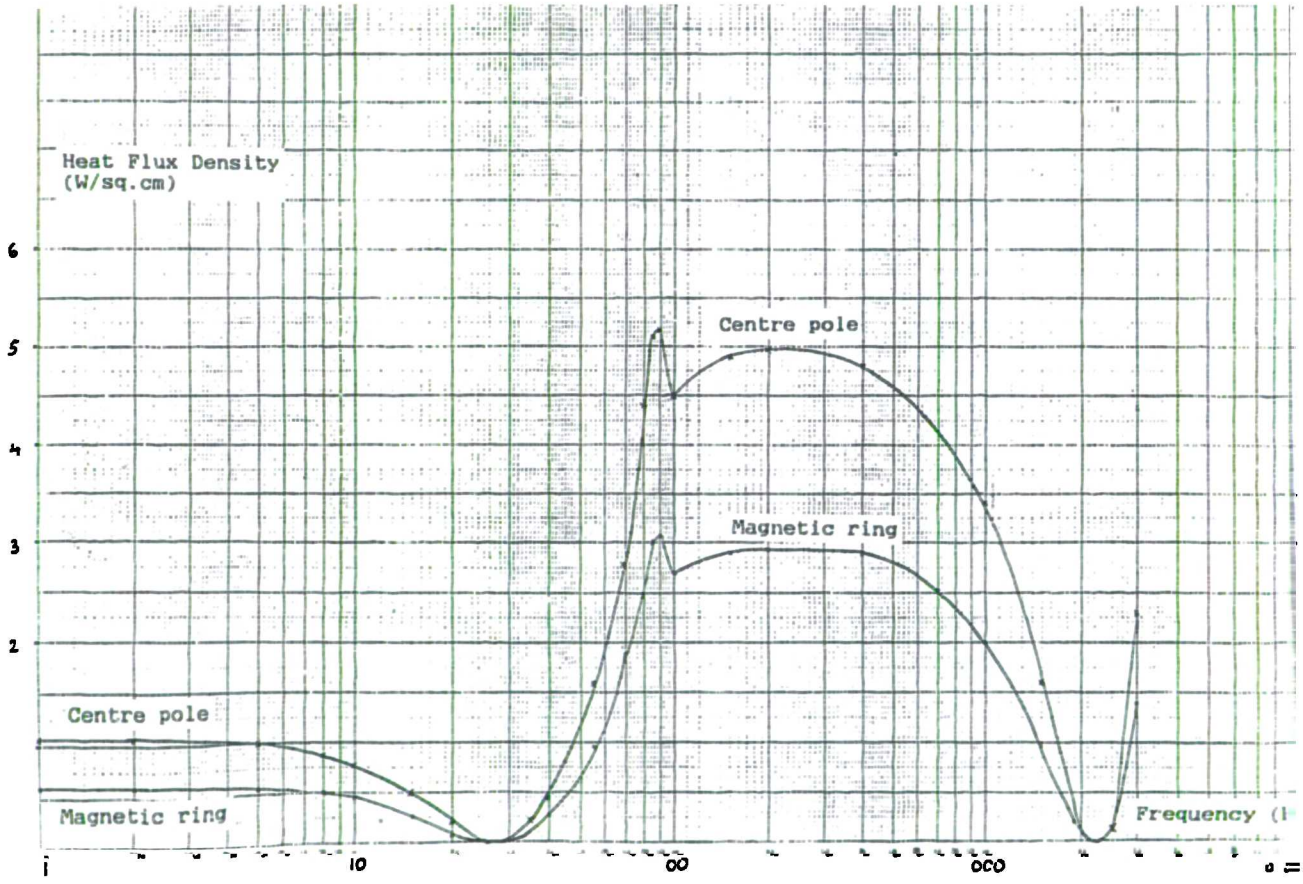


Fig. 4m VP700 - Copper Plating Heating Levels

4.5. Further Comparisons Using the VP85 and VP30 Machines

During the initial phase of the project and also throughout the development of the prediction model, several comparisons were also made using test data obtained from two

other machines, the VP30 and VP85 machines. These are now presented here.

VP85

The performance profile for the VP85 machine as used for the tests is as shown.

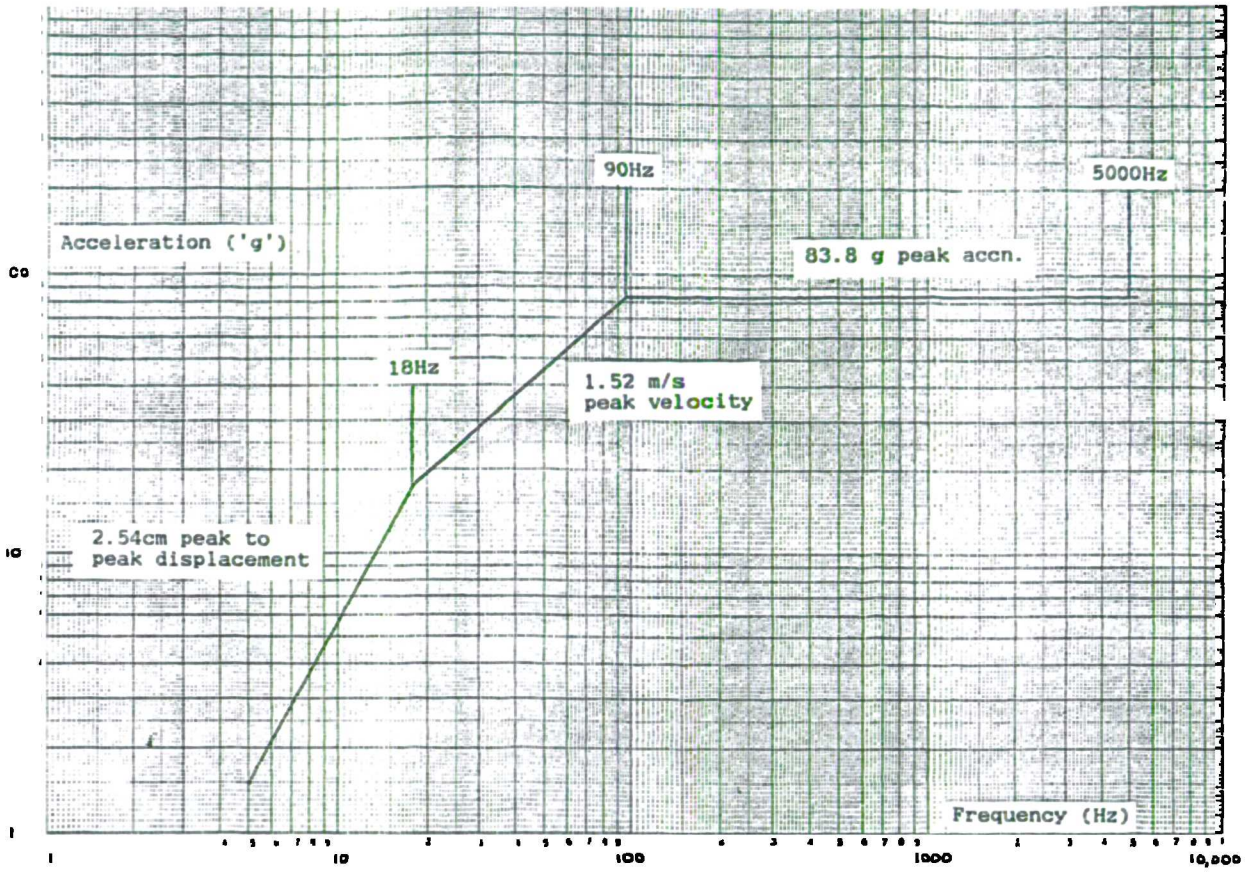


Fig. 4n VP85 - Performance Profile

The shaker is driven by a 6 kVA amplifier and has a total moving mass of approximately 9.2 kg. The a.c. coil has 26.5 turns of 3.15 x 4.5 mm copper and has a resistance of about 0.041 Ω at 100°C. The test was carried out at a slightly reduced output level of 83.8g peak acceleration instead of the usual 96g. The current and voltage curves below are followed by several circuit diagrams indicating the various current flows and parameter values during shaker operation as predicted by the model.

It should be noted that the input currents and voltages shown in the circuit diagrams below for both the VP85 and VP30 shakers do n t always match the values read off from the current and voltage curves. This is due to the fact that the circuit diagrams represent shaker operation with slightly different performance specifications and have been included for purely illustrative purposes.

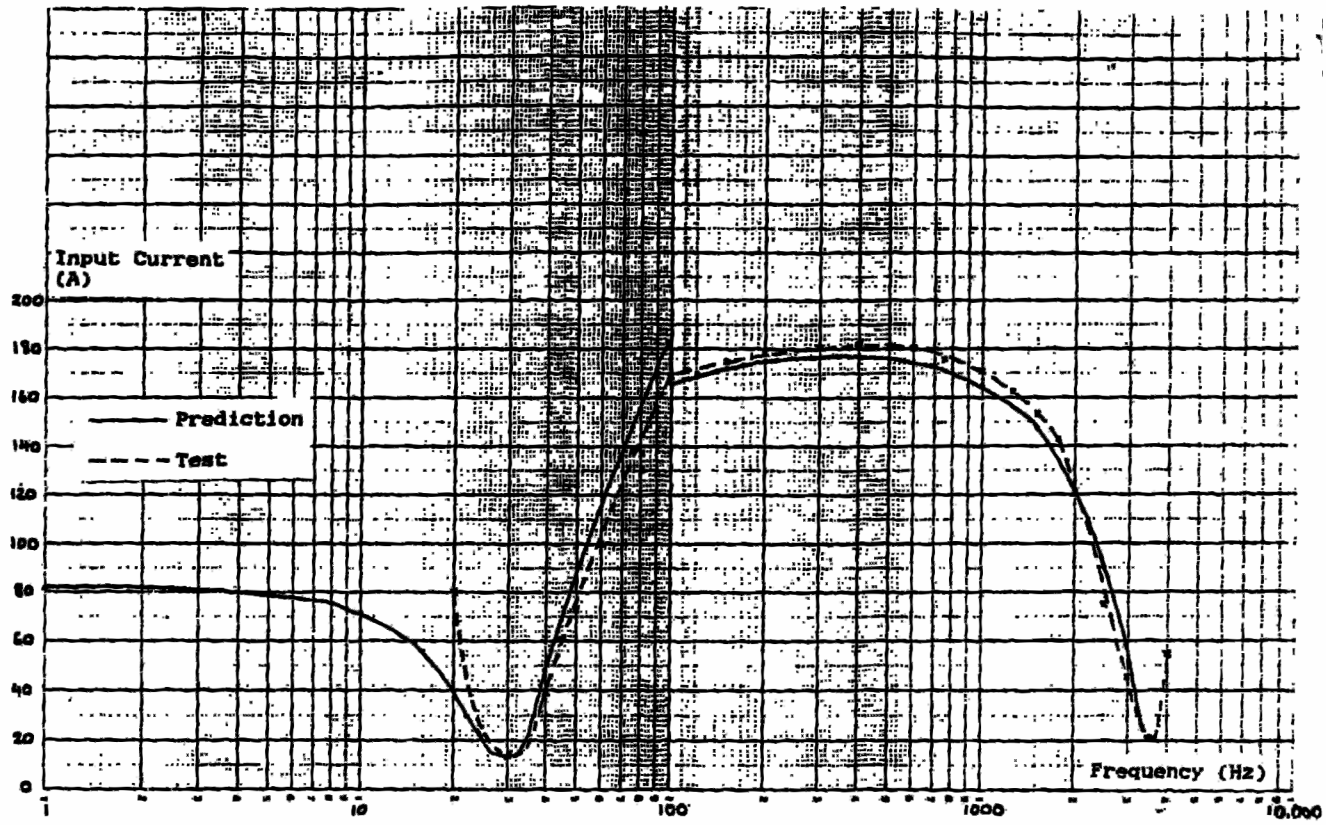


Fig. 4o VP85 - Current v Frequency

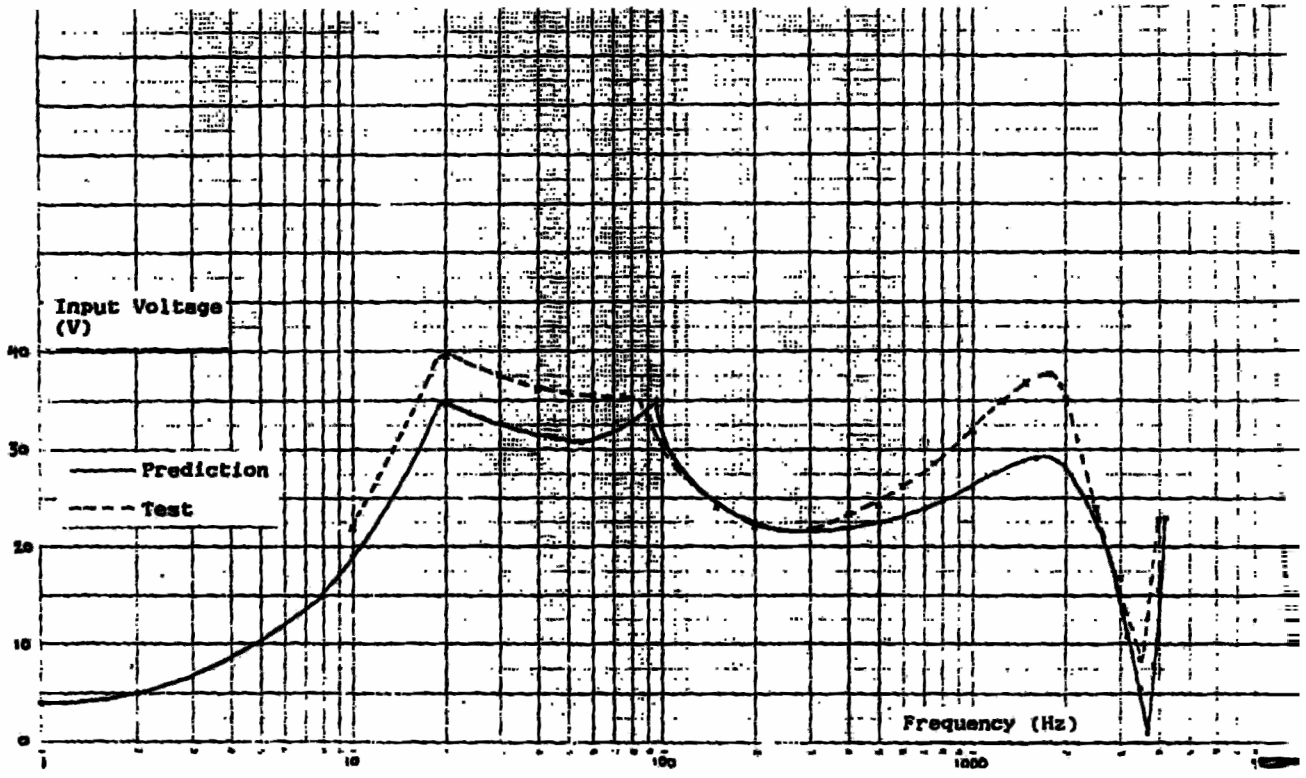


Fig. 4p VP85 - Voltage v Frequency

The current curves indicate a very good tie up between test and predictions with a difference of between 3 and 11 %, (on the optimistic side), over the frequency range shown which is perfectly acceptable for our purposes. The voltage comparison shows a bigger difference of between 8 and 22 % again on the optimistic side but still within acceptable limits for this size of machine.

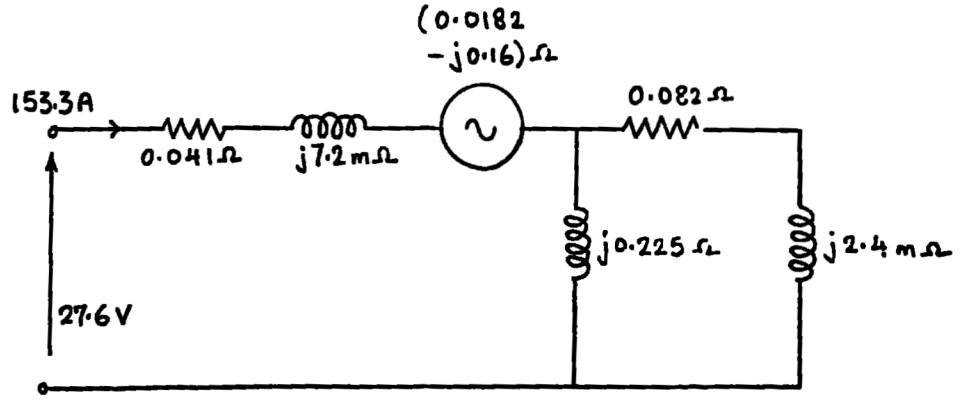


Fig. 4q VP85 - Equivalent Circuit at f = 100 Hz

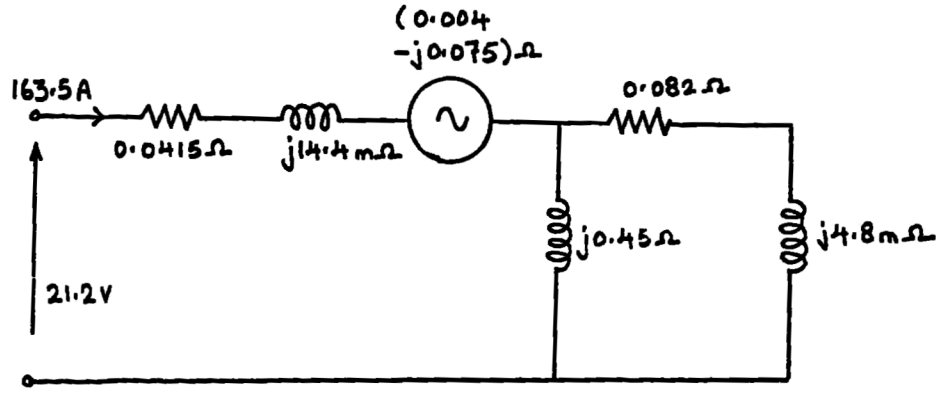


Fig. 4r VP85 - Equivalent Circuit at f = 200 Hz

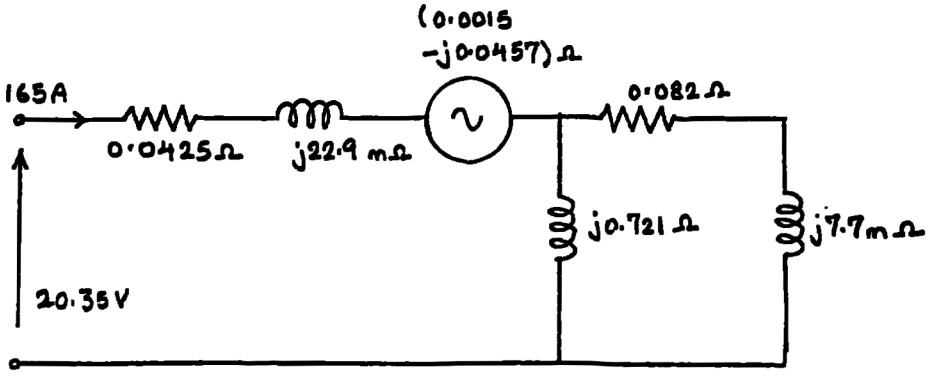


Fig. 4s VP85 - Equivalent Circuit at f = 320 Hz

The dip in the voltage profile at approximately 320 Hz, can be explained by examining the equivalent circuit, where it can be seen that the total inductive leakage reactance is almost equal to the capacitance of Z_m, leading to a fall in overall circuit reactance.

At f = 320 Hz,

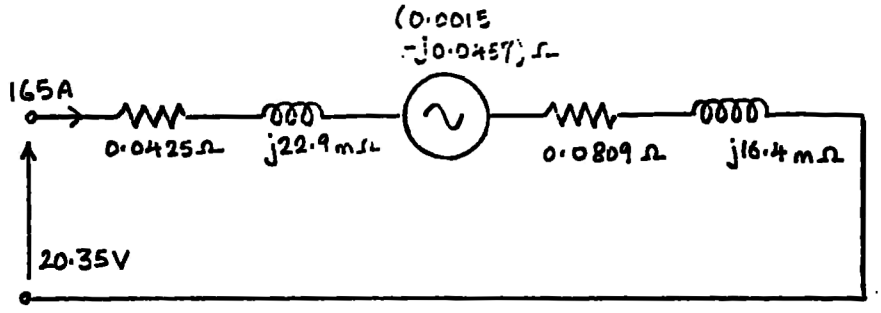
$$(R_2 + j.\omega.L_2) \quad \text{in parallel with} \quad j.\omega.L_m$$

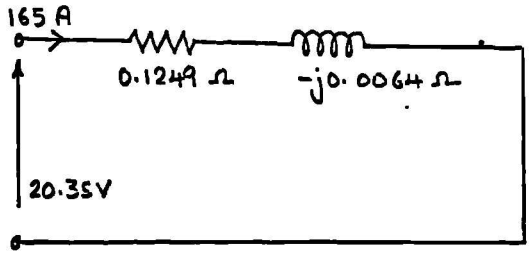
$$= \frac{(0.082 + j0.0077).(j0.721)}{(0.082 + j0.7287)}$$

$$= \frac{0.000455 + j0.00404 + j0.0048 + 0.043}{0.5377}$$

$$= (0.0809 + j0.0164)\ \Omega$$

Therefore, the equivalent circuit becomes :





VP30

The performance profile for the VP30 used in the tests is as follows.

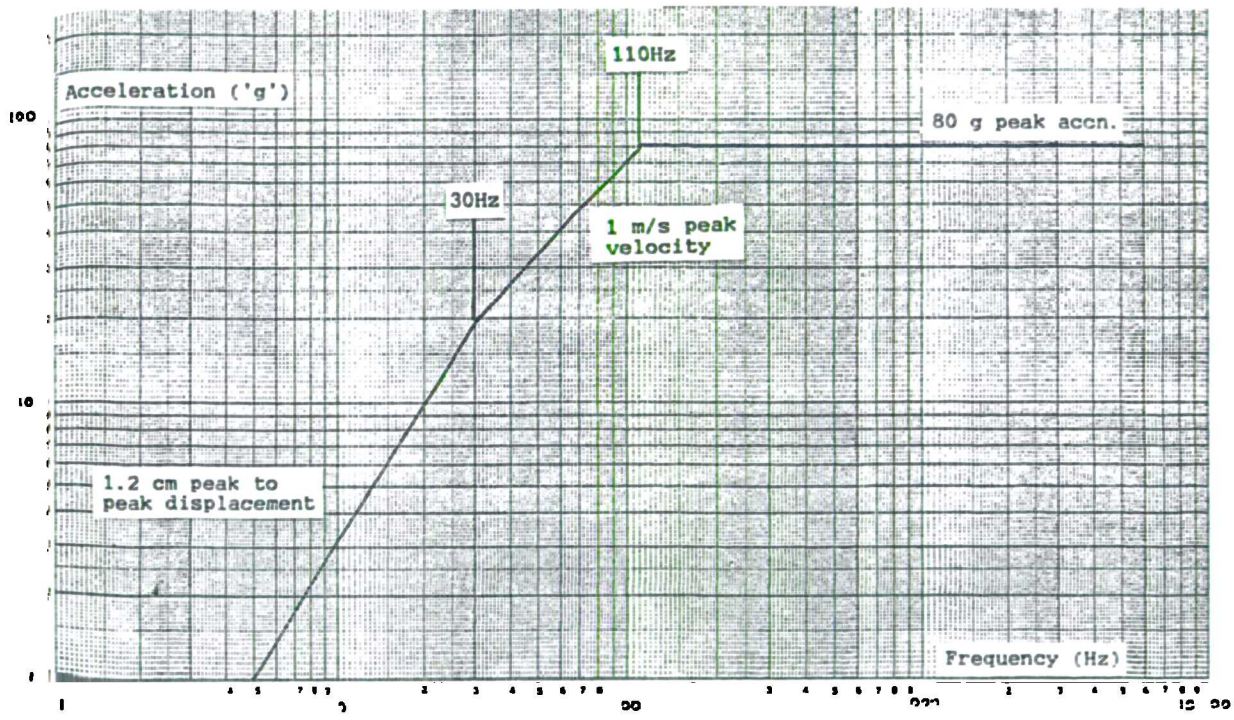


Fig. 4t VP30 - Performance Profile

The VP30 machine is the next machine down from the VP85 in the existing range of shakers and is driven here by a 1.5kVA amplifier. The total moving mass is approximately 2.27 kg, the a.c. coil has 26.5 turns and has a resistance of 0.0935 Ω at 100°C. The test was carried out at a slightly reduced output level as shown in Figure 4t above compared with the usual 17.8mm peak to peak displacement, 1.52 m/s peak velocity and 100g peak acceleration.

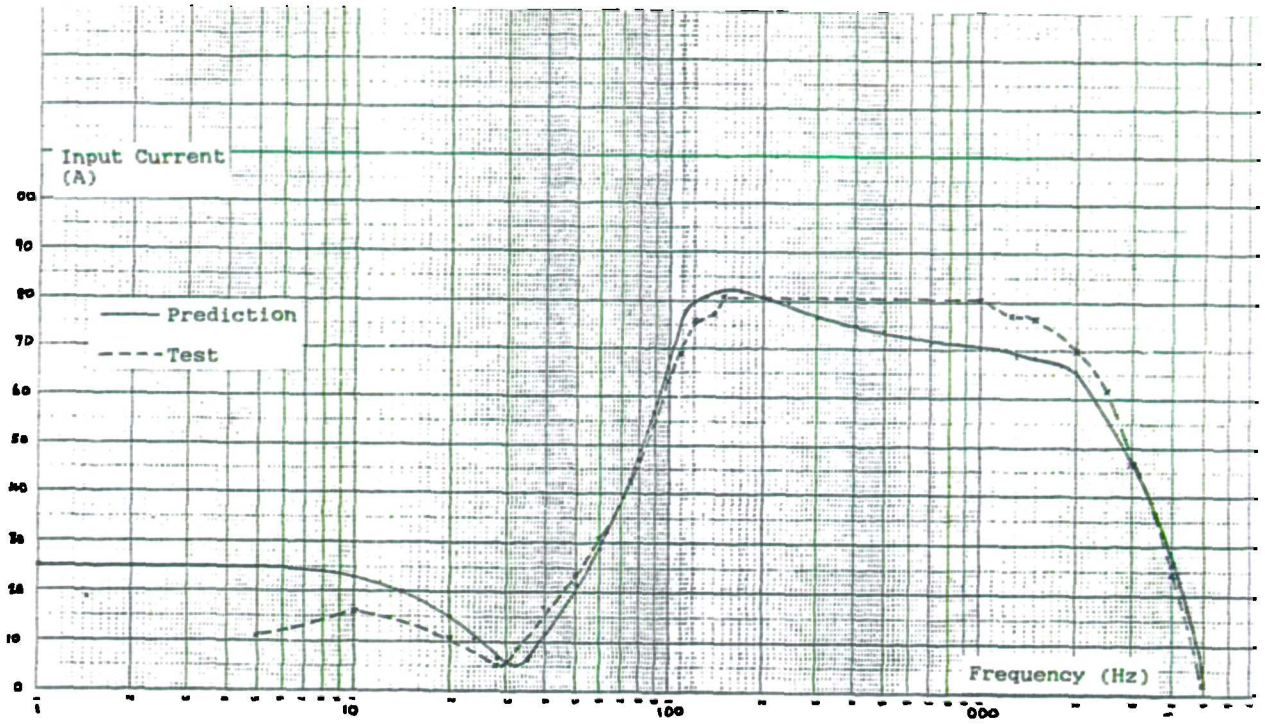


Fig. 4u VP30 - Current v Frequency

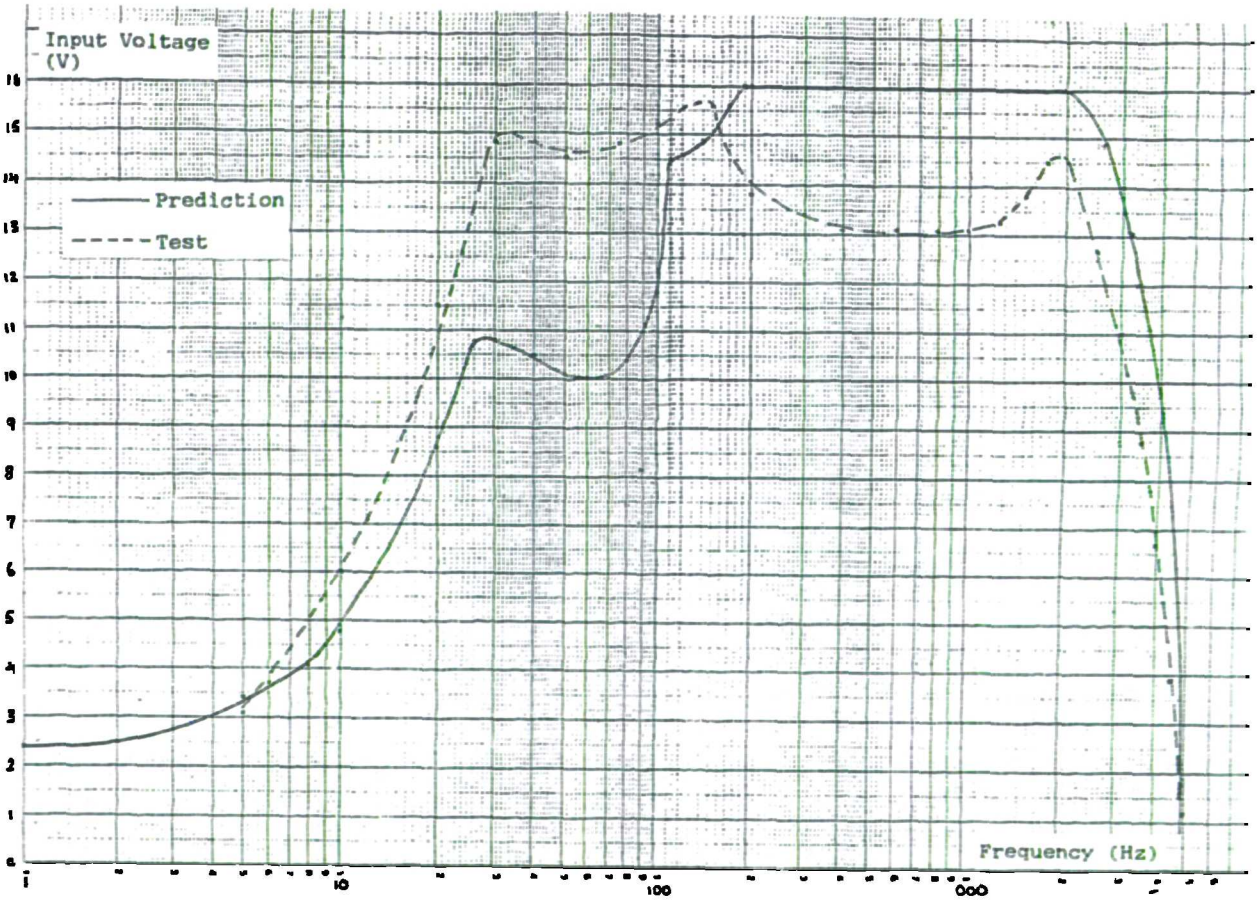


Fig. 4v VP30 - Voltage v Frequency

As for the VP85 machine previously, the current curves tie up quite well except around about the 300 to 2000 Hz region where the difference is about 12.5 %. The voltage curves, however, seem to indicate differences ranging between 18 and 32 % and there is even a 42 % difference at about 4000 Hz. Not all the differences can be attributed to experimental error, so this seems to suggest that the prediction model works well for the larger shaker sizes (e.g. the VP700 machine described earlier) and tends to get worse as the shaker size reduces, i.e. for the VP85 and VP30 machines. The predicted voltage curve for the VP30 does not show the expected dip in the 200 to 1000 Hz region. This has been put down to the underestimation of the leakage inductances at these frequencies. The prediction code was altered to allow the user to artificially increase the leakage inductances and this succeeded in producing the characteristic dip in the voltage requirement, thus confirming the above suspicion.

The circuit diagrams below indicate that the majority of the voltage is dropped across the resistances, which is to be expected in a smaller machine having higher resistances and lower reactances.

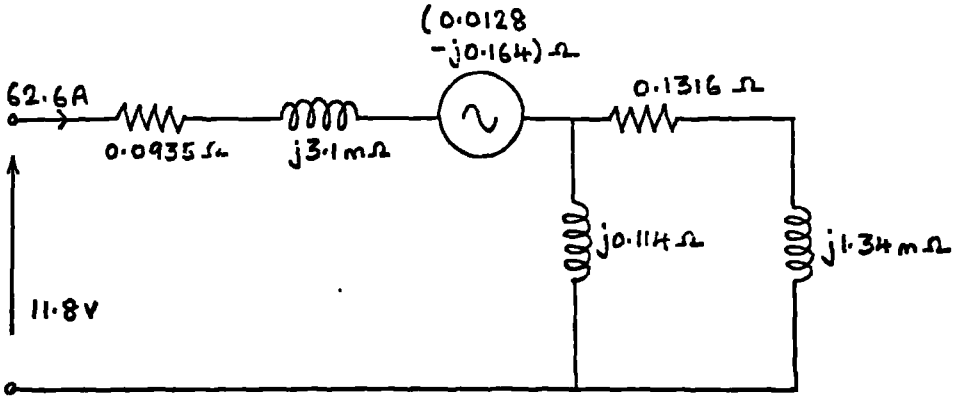


Fig. 4w VP30 - Equi alent circuit at f = 100 Hz

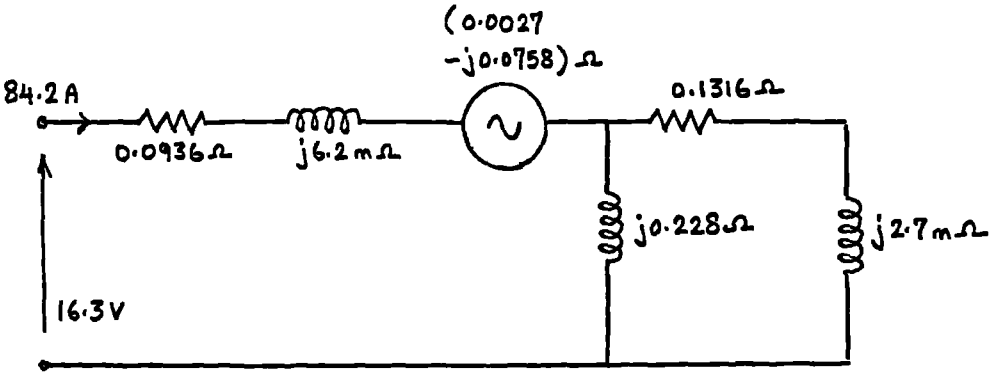


Fig. 4x VP30 - Equivalent circuit at f = 200 Hz

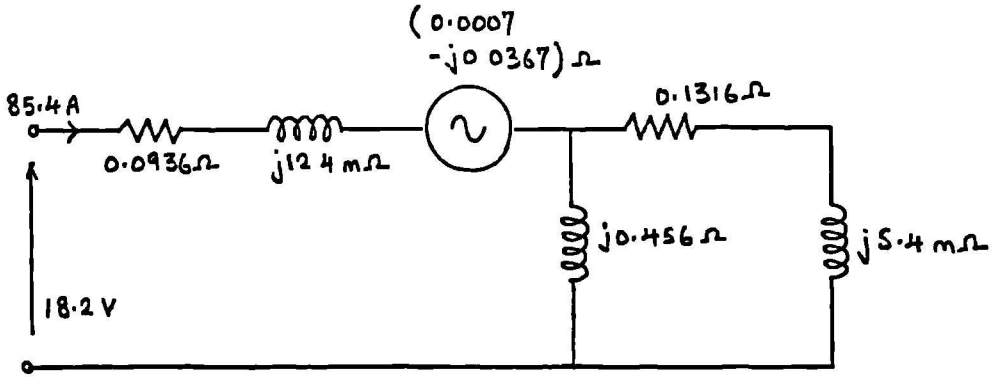
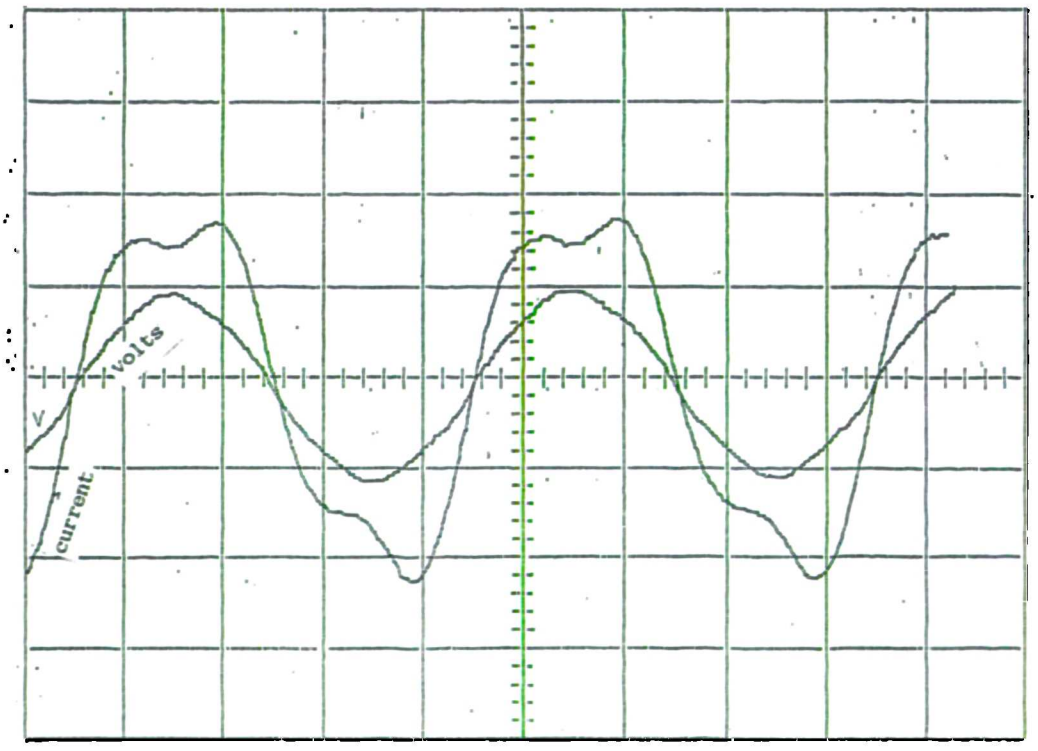
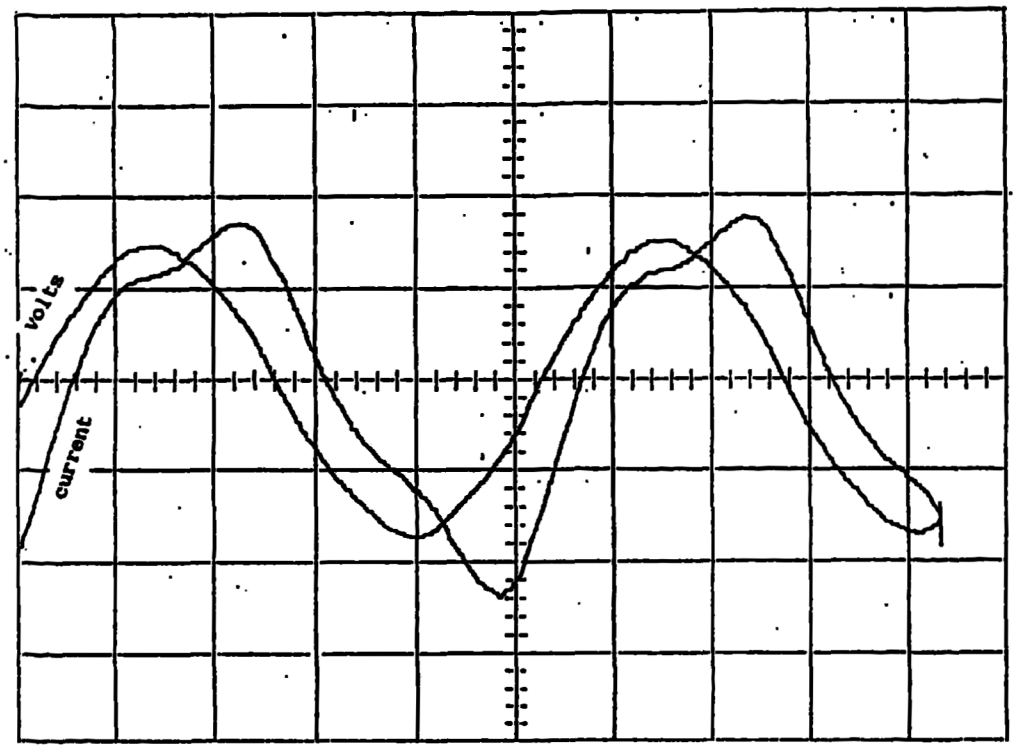


Fig. 4y VP30 - Equivalent circuit at f = 400 Hz

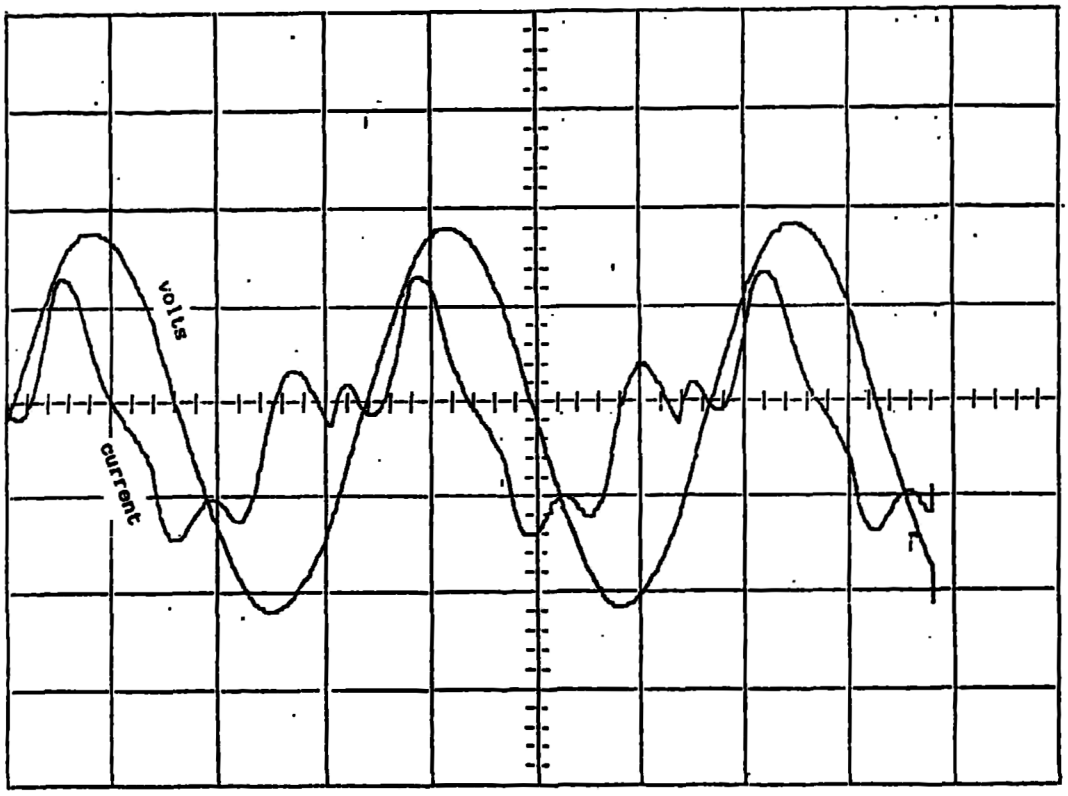
The set of 5 oscillographs below demonstrates the effects on the current and voltage waveforms as the shaker operation passes through the first mechanical resonancepoint and progresses through to the higher frequencies At low frequencies and at the mechanical resonant frequency, (see the 29 and 31 Hz traces), the current distortion seen could be due to the non-linearity of the suspension. Current distortion reduces at the frequencies beyond this. Note that the voltage waveform throughout remains sinusoidal since the amplifier and control system act as a voltage source.



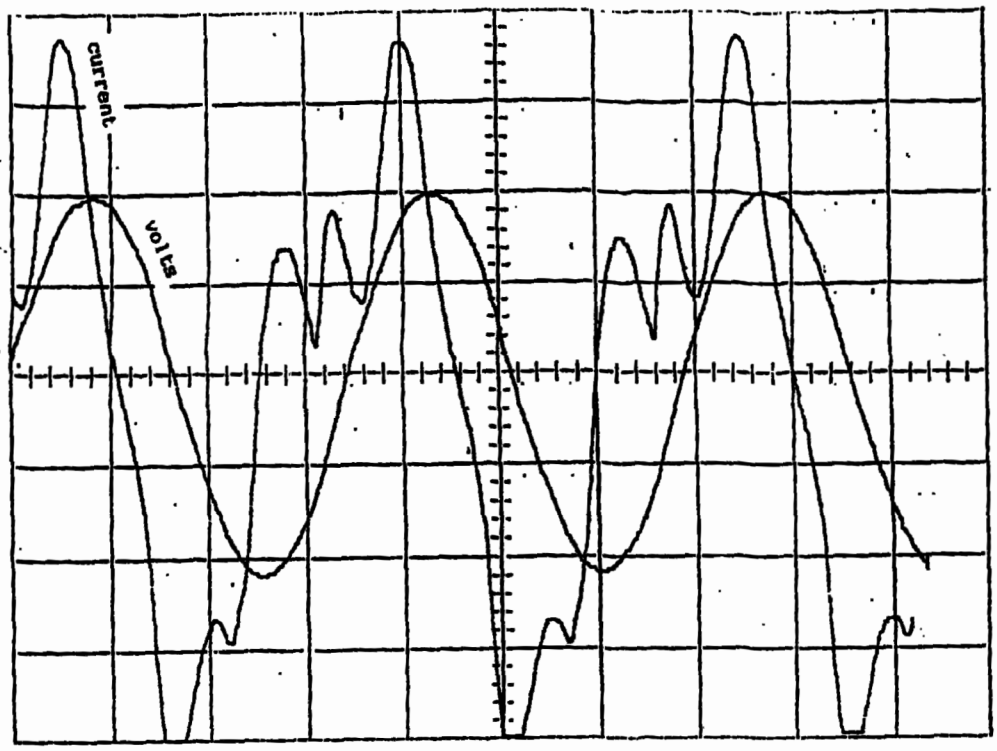
f = 6 Hz
V = 7.6 V cm I = 15.4 A cm t 77.9 ms'cm



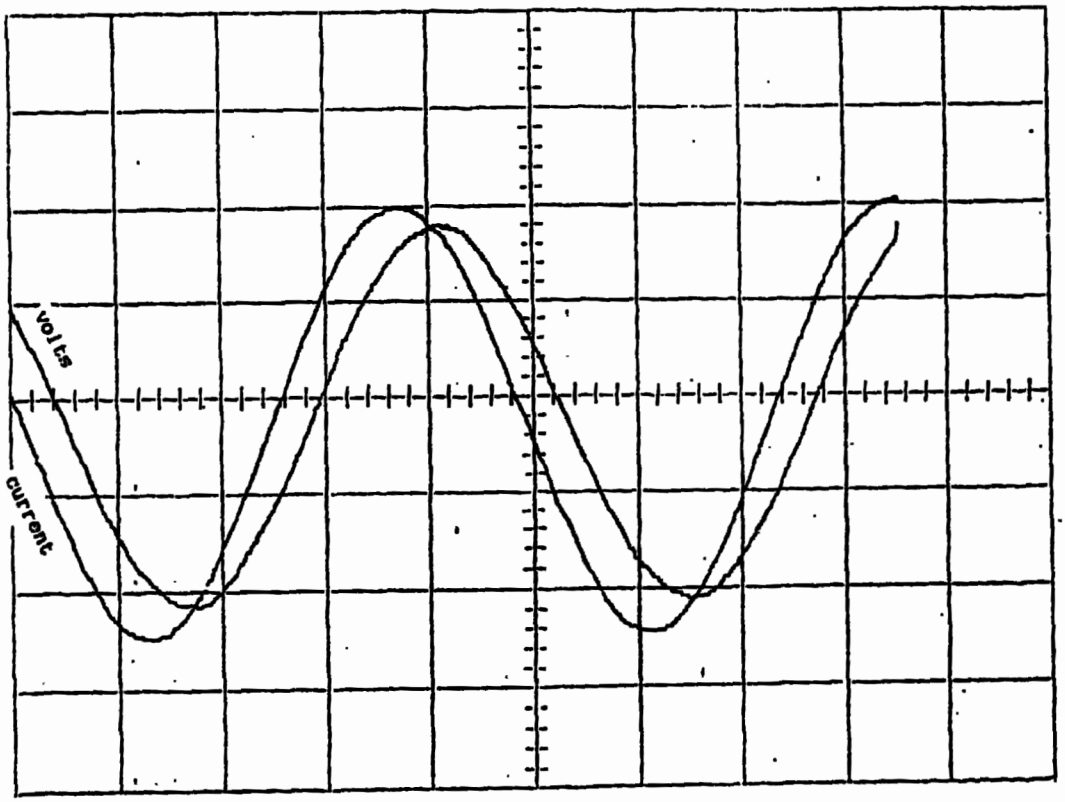
f = 10 Hz
V = 7.5 V/cm I = 15.9 A/cm t = 31.2 ms/cm



f = 29 Hz
V = 15.5 V/cm I = 7.8 A/cm t = 15.8 ms/cm



f = 31 Hz
V = 15.9 V/cm I = 3.1 A/cm t = 15.2 ms/cm



f = 200 Hz
V = 16.1 V/cm I = 77 A/cm t = 1.5 ms/cm

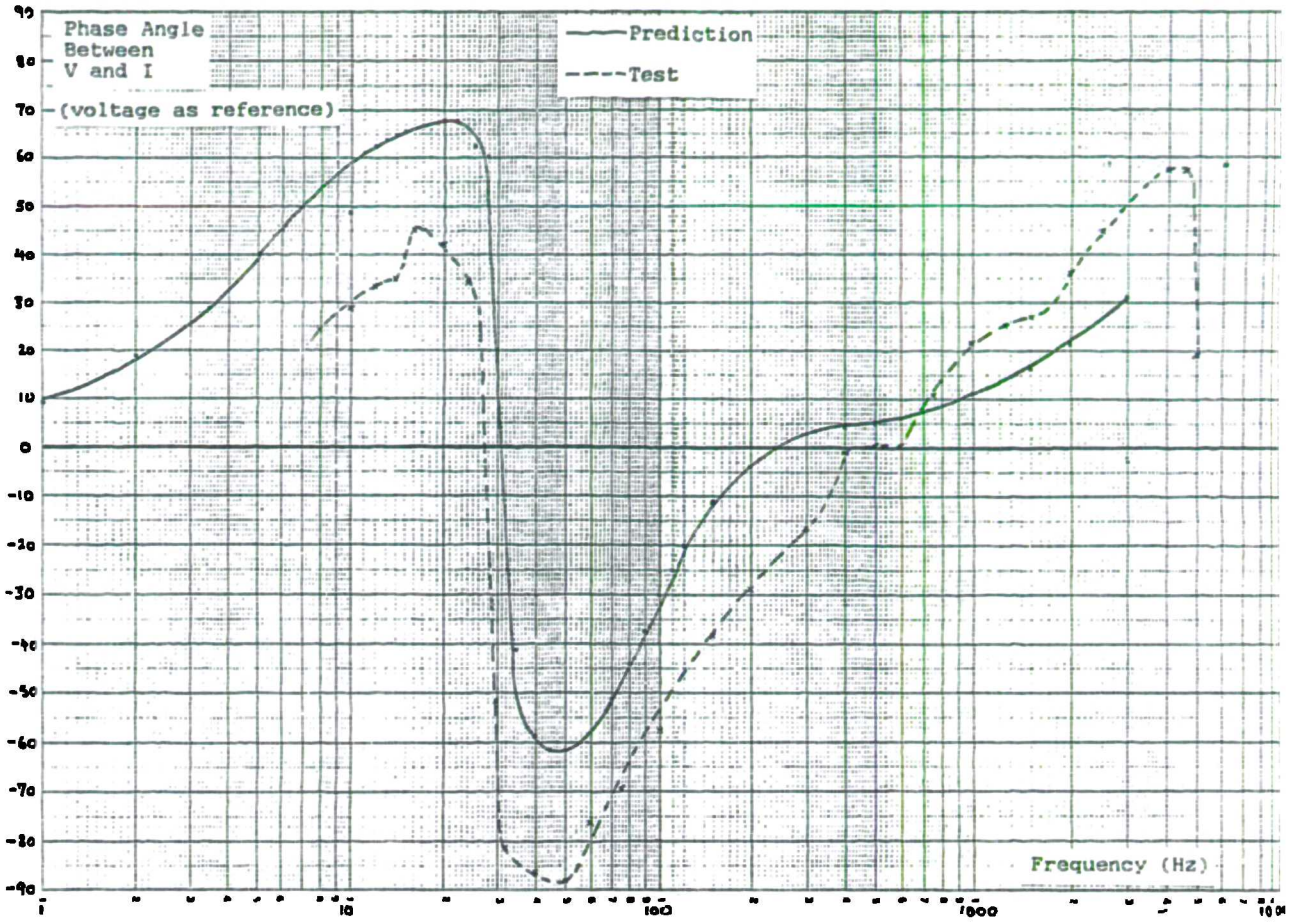


Fig. 4z VP30 - Phase Angle Between Input Voltage and Input Current

The predicted curve above has the same shape as the test curve which is encouraging even though the actual values show quite a big difference. The test curve is a bit 'jerky' due to the difficulty in obtaining accurate phase measurements using an oscilloscope. The voltage vector is taken as a reference here. It can be seen quite clearly that from 1 Hz to the mechanical resonance point at about 30 Hz the main circuit reactance is inductive. Past the mechanical resonance point , it becomes capacitive, (due to the motional impedance), and then becomes inductive again at about 500 Hz or so as the motional impedance ceases to dominate the circuit, the leakage inductances taking over at this point. This set of curves also serves to indicate the changes ocurring to the power factor of the machine which varies between about 0.94 lagging and almost zero leading, according to the test curve.

The comparison of flux densities below serves to confirm the fact that the correct value of flux density was being used for the predictions.

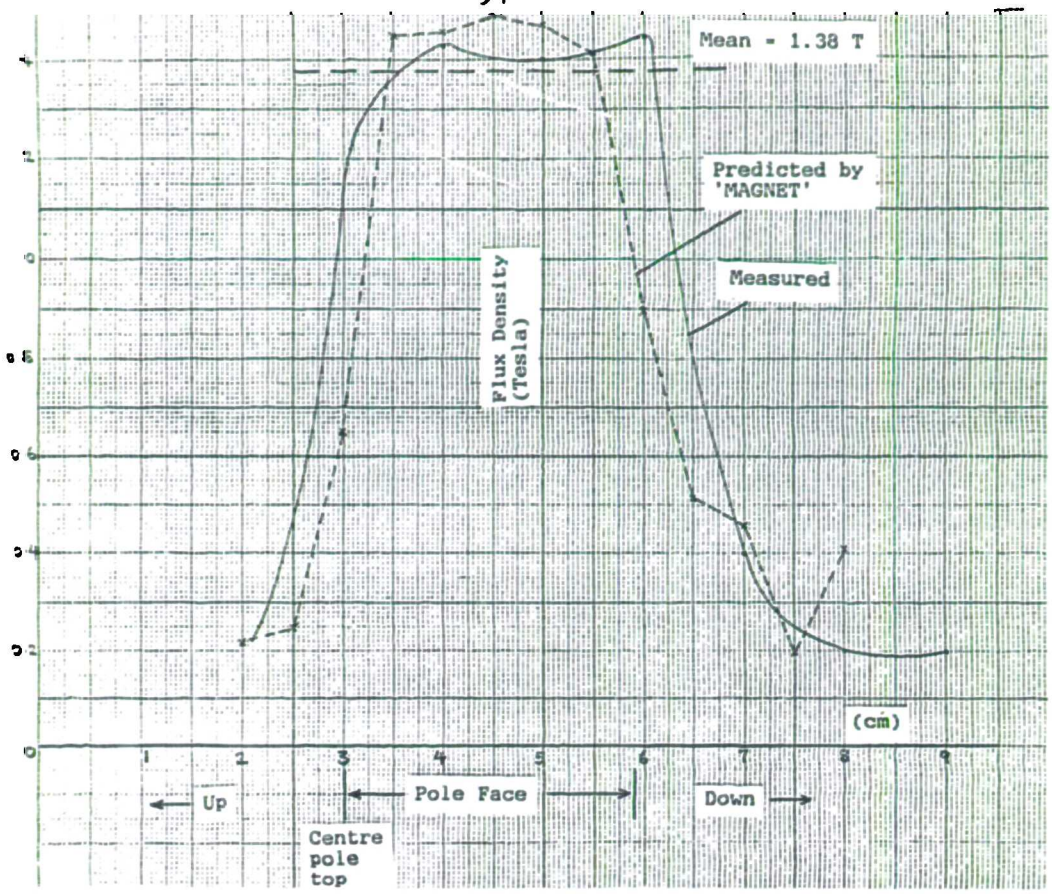


Fig. 4z1 VP30 - MAGNET Predicted v Measured Air-Gap Flux Density

Overall, these results seem to suggest that the model, even in its simplified form, does serve to predict the behaviour of the moving coil shaker with acceptable accuracy. The approximations made to the equivalent circuit and hence the equations, at various frequency points seem to be sufficient in explaining the shaker response at those points and will thus serve to provide useful information for 'tuning' the shaker design. The comparisons made for three shakers from the sponsor's existing range has helped to build up confidence in the use of these prediction techniques as a design tool for use in the further investigations of moving coil shakers by the sponsors. The success of the electrical and electromagnetic design of the prototype shaker, (discussed in Chapter 6 in more detail), further strengthens the argument for adopting a simple equivalent circuit approach to moving coil shaker design. However the presence of significant differences between test and predicted results under some conditions suggests that work on more complex models could be worthwhile.

CHAPTER FIVE
ELECTRICAL DESIGN

The electrical design procedure has to take into consideration not only electrical and magnetic factors but also mechanical aspects. Manufacturing techniques and factory practices also play an important part, e.g. in deciding which magnetic circuit configuration and a.c. coil design to opt for. Some material is based on an earlier report prepared during the course of the project (Reference 15).

5.1. Design Procedure

The design flowchart below outlines the basic steps used in the electrical design process.

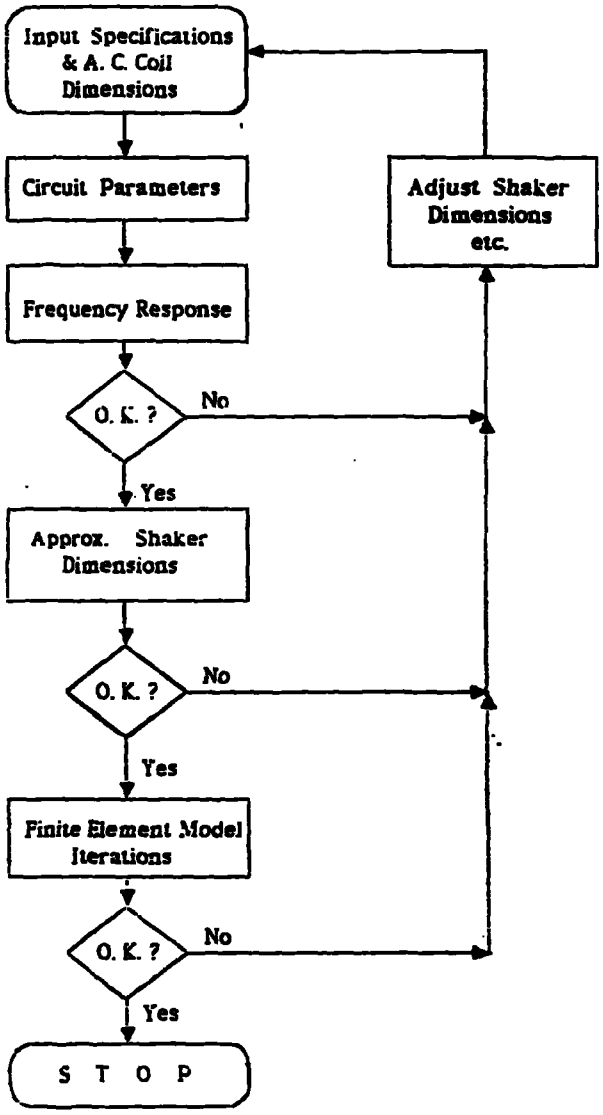


Fig. 5a Flowchart of Basic Design Methodology

5.1.1. Stage One - Required Specifications & Shaker Detail

(i) Specifications

The design process normally begins with a company or customer performance specification. To summarise, typical specifications are,

- *peak to peak maximum displacement*
- *peak maximum velocity*
- *peak maximum acceleration*
- *operating frequency range and frequency boundaries between the maximum displacement, velocity and acceleration-limited phases*
- *amplifier rated voltage and current*
- *likely table mass*
- *likely suspension stiffness, table/armature stiffness, damping coefficients*

The complications here are occasional uncertainties about,

(a) thrust versus velocity tradeoffs,

(b) amplifier performance, and

(c) the need for a single shaker design to be able to operate well with several amplifier sizes and performance specifications.

Fortunately, many of these uncertainties can be catered for by simple changes to a.c. winding turns and conductor sizes.

The first decision the designer has to make concerns the configuration to opt for. The decision has to be made whether the shaker should use a single-ended, double-ended or a c-core configuration, i.e. should the company's usual configuration

be used or a new one tried.

In the present case, the shaker manufacturer produced a range of shakers that he wanted to update so configuration changes were not ruled out. It was decided, as a test case, to evolve a new design for a shaker performance specification in the middle of the existing shaker range. The existing shaker model was of a size that was quite popular in the vibration test field, so development costs could hopefully be recovered quickly. It is often not possible to be certain before trial designs have been drawn up which configuration is likely to be 'best', and it is therefore necessary to proceed on a trial and error basis. In the present case, the company was keen to evaluate the c-core configuration's merits so the choice of configuration for much of the project work was virtually preset.

The second design decision concerns the a.c. coil type, viz. the number of winding layers. If the coil has 2 layers, with ribbon, (i.e. rectangular strip), conductors either side of a central composite-material tubular core, the total cooling area available is greater than with a single layer coil wound onto the outside of a composite tube, where heat flow inwards is greatly restricted by the tube. However, with the double-layered coil construction, the middle of the coil, (next to the tubular core), is inadequately cooled and can lead to high thermal stressing. The coil type selection hence affects the feasible a.c. loading, (amperes per axial centimetre), and in turn the thrust per cm^2 of air-gap area. The choice of a.c. coil type is hence highly dependent on production and cooling factors. Both types of coil construction were considered in the present project.

The next decision concerns the a.c. coil cooling method, viz. forced air or oil spray, (other techniques, e.g. direct oil or water cooling are not considered viable in the size range concerned). This choice is often highly dependent on company practice or on customer preferences. Established figures of watts/cm^2 of coil surface were available for each type of cooling. A similar decision was also required as regards the d.c. coil cooling method. Direct water or oil cooling is more of a possibility here. Hopefully each cooling method leads to a known figure of feasible amps/mm^2 or watts/cm^2 of d.c. coil cooled surface.

(ii) Determination of k_v with Specified F and Amplifier I_{max}

k_v, the shaker's thrust per amp constant, is defined generally by :

$$F = k_v . I$$

where I is the a.c. current and F is the thrust. Hence to satisfy the specified I_{ref} and F, the required k_v is,

$$k_v = \frac{\hat{F}}{I_{ref}} \qquad \text{..... (5.1)}$$

where F is the required peak thrust.

(iii) Velocity Check

It is then possible to check that the velocity requirement in the specifications is achievable . The maximum velocity is given by,

$$\dot{x} = \frac{V_{ref}}{k_v} \qquad \text{..... (5.2)}$$

where $\dot{x}$ is the maximum feasible velocity and V_{ref} is the voltage rating of the amplifier in question. This holds because, F = Bil and hence k_v = bl. Also E = Bl$\dot{x}$, thus giving E = $k_v\dot{x}$. Thus, given the required maximum thrust and velocity figures, the amplifier Volt-Ampere rating can be determined, (if necessary), from :

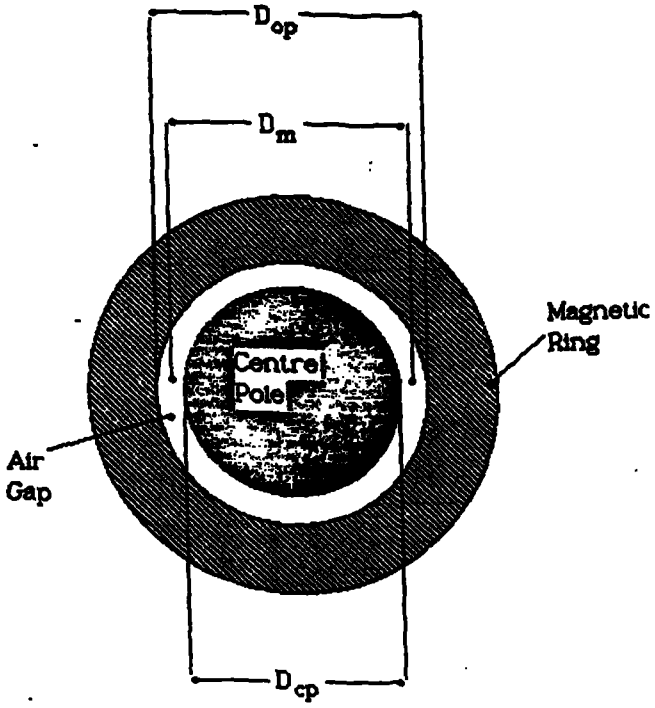
$$V_{ref}.I_{ref} = F.\dot{x} \qquad \text{..... (5.3)}$$

(iv) Determination of Mean A.C. Coil Diameter

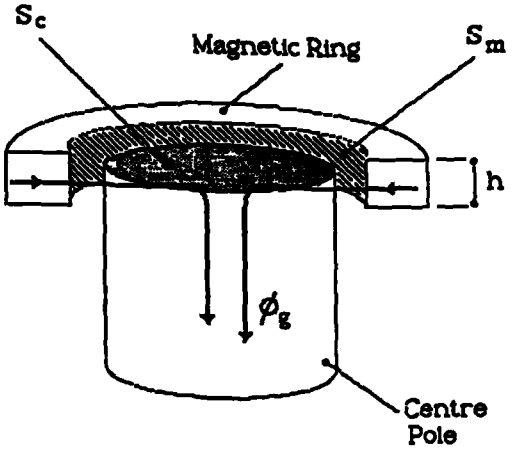
The shaker's D_m and h are then provisionally set by fixing a trial value of h, calculating a corresponding D_m on the basis of feasible centre pole flux density conditions, checking the resulting $\pi D_m h$ product for correct F, and iterating as necessary with successive trial values of h. The initial assumption of B_g is usually based on measurements taken from an existing shaker of

about the same size. Experience has shown that B_g often lies in the approximate range 1.40 to 1.50 Tesla, so 1.45T is a good initial assumption.

In determining D_m, it is assumed that all the generated d.c. flux that crosses the air-gap passes into the centre-pole, (i.e. there is no fringing and all the flux is conserved), as shown in Figure 5b.



(i) Plan View of Shaker



(ii) Cutaway View of Side Elevation

Fig. 5b D.C. Flux Path

Thus, flux crossing the air-gap is, (referring to the figures above),

$$\phi_g = B_g . S_m$$

where,

$$S_m = \pi . D_m . h$$

The flux entering the centre-pole is,

$$\phi_{cp} = B_{cp} . S_c$$

where,

$$S_c = \frac{\pi . D^2_{cp}}{4}$$

Then, using the assumption above,

$$\phi_g = \phi_{cp}$$

giving,

$$D_m = \frac{B_{cp} . D^2_{cp}}{4 . h . B_g} \qquad \text{..... (5.4)}$$

D_m is related to D_{cp} by,

$$D_{cp} = D_m - g \qquad \text{..... (5.5)}$$

Substituting for D_{cp} from eqn. 5.5 in eqn. 5.4, a quadratic in D_m is obtained,

$$B_{cp}.D_m^2 - (4.h.B_g + 2.g.B_{cp}).D_m + B_{cp}.g^2 = 0$$

$$D_m = \frac{(4.h.B_g + 2.g.B_{cp}) + \sqrt{[-(4.h.B_g + 2.g.B_{cp})]^2 - 4.B^2_{cp}.g^2}}{2.B_{cp}}$$

..... (5.6)

Note that trial figures of d.c. ampere-turns and hence d.c. slot area and shape, and magnetic circuit trial dimensions are not calculated now but are dealt with later, (see section 5.1.4.), once a satisfactory a.c. design has been achieved.

(v) A.C. Coil Height

As the a.c. coil moves up and down in the air-gap, it will encounter differing mean levels of d.c. flux, thus producing non-uniform thrust, (this is dealt with in slightly more detail in section 5.1.5. (iii)). To allow for this possible variation the d.c. fringe fields at the top and bottom of the a.c. coil are taken into account when working out the approximate a.c. coil height. The height of each fringe field, h_{fdc}, is taken as g/2 and,

$$h''' = h + 2.h_{fdc} \qquad \text{..... (5.7)}$$

In practice, as will be seen, the axial coil height is taken as 15 % longer than the magnetic ring pole face height.

(vi) A.C. Coil Turns

The k_v factor given by B_g x (conductor length) is,

$$k_v = B_g.\pi.D_m.N_T \qquad \text{..... (5.8)}$$

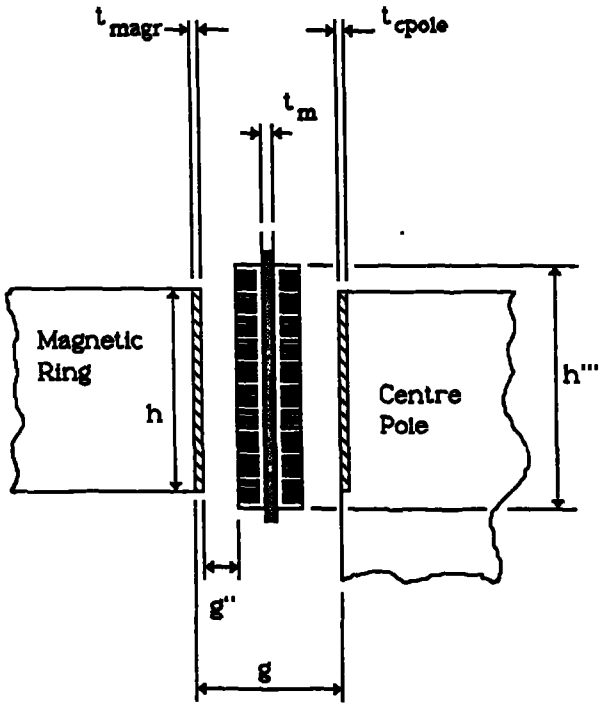
Eqn. 5.8 is now used to obtain the total number of a.c. coil turns required to produce the specified thrust.

$$N_T = \frac{k_v}{B_g . \pi . D_m} \qquad \ldots\ldots\ldots\ldots\ldots (5.9)$$

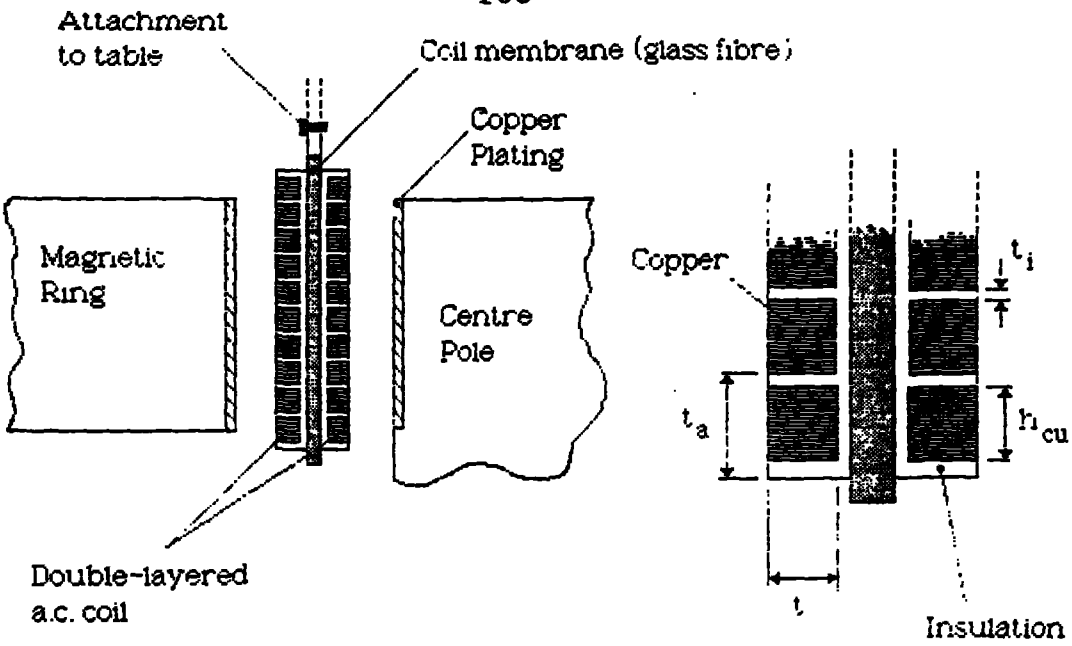
It should be noted that only a fraction of the total coil turns will be immersed in the d.c. flux at any instant, and this is allowed for by multiplying N_T by a factor k_1, where $k_1 = h/h'''$.

(vii) Detailed A.C. Coil Construction

Figure 5c indicates the constructional details of the moving element.



(i) General Detail (including a.c. coil)



(ii) Dimensional Detail

Fig. 5c Details of Moving Element

Note that rectangular conductors are used in most shakers in order to maximise the amount of copper that can be used in the space available. The overall axial thickness of one coil turn, t_a , is given by :

$$t_a = \frac{h'''}{N_T/2} \qquad \text{..... (5.10)}$$

The axial conductor copper thickness h_{cu} is given by :

$$h_{cu} = t_a - 2.t_i \quad ; \quad t_i = 1 \text{ layer of insulation thickness}$$

..... *(5.11)*

Insulation and coil mounting tube, ('membrane'), thicknesses are specified by the manufacturer as standard items currently used by them. For a double-layered a.c. coil, the radial thickness of the conductor, per layer, is given by,

$$t = \frac{g - (t_{cpole} + t_{magr} + 2.t_i + 2.g'' + t_m)}{2} \qquad \text{..... (5.12)}$$

This calculation depends on the total 'magnetic' air-gap length, g, (i.e. as seen by d.c. flux crossing the gap), and includes the copper plating thicknesses on the pole faces. The choice of g as in any electrical machine is critical since it affects the entire set of magnetisation conditions. In shakers, (and other air-gap wound machines), it also determines, (as eqn. 5.12 states), the allowable conductor thickness. As in induction machines, a very short air-gap is desirable, providing a high value of magnetising inductance, and thus increasing the coupling between the primary and secondary parts of the machine. Because of the presence of the moving element in the air-gap of a shaker, and constraints on the heating levels that can be tolerated, the air-gap length is usually predetermined for a given size of machine.

After h_{cu} and t have been calculated, the nearest conductor cross-section is chosen from a standard conductor table, and appropriate adjustments made to N_T.

The first iteration of a.c. coil design is now complete and the design process can move on to the next design stage.

5.1.2. Stage Two - Circuit Parameters

The equivalent circuit parameters can now be evaluated. Note that some frequency-dependent variation in the resistances and leakage inductances occurs due to skin effect, and that resistance estimates are usually made for an assumed operating temperature of 100°C. The derivations of the various parameters have been dealt with in Chapter Three and Appendix A. In calculating the parameters, account must of course be made for the particular type of magnetic circuit configuration and a.c. coil construction involved.

5.1.3. Stage Three - Frequency Response

The equivalent circuit is now used to provide estimates of a.c. coil total impedance and input current, voltage etc. Maximum currents and voltages are set by amplifier capabilities, (either the current or voltage being limited at any given frequency). Knowledge of the current then enables the velocities, accelerations and thrusts to be evaluated for each frequency point over the frequency band of interest, using the equations developed in Chapter Three. Careful examination of all circuit parameter values and the branch currents and voltages together with the resulting shaker performance curves will give the designer an indication of which 'lead' to follow in order to achieve

the desired shaker performance without exceeding any of the imposed limits. This might involve thickening a copper plating layer to reduce secondary resistance, or increasing the a.c. coil conductor cross-sectional area in order to reduce heating levels, etc.

5.1.4. Stage Four - Approximate Shaker Dimensions

If the frequency response determined in Stage 3 is satisfactory, (i.e. provides an acceptable level of performance for given amplifier ratings), the shaker's d.c. design can be considered in more detail, viz. centre-pole diameter, d.c. slot area and shape, cross-sectional areas of the outer limbs of the shaker, can be obtained. The approximate iron weight can also be calculated at this point and comparisons made with an existing equivalent sized machine.

(i) Specifications

Key input parameters for the d.c. design process are :

- Mean a.c. coil diameter (Stage 1)
- Pole face height (Stage 1)
- Air-gap flux density (Stage 1)
- Air-gap length (Stage 1)
- D.C. current density averaged over slot area
- D.C. current density in actual copper
- D.C. coils packing factor (ratio of actual copper to slot area)
- Density of ferromagnetic material used (usually steel)
- certain shaker dimensions from existing machine (used for scaling calculated dimensions of new design).

(ii) Ampere-Turn Calculations

The number of ampere-turns dropped across the air-gap is,

$$AT_g = \frac{B_g . g}{\mu_o}$$

Therefore, the estimated total ampere-turns for the new design is,

$$AT_T = \frac{B_g . g}{\mu_o} . (1 + k_1) \qquad \text{..... (5.13)}$$

where,

$$k_1 = \frac{AT_T - AT_g}{AT_g} = \frac{\text{ampere turns dropped in iron circuit}}{\text{ampere turns dropped across airgap}}$$

In later stages in the design process, several iterations on the magnetic circuit using finite-element techniques, will provide an accurate value for k_1 . Initially an intelligent estimate has to be made about the number of ampere-turns dropped in the iron circuit. For single-ended shakers of the type being discussed here, a typical k_1 figure is about 0.43.

(iii) D.C. Slot Area

Using the d.c. current density averaged over the d.c. slot and the total ampere-turns required, the slot area is given by,

$$A_s = \frac{AT_T}{\delta_{DC}} \qquad \text{..... (5.14)}$$

For forced air-cooled designs, d.c. current densities of about 1.62 x 10^6 to 2.0 x 10^6 A/m^2 are quite common.

(iv) Shaker Dimensions

Figure 5d shows all the major dimensions that can now be estimated approximately.

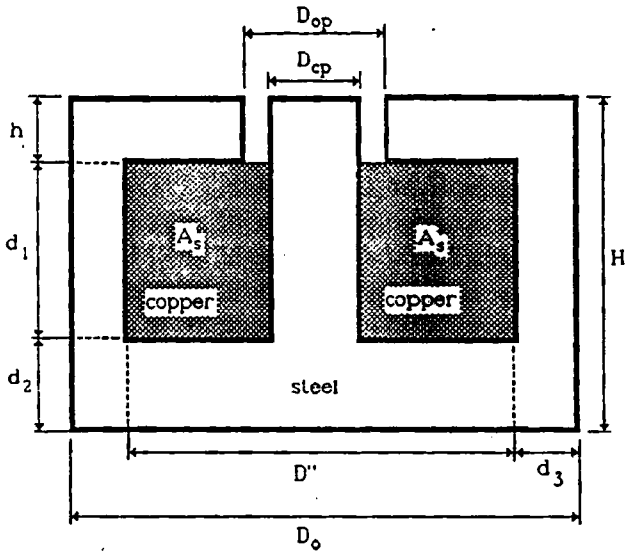


Fig. 5d Approximate Shaker Dimensions

The approximate estimation process proceeds as follows :

The d.c. slot is initially assumed to be of square cross-section giving,

$$d_1 = \sqrt{A_s} \qquad \ldots\ldots\ldots\ldots\ldots (5.15)$$

and, the other dimensions are as follows,

$$D'' = D_{op} + 2.d_1 \qquad \ldots\ldots\ldots\ldots\ldots (5.16)$$

Side Limb Thickness

$$d_3 = d_3{}^{vp85} \cdot \left[\frac{D_{cp}}{D_{cp}{}^{vp85}}\right]^{\lambda} \cdot \left[\frac{D''{}^{vp85}}{D''}\right] \qquad \ldots\ldots\ldots (5.17)$$

where, d_3^{VP85} , D_{cp}^{VP85} and D''_{VP85} are dimensions obtained from an equivalent sized machine, (model no. VP85), and are used to proportion the machines d_3 dimension to the new flux level, (which is taken as proportional to D^2_{cp}), and the new peripheral length of the outer iron annulus, (i.e. proportional to D").

Thickness of Base Disc

$$d_2 = d_2^{VP85} \cdot \frac{D_{cp}}{D_{cp}^{VP85}} \qquad \text{..... (5.18)}$$

Again, this proportions the d_2 dimension used in the existing VP85 machine to the new flux level, (proportional to D^2_{cp}), and to the new peripheral length at the inner diameter of the bottom and top iron discs, (proportional to D_{cp}).

Thickness of Top Annulus (equal to pole face height)

$$h = d_2 \qquad \text{..... (5.19)}$$

Overall Diameter of Magnetic Circuit

$$D_O = D'' + 2.d_3 \qquad \text{..... (5.20)}$$

Overall Height of Magnetic Circuit

$$H = d_1 + d_2 + h \qquad \text{..... (5.21)}$$

Using these approximate dimensions, the total iron weight of the magnetic circuit can be evaluated and a decision made as to whether the design is too heavy for its force rating. If so, weight can be reduced by reducing iron sections, (raising AT_{dc} requirements and d.c. saturation levels), and/or by raising a.c. coil ampere-turns and reducing total d.c. flux.

(v) D.C. Losses

The approximate losses in the d.c. coils are calculated using the following expression,

$$D.C.\ Losses = A_s.C_j^2.\rho_1.L_{mt}.k_p.k_1 \qquad \ldots\ldots\ldots\ldots\ldots (5.22)$$

where,

A_s - d.c. slot area

C^2_j - d.c. current density in the actual copper

ρ_1 - resistivity of copper

L_{mt} - length of mean turn of d.c. winding

k_p - packing factor (ratio of actual copper to slot area, approx 0.74)

k_1 - number of d.c. slots (1 for the S.E. configuration)

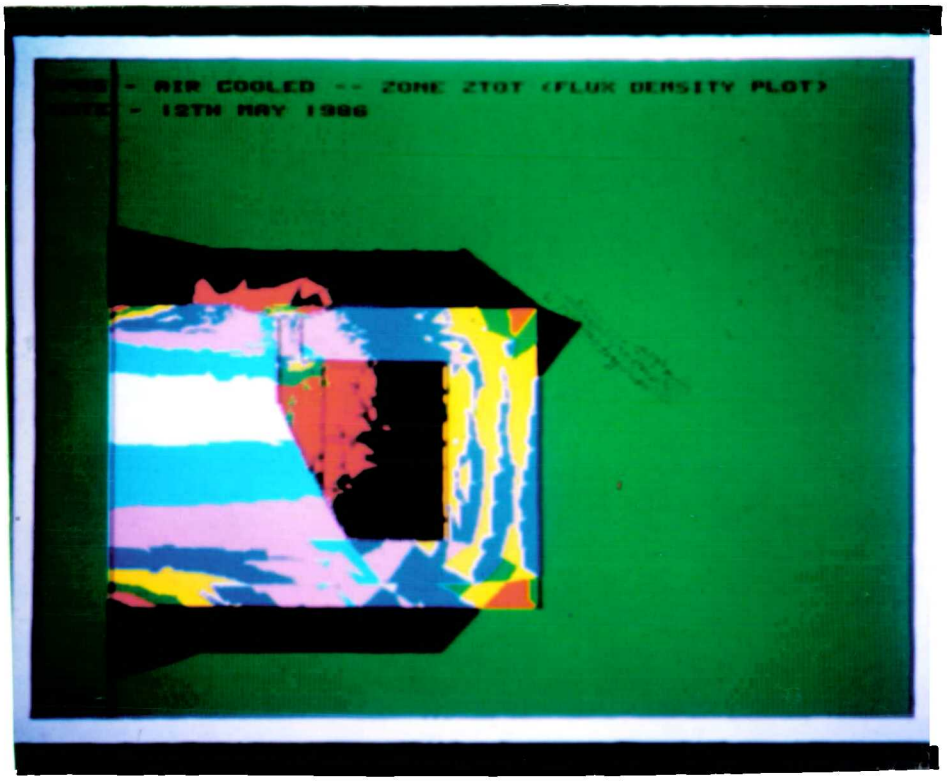
5.1.5. Stage Five - Finite Element Modelling

The commercially available C.A.D. software package MAGNET for the solution of electromagnetic field problems in electromechanical and electromagnetic devices, using finite-element techniques was introduced for the magnetostatic flux calculations. Its primary role was to determine the magnitude and distribution of the main d.c. air-gap flux for a prospective magnetic circuit design and a trial value of d.c. ampere-turns. This is a vital step in the determination of the shaker's mean B_g and hence k_v and a.c. coil impedance, etc. It was also used in the detailed design of the magnetic circuit steel-work and for evaluating degaussing requirements to reduce stray flux levels at the table surface. Experimental results, such as air-gap flux densities, stray flux values and force measurements, taken from existing shakers were used to build up confidence in the results obtained using the package.

(i) Flux Saturation Levels

Running on an IBM PC/XT 286 desk-top personal computer, the package served to highlight areas in the shaker design that could be improved upon. For instance, flux saturation levels in the steel cross-sections could be calculated and displayed,(using different colour shadings for each different level), on the computer's high-resolution

monitor as indicated in Figure 5e below.



White - very saturated
Light blue - less saturated
Pink - slightly saturated
Dark blue - not saturated

Fig. 5e Flux Density Saturation Levels

Thus, at a glance the de igner can tell which parts of the magnetic circuit are saturating and which are not. This helps in optimising the amount of steel required f r each part of the circuit. This also helps to identify 'leaky' parts of the circuit, including the source regions for undesirable stray fields at the table top.

(ii) Flux Line Plots

Flux line plots help in the actual sizing of the d.c. slots, to minimise d.c. slot leakage and stray flux in the pole tip area. By varying the cross-sectional area of the d.c. slot, either the width or the height of the magnetic circuit can be optimised, depending on which is the more imp rtant. Another use of such a pl t is in spotting irregularities in the finite-element mesh used to model the shaker, which may cause the solution to converge at a slower rate and may even lead to

inaccuracies in the final results obtained.

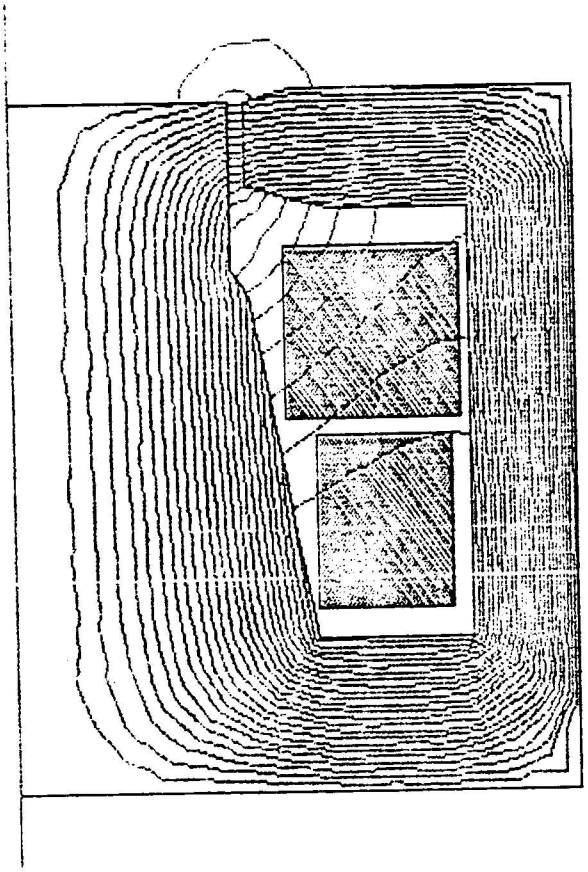


Fig. 5f Typical Flux Line Plot

The designer can 'zoom-in' on a particular area of interest to examine it in more detail.

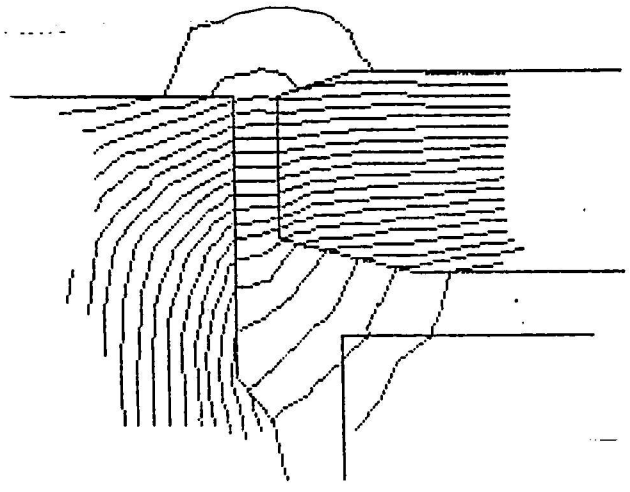


Fig. 5g 'Close-Up' of the Air-Gap Region

(iii) Air-Gap and Iron Flux Densities

Close examination of the flux density in the air-gap is permissible, enabling comparisons to be drawn up with experimental test data obtained using a hall-probe.

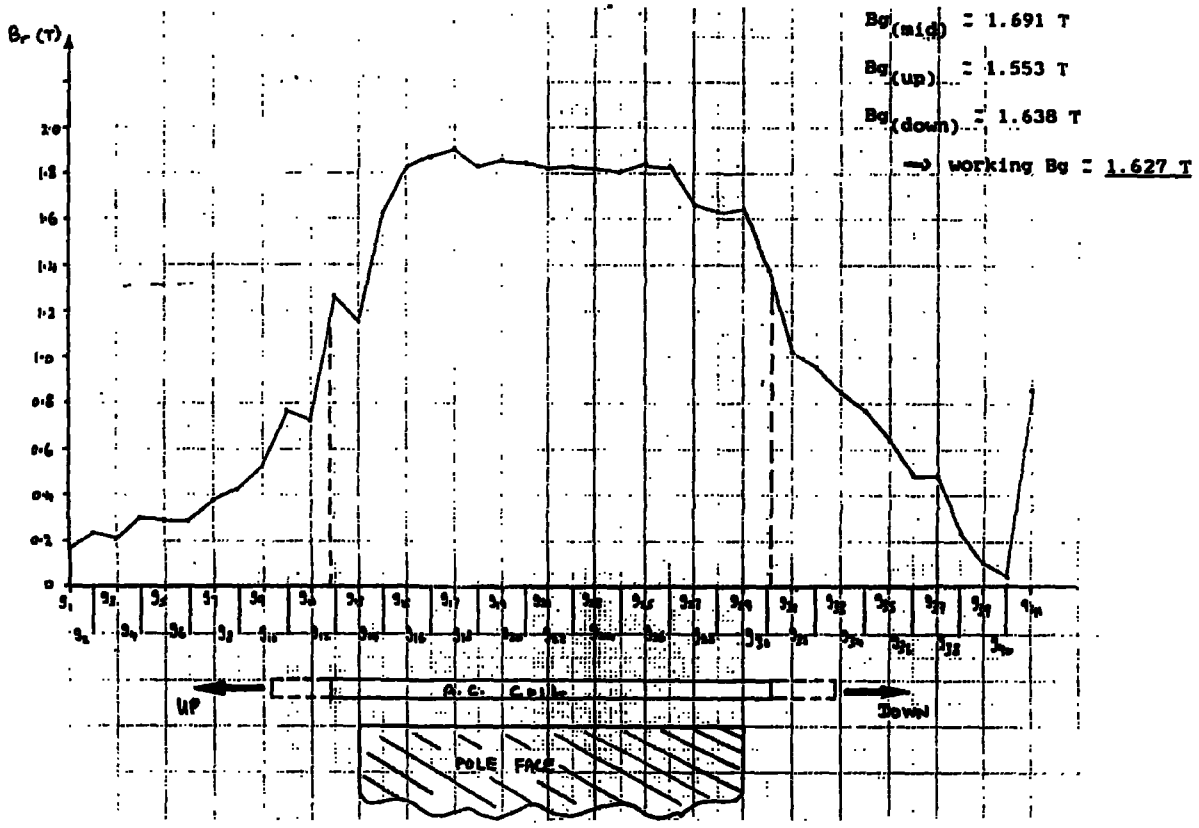


Fig. 5h Air-Gap Flux Density (axially)

The 'sky-line' effect noticed in the above plot is due to the size of the elements used to model the air-gap region. This effect will be less noticeable if a finer mesh is created, but the number of elements that can be used is limited, chiefly, by the amount of memory available on the personal computer.

Both the radial as well as the axial components of flux density can be examined throughout the magnetic circuit allowing the designer to keep a check on the levels of flux present in various parts of the circuit. Figure 5i indicates the 'contours' along which the flux density level is plotted and integration carried out.

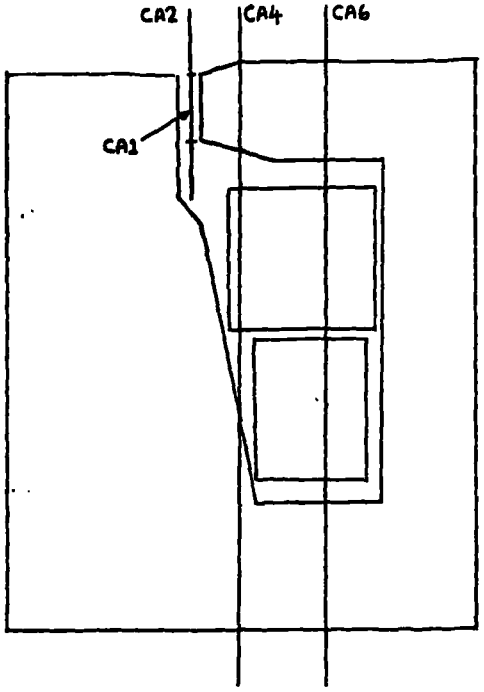
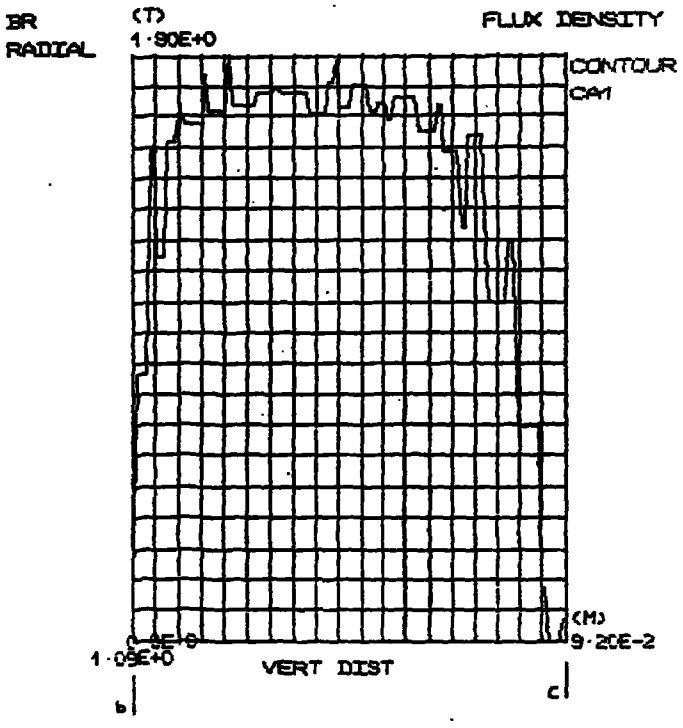
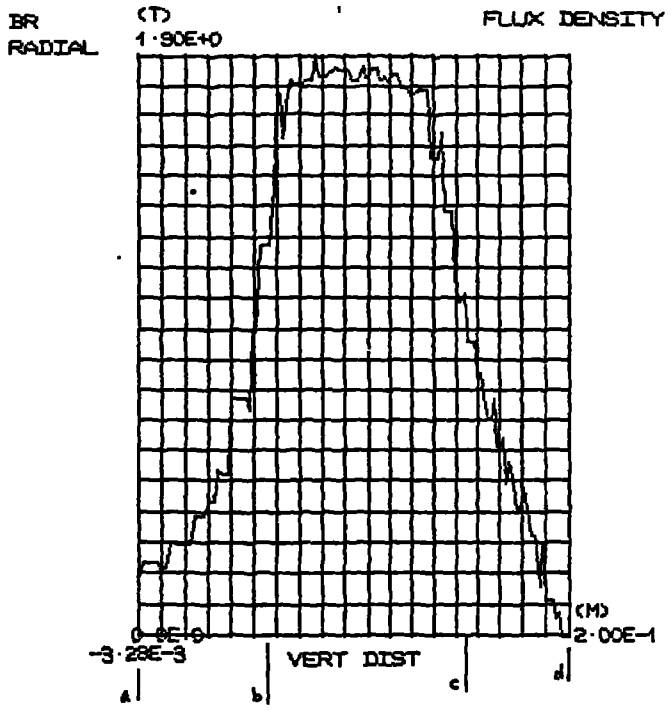


Fig. 5i Position of Typical 'Contours' Used in Shaker Design

Figures 5j and 5k show the flux density levels along the various 'contours'.

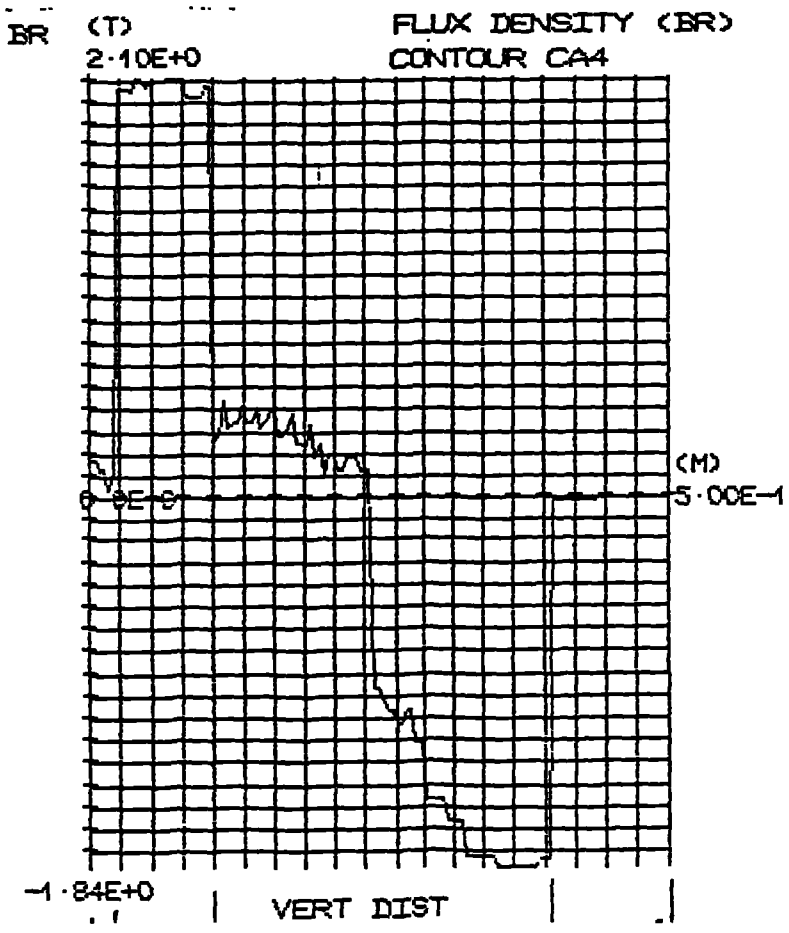


(i) Contour CA1

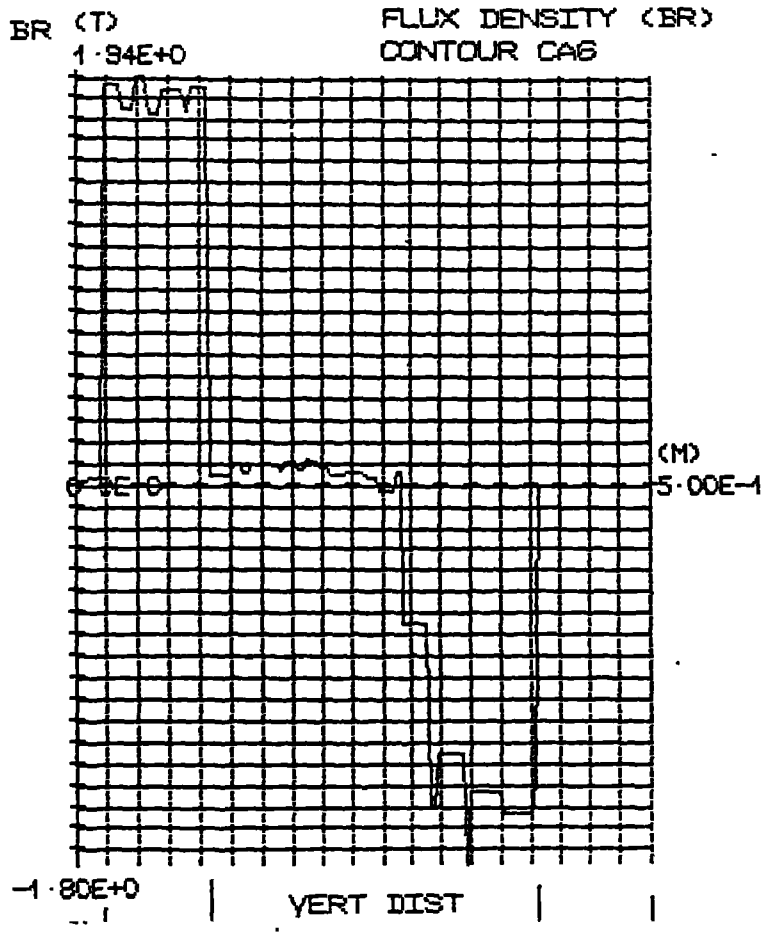


(ii) Contour CA2 (along a.c. coil height)

Fig. 5j Radial Components of Flux Density in the Air-Gap



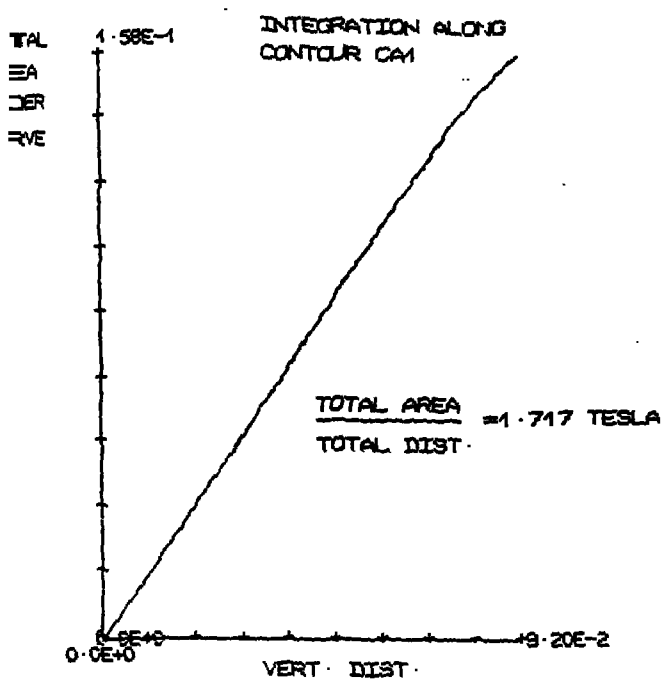
(i) Contour CA4



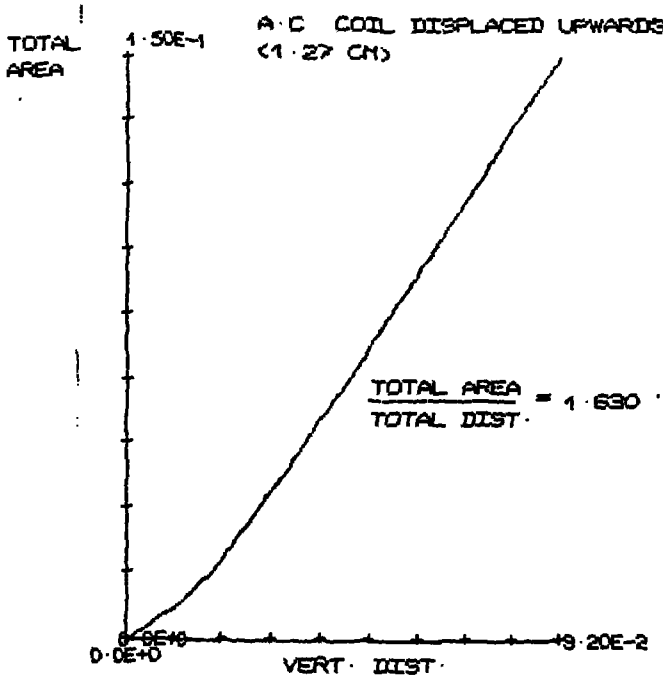
(ii) Contour CA6

Fig. 5k Radial Components of Flux Density in the Iron

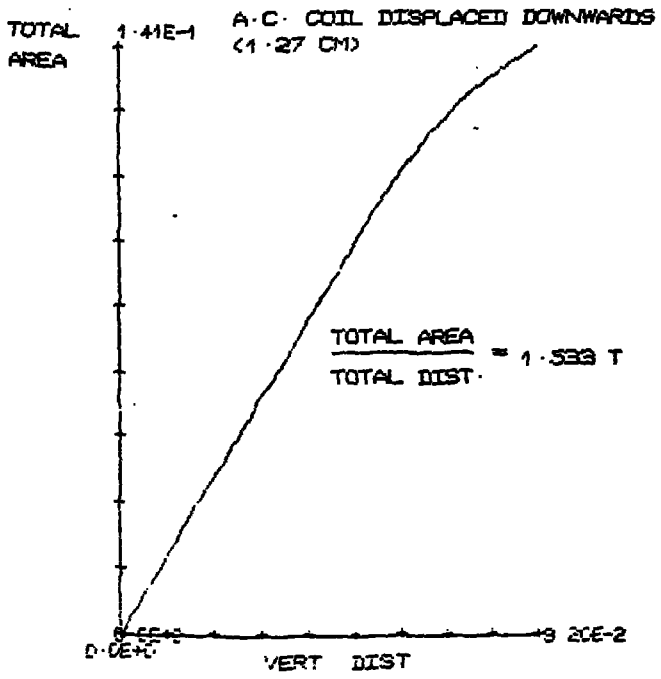
This type of examination can also provide important information about the constancy of the thrust per amp on the a.c. coil produced by the interaction of the alternating current with the d.c. flux. As the a.c. coil moves up and down, the ends of the coil may possibly move out of the area of high d.c. flux. Thus the average d.c. flux 'seen' by the coil will vary, (as shown by integrating along the relevant 'contours', in Figure 5l), producing a varying thrust per ampere which is, of course, undesirable since distortion in the back e.m.f. and coil motion waveforms will then occur. The resulting flux density plots, (axial variation along the air-gap), will aid the setting of the allowable axial length of the a.c. coil.



(i) Mid-Position



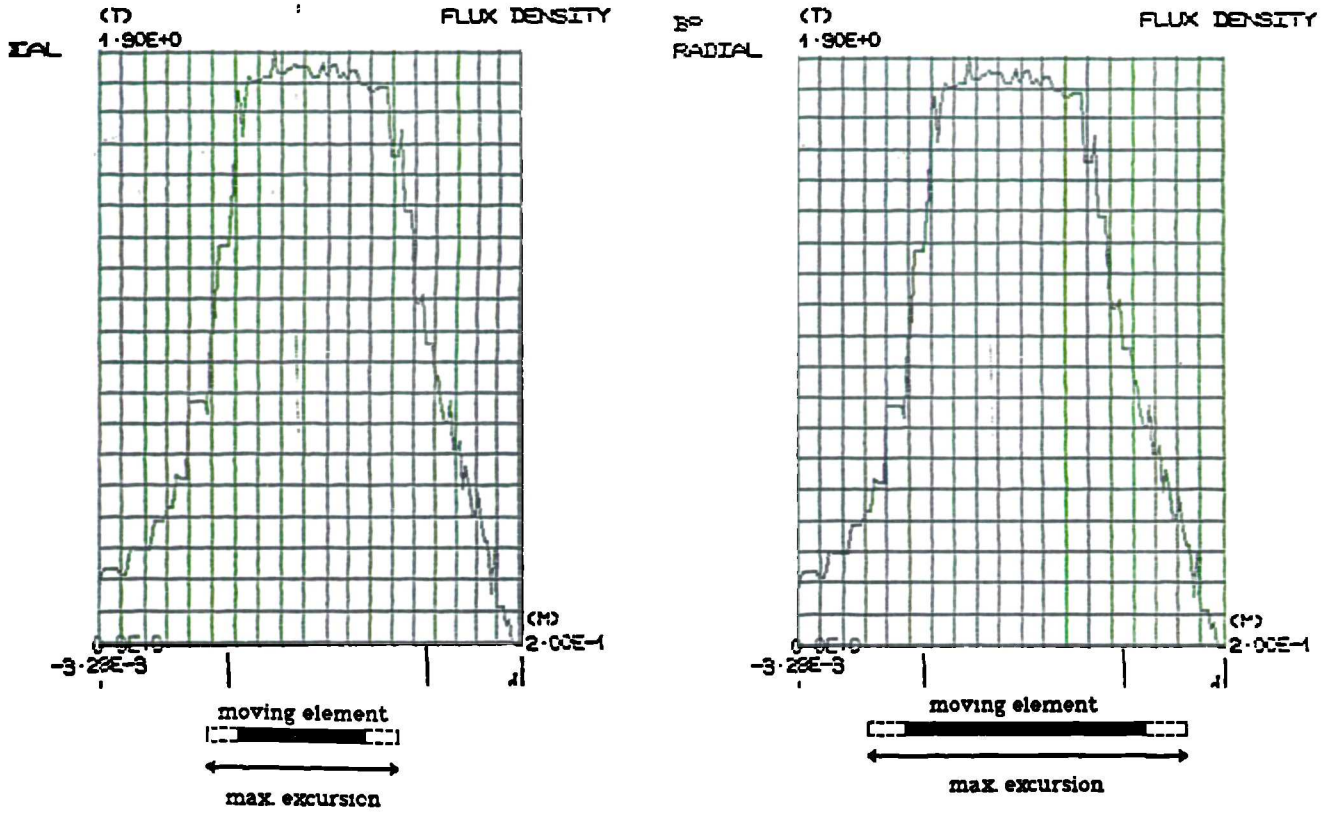
(ii) Upwards Position



(iii) Downwards Position

Fig. 51 Average Flux Density Plots for the 3 Main A.C. Coil Positions

A very short coil or a very long coil (axially) will reduce the problem of non-uniform thrust being developed, even at the extreme excursion points, as shown in Figure 5m.



(i) Short Coil *(ii) Long Coil*

Fig. 5m Different Axial Lengths of A.C. Coils for Same Flux Distribution in the Air-Gap

As long as the coil-ends stay within either the high flux area or the low flux area, there will be no, (or only very slight), variation in thrust at a given frequency. However, too long a coil will produce unnecessary losses as only a small proportion of the copper will be fully immersed in the d.c. flux at any instant, and hence inv lved in producing thrust. Also, there will be a slight weight increase due to the additional copper, membrane and bonding materials required for the longer length. On the other hand, a very short coil will mean reducing the conductor cross-section since the active number of turns must be preserved to produce the same thrust at the amplifier current limit. This will raise current densities and aggravate heating problems. The compromise typically reached involves choosing an a.c. coil axial

length some 15% longer than the pole face height, and this is applied to all sizes of machine. This is partially justified on the grounds that virtually the entire local fringe field then contributes to thrust production at medium and high frequencies, and low frequency specified maximum displacements tend to scale with shaker size.

(iv) Stray Flux Levels

The level of flux at the table top should ideally be eliminated or at least minimised, as certain test loads may be adversely affected. A steel screen can be used to reduce d.c. flux and a copper screen for a.c. flux. In addition, a d.c. degaussing coil can be included in the shaker design, positioned between the top of the magnetic ring and the table, as can be seen in Figure 5n. Stray flux values at the table surface can be calculated using MAGNET and used to determine the size of degaussing coil required, if any.

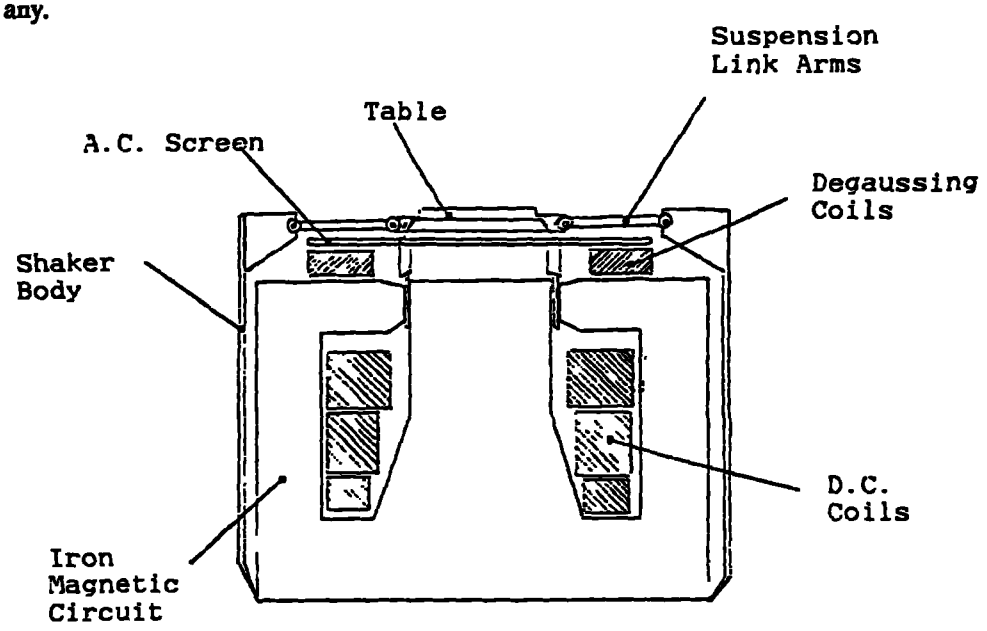


Fig. 5n Position of Degaussing Coil and Screens

Once the average level of stray flux at the table top has been established, the number of ampere-turns required to nullify this level, (or reduce it to an acceptable level), can be determined reasonably accurately using the standard equation [8],

$$B_z = \frac{\mu_o . N . I . r^2}{2(r^2 + z^2)^{3/2}} \qquad \ldots\ldots\ldots\ldots\ldots (5.23)$$

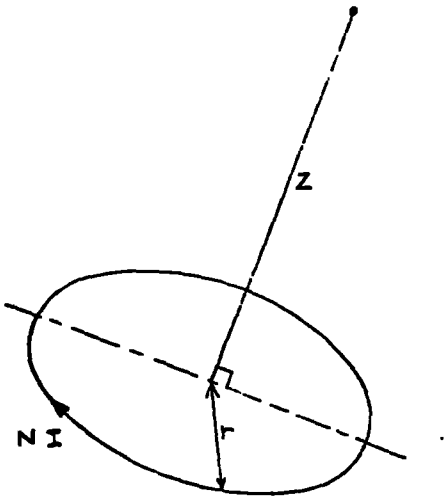
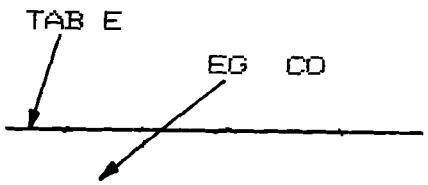


Fig. 5o Flux Density on the Axis of a Circular Coil

The resultant ampere-turn value for the degaussing coil is then used in a further MAGNET run to confirm the reduction in stray flux at the table top. Figure 5p indicates the stray flux fields with and without the degaussing coil, (no extra screening is present here).





(i) Without Degaussing *(ii) With Degaussing*

Fig. 5p Stray Flux Fields

(v) General Comments on Use of MAGNET

This software tool has proved to be helpful for our design purposes and is certainly useful in providing the designer with useful, relevant information with a minimum of effort on his part. A designer can take a maximum of about 4 days to be able to use most of the package's major facilities with relative ease. The user requires a fair understanding of his or her problem and how to set it up according to MAGNET's data input requirements, e.g. which nodes to constrain according to whether the boundary is a Dirichlet or Neumann boundary, etc. A detailed knowledge of the internal workings of the solution method, (i.e. the finite-element methods used and the approximations made), is usually of academic interest only and is not strictly essential for the routine use of the package.

There are five distinct sub-programs within the main package that the user needs to use to be able to form his problem and solve it.

Mesh Definition

Since the version of the package used could only deal with problems in two dimensions, (though a three-dimensional version has recently become available), the first stage involves deciding which two-dimensions are of importance, which axis or axes of symmetry, (if any), to use in building the mesh, (which takes the form of triangular elements), and what are the salient features of the machine being modelled. The geometry of the model is usually defined using rough sketches on sheets of graphed paper. The main x and y coordinates of the total mesh are then supplied to the automatic mesh generator. Each material used in the model, (steel, copper and air for shaker design), is defined by labelling the relevant triangular elements. After the mesh is suitably refined and all irregularities, like badly-defined elements or misplaced nodes, have been eliminated, the relevant boundaries are set and labelled.

Material Specification

All magnetisation curves, (B/H curves), for magnetically permeable materials are then defined. Each material is described by a mean magnetisation curve and two further curves, which may denote loss density, incremental permeability or some other quantity, can also be defined. The curve library within MAGNET can hold up to 128 material descriptions. the curve for the particular type of steel used in existing shakers and also for the prototype machine is shown below.

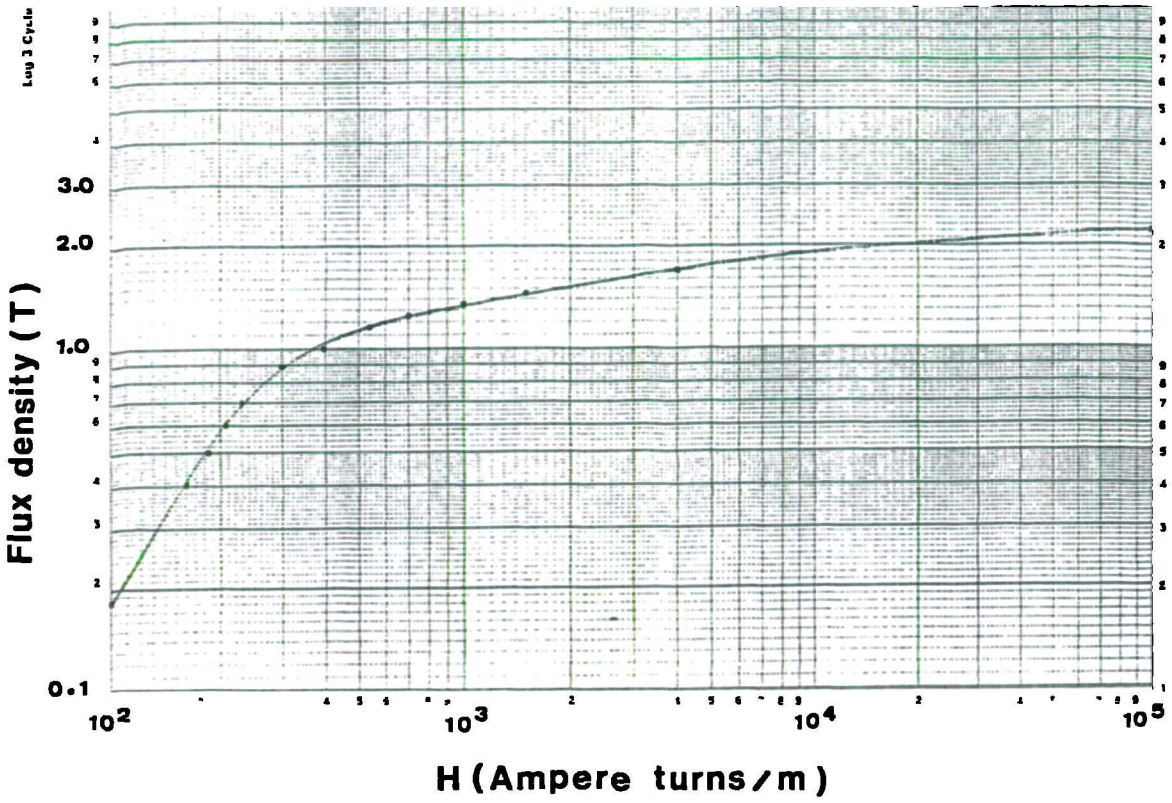


Fig. 5q Magnetisation Curve for Cast Steel of Shaker (BS1617 Grade A)

Problem Description

This next stage allows the user to define the problem type, (whether it includes hard or soft materials), excitation sources, e.g. d.c. coils in this case), boundary constraints, (e.g. the outermost boundary of the model, which is usually the air space surrounding the shaker iron, is forced to be at zero potential, which is the theoretical case at infinity), etc.. Several different problems can be set up at once, so that the effect of altering, say, the d.c. ampere-turns can be observed. The finite-element solver will then solve the first problem and then go on to the next, using the solution of the previous problem as the next starting point.

Solving

The solver type should be cho en with care depending on whether the problem involves linear or non-linear materials or a combination of both, and whether the solution is required in the x-y or r-z plane, etc. The electromagnetic shaker designed here made use of the r-z plane, so the RZPM solver, (Axisymmetric Non-Linear Magnetostatic solver), was selected. Typical solution time for a heavily saturated model of about

900 nodes and 1700 elements was about 20-25 minutes on the IBM PC XT/286 personal computer with an EGA (Enhanced Graphics Adapter) board running off the hard disk.

Post-Processing Results

The post-processor is then invoked to deal with the mass of information produced by the solver. The solution obtained from the solver stage is usually in terms of a field of magnetic vector potentials, A. Manipulation of this field of values will then yield the required items of interest, e.g. flux line plots, flux density levels, forces, etc.. The user can create his or her own little 'subroutines', called 'user-verbs', within the post-processing sub-program to perform various calculations on the vector potential field with ease.

5.2. Comparison Between the Single-Ended, Double-Ended and C-Core Configurations [15]

It is quite difficult to make general comparisons and conclusions about existing shaker designs, let alone new ones, as there are so many design variables and second-order performance criteria that need to be taken into account. Thus, it is doubly difficult to generalise about the three current shaker configurations. An attempt has been made here to try and minimise these difficulties by :

(a) considering 3 equivalent hypothetical shaker designs, one of each configuration, having simply related values of major design features;

(b) concentrating on just a few of the important assessment criteria (e.g. thrust, iron weight, equivalent circuit parameters);

(c) not considering second-order phenomena such as d.c. flux fringing.

The author feels that the comparison should be carried out in two stages, one dealing with the electrical aspects and the other with the mechanical aspects.

5.2.1. Electrical Aspects

Assumptions

(a) The three designs are assumed to have :

(i) equal maximum thrust

(ii) equal a.c. ampere-turns per axial cm of coil height
(i.e. equal a.c. amps in a given conductor size, or equal a.c. current density, or equal watts/cm² of coil surface area).

(iii) equal d.c. flux density in gap

(iv) equal iron saturation

(v) equal radial gap length

(vi) equal number of a.c. coil layers

(b) Maximum thrust, F, is taken as equal to :

= air-gap flux density x axial AT/cm x pole face area

$= B \times AT/cm \times \pi . D_m . h . N_p$

where,

D_m = mean gap diameter
N_p = number of air-gaps in the shaker
h = axial pole face height

or,

$$F = B.I.\pi.D_m.N.N_p$$
$$= B.J.\pi.D_m.h.N_p$$
$$= B.J.A$$
$$= (N_p.\phi_{DC}).J$$

where,

A = total pole face area = $\pi.D_m.N_p.h$
ϕ_{DC} = d.c. flux in the shaker = $\pi.D_m.h.B$
J = NI/h
N = number of a.c. coil turns immersed in d.c. flux per air-gap

Note that $N_p = 1$ for the single-ended and double-ended configurations, and $N_p = 2$ for the c-core configuration.

Discussion Points

(i) Since the three shakers share common values of B and J, and we need equal maximum thrusts, each must be given the same total pole face area, ($\pi D_m h N_p$).

(ii) Since the ϕ_{DC} values in the single-ended and double-ended shakers are equal, the ϕ_{DC} in the c-core shaker is half this value.

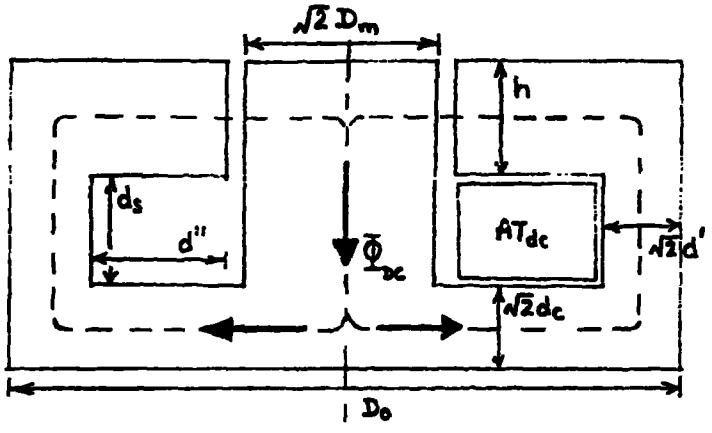
(iii) The d.c. flux in the double-ended shaker splits two ways on reaching the centre pole, and the centre pole cross-sectional area can hence be half that of the single-ended shaker. Thus, the centre pole diameter in the double-ended shaker can hence be $1/\sqrt{2}$ that needed in the single-ended case. The centre pole diameter in the c-core machine can also be $1/\sqrt{2}$ that of the single-ended case, again due to the halved value of ϕ_{DC}.

(iv) The pole face height, h, must be increased in the double-ended shaker by $\sqrt{2}$ to preserve the ($\pi D_m h$) and hence the thrust.

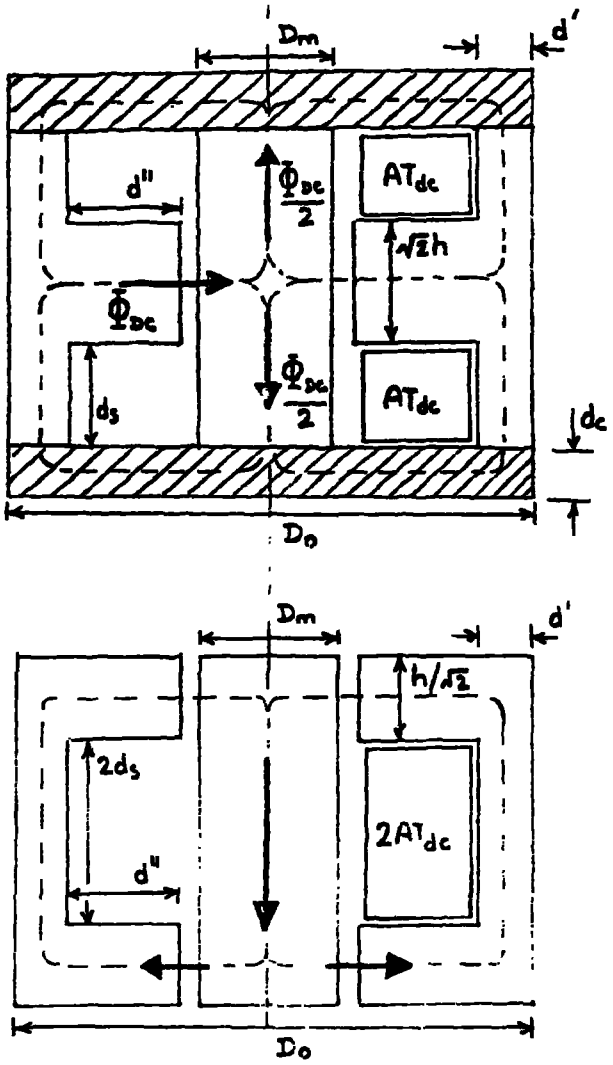
(v) The c-core can be envisaged as simply half a double-ended, (say the upper half), with the top iron disc interrupted by an airgap. The total pole area at ($2hD_m N_p$) is unchanged, and the pole height at each airgap is $1/\sqrt{2}$ that of the single-ended and $1/\sqrt{2}$ that of the double-ended.

A diagrammatic comparison has been made of the three shaker configurations.

Comparison of Cross-Sections



Single Ended



Double Ended

C Core

Fig. 5r Typical Cross-sections

In the cross-sections detailed above, the symbols h, D_m, etc. are supposed to have equal numerical values for all three configurations. Typical aspect ratios, (average taken for two standard current machines, the VP85 and the VP700LT), for the single-ended unit, are :

$D_o/D_m = 1.85$

$d'/d'' = 0.76$

$d''/D_m = 0.3$

$d'/D_m = 0.22$

$d_c/h = 3.2$

Equivalent Circuit Parameters

Here we can show that if the shakers' a.c. coils employ equal turns per axial cm., their a.c. equivalent circuits in almost all respects are identical, given the assumptions made earlier.

(a) Motional Impedance

$$Z_m = E/I$$

$$= \frac{k_v^2 . \hat{\dot{x}}}{\hat{F}}$$

where,

$$k_v = F/I$$
$$= B.\pi.D_m.N.N_p$$
$$= A.N/h.B$$

Hence if the shakers use the same values of turns per axial cm of pole height N/h, they will have equal k_v. Hence for equal maximum velocity and thrust, (or equal thrusts, total moving mass and suspension characteristics), the shakers will also share a common value for Z_m.

(b) A.C. Winding Resistance

$$R_1 = \pi.D_m.N.N_p/\text{conductor cross section } a_c$$
$$= \pi.D_m.h.N_p.(N/h).(1/a_c)$$
$$= A.(N/h).(1/a_c)$$

The three shakers share common values of A and N/h. Since they also share common values of gap length and number of layers, and have equal N/h, the a_c values will also be equal. hence a.c. winding resistances will be equal.

(c) A.C. Leakage Inductances

$$\text{A. C. Leakage Inductance} = N_p.N^2/\text{path reluctance}$$
$$= \frac{N_p.N^2}{(h/\pi.D_m.\mu_o).k.g}$$

where g is the radial gap length and k is a design related constant. (k . g) will be equal for all three shakers, given the common gap lengths, winding thicknesses and

so on.

Hence,

$$L \propto N_p.(N/h)^2.h.D_m$$
$$\propto N_p.(N/h)^2.A/(\pi N_p)$$
$$\propto (N/h)^2.A$$

Hence leakage inductances for each of the three layouts will be equal. So far as the secondary leakage inductances, (referred to the a.c. coil), are concerned, a similar argument applies.

(d) Plating Resistances Referred to the A.C. Coil

$$R'_2 = N_p.(\pi D_m/\text{plating cross section}).N^2$$
$$= N_p.\pi D_m.N^2/t.h$$

where t = plating thickness on centre pole + plating thickness on magnetic ring.

$$R'_2 = \frac{A.(N/h)^2}{t}$$

Hence if the shakers employ a common t, they will possess equal values of R'_2.

(e) Magnetising Inductance, L_m

$$L_m \propto N_p.N^2.\mu_o.(h/3).\pi.D_m.(1/g)$$
$$\propto (N/h)^2.h^2.A.(1/g)$$

If, as before, we compare shakers having equal N/h, A and airgap length g, the magnetising inductances will be in the ratio 1 : 2 : 0.5 for the single-ended, double-ended and c-core shakers respectively.

These are substantial differences. However since the L_m is shunted by the plating branch in the equivalent circuit, the author is reasonably certain that the differences are of second order importance only to the overall operation of the shaker, though they considerably affect the frequency at which the plating starts to carry substantial

eddy currents.

(f) Conclusion

Except for the magnetising inductance, L_m, the value of each component in the equivalent circuit would hence seem to be independent of the shaker's configuration, given the assumptions made. This means that the input voltages, currents, kvas etc. will be very similar over the entire frequency range.

From the above section it is possible to state immediately that the watts/cm^2 for both the a.c. coil, (I_1^2 . R_1 / A), and plating, (I_2^2 . R'_2 / A), will be independent of the configuration.

5.2.2. Quantitative Mechanical Aspects

The following sections refer to Figure 5r.

Iron Weight Comparison

(a) Unshaded volume of double-ended unit = volume of c-core unit.

(b) Volume of single-ended unit (on Assumption A ; see below)

= $(\sqrt{2})^3$ x volume of 1/2 the double-ended unit

= $\sqrt{2}$ x volume of double-ended unit.

Assumption A - All main dimensions of the single-ended unit, D_m, h, d_s, d", d', d_c are $\sqrt{2}$ up on those of the double-ended unit. In fact, the d.c. slot dimensions d_g x d" will be the same. Hence the single-ended unit's iron weight will be somewhat less than $\sqrt{2}$: 1 up on that of the double-ended.

(c) Conclusion in Respect of Iron Weight

Single-Ended - *heaviest*
Double-Ended - *medium*
C-Core - *lightest*

D.C. Copper Weight Comparison

Total d.c. ampere turns are :

Single-Ended	*1*
Double-Ended	*2*
C-Core	*2*

The single-ended d.c. coil's mean diameter is $\sqrt{2}$ higher than the other two. Hence, the d.c. I^2R and copper weights will be in the ratio :

Single-Ended	$\sqrt{2}$
Double-Ended	*2*
C-Core	*2*

Hence d.c. copper weight and d.c. power are equal for the double-ended and c-core shakers, and smaller in the single-ended shaker by a factor of $\sqrt{2}$.

Moving Element Comparison

The sketches below are drawn to a common scale and indicate the electrical portions of each moving element.

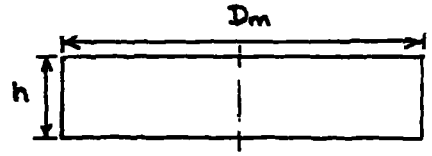
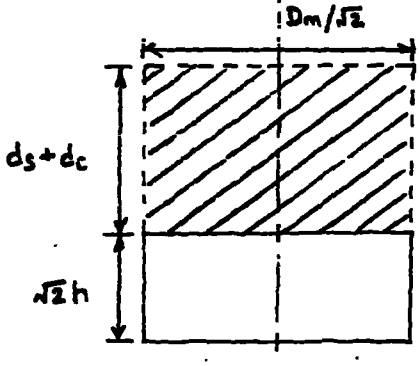
Copper weight	*Ampere-turns*	*I^2R loss*		
1	*1*	*1*		Single Ended
1	$\sqrt{2}$	*1*		Double Ended

Fig. 5s (i) Moving Element Comparison (Single Ended and Double Ended)

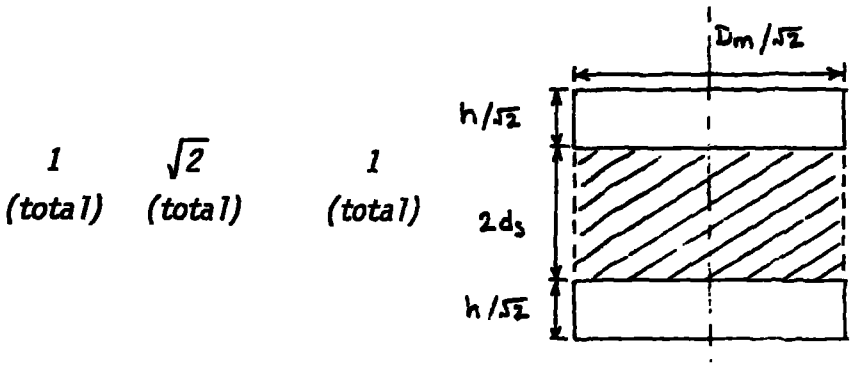


Fig. 5s (ii) Moving Element Comparison, contd. (C Core)

A.C. Winding Copper Weight

$$Weight = N_p.\pi.D_m.N.a_c.\sigma = A.(N/h).a_c.\sigma$$

where,

σ = *current density*

A.C. winding copper weights will hence be independent of the configuration.

A.C. Coil Overhang

It has been assumed so far in comparing resistances, copper weights and so on that the a.c. coil height is simply h. In practice it must be at least $(h + \hat{\hat{x}})$, unless a short coil construction is used in which case the pole face height must ideally be at least = (coil height + $\hat{\hat{x}}$). The percentage penalty on a.c. copper weight, I^2R loss, etc. for this extra coil height will be $(h + \hat{\hat{x}})/h = 1 + \hat{\hat{x}}/h$.

Hence shakers having a large h come off best here. With $\hat{\hat{x}}$ = 2.5 cm and h values for the single-ended, double-ended and c-core of 14 cm, 20 cm and 10 cm respectively, the percentage penalties are :

Single-Ended 18 %

Double-Ended	*12.5 %*
C-Core	*25 %*

The double-ended configuration is hence at a slight advantage here in respect of coil weight and coil power loss, (though not in respect of watts/cm^2), and very slightly better off in respect of input kVA, (the kVA $= \sqrt{P^2 + Q^2}$ relation minimises the importance of P over much of the frequency range). Though the c-core configuration comes off worst so far as these penalties are concerned, the differences are only just large enough to be worth considering, (6% and 11% with respect to single-ended and double-ended configurations respectively).

5.2.3. Qualitative Mechanical Features of the Three Configurations

(a) Single-Ended Machine

Moving Element Length

For this configuration, helped by the short axial distance between coil and table and by the small L/D aspect ratio of the coil, the moving element axial length tends to be short. This will mean a reduction in 'axial resonances' in the moving element during high frequency operation of the shaker. Using the shaker in the horizontal position will pose no problems since the support for the moving element at the top will be sufficient to prevent the element from acting like a cantilever. The total moving mass will tend to be low and the short coil is easier to wind.

Servicing the A.C. Coil

The short length means that the entire suspension system can be above the shaker's magnetic circuit, reducing mechanical complexity. It will hence be relatively easy to service/change the a.c. coil on site since this just involves unbolting the suspension link arms, detaching the a.c. coil leads, and then lifting out the moving element. Special lifting equipment should not be necessary.

D.C. Degaussing

Because the air-gap is situated at the top of the magnetic circuit, airgap fringe fields tend to extend into the table region and a d.c. degaussing coil may hence be required. The number of ampere-turns required can be quite considerable, in order

to reduce the flux at the table surface to acceptable levels.

Mechanical Construction

The single-ended configuration is mechanically simple to construct. It may be possible to further reduce the machining necessary. If flat magnetic rings were to be used instead of sloping pole tips, and if a cylindrical centre-pole piece could be used instead of the tapered centre-pole base which is currently used, then further savings in machining costs would be possible at some possible cost in electrical performance. Trial solutions using flat-topped pole pieces and cylindrical centre-poles have been investigated theoretically and in fact no adverse effects have been noticed apart from slight increases in iron weight.

(b) Double-Ended Machine

Moving Element Length

Here, the moving element length will be longer than for the S.E. case as the air-gap is situated in the middle of the magnetic circuit. Because of this longer element, 'axial mechanical resonances' may be more of a problem at the higher frequencies. Hence, the moving element may well require a bottom-end support, for example a second set of link arms or roller supports built into the centre-pole. Shaker operation in the horizontal mode may accentuate the need for a bottom-end support. The total moving mass will tend to be heavier than for the S.E. case.

Servicing the A.C. Coil

It will be difficult to service/change the coil on or off site. This is because, with the D.E. configuration, the top iron structure, (which forms part of the magnetic circuit), will have to be removed to gain access to the coil, and lifting equipment is more likely to be needed due to the weight of the top iron structure.

D.C. Degaussing

Because the air-gap is situated in the middle of the magnetic circuit, the top iron structure will provide some shielding. Hence, the d.c. degaussing coil required can have fewer ampere-turns than for the S.E. configuration.

Mechanical Construction

The D.E. magnetic circuit is mechanically more complex, due to the top iron structure which needs to be segmented to allow mechanical connection of the table to the a.c. coil. As regards reducing machining costs and simplifying the magnetic circuit further, the same points that apply to the S.E. case also apply here.

(c) C-Core Machine

Moving Element Length

The moving element for the c-core configuration is likely to be the longest due to the presence of the two air-gaps, top and bottom of the magnetic circuit. There is thus a risk that the axial stiffness of the moving element is likely to be less and problems associated with 'axial mechanical resonances' may be more pronounced. This also points to the need for a lower-end support, particularly during large coil displacements and horizontal shaker operation. Because the moving element is quite long, it is important that the former, on which the a.c. coils are wound, is in fact designed to be relatively stiff, (radially as well as axially) so that, with the help of a lower end support, any likelihood of the moving element 'flapping' about during shaker operation is reduced. However, the total moving mass will also be increased unless high performance materials are used. If such materials are used, significant cost penalties may be introduced partly because, unlike the formers for the S.E. and D.E. configurations, which can be produced in-house, such a former is likely to have to be built by a sub-contractor.

Servicing the A.C. Coil

Servicing the a.c. coil on or off site should not prove to be too difficult provided only a top-end support is required for the moving element. Just as for the S.E. configuration, the link arms will have to be unbolted, the coil leads detached and the moving element lifted out. However, if a lower-end support is being used, then the removal of the moving element will be more difficult. This again depends on the type of lower-end support being employed. If it is a second set of link arms then it will be quite difficult to remove. On the other hand, if rollers were used, (recessed into the centre pole), then removal should be no real problem.

D.C. Degaussing

As for the S.E. case, fringe fields from the top gap are likely to be a problem. To

reduce d.c. flux levels at the table top, a top degaussing coil will be needed. If it is also necessary to reduce stray d.c. flux levels outside the shaker, and not just at table top level, it may be wise to use a second degaussing coil situated at the bottom of the machine, due to the presence of the bottom air-gap.

Mechanical Construction

The c-core configuration is easier to construct, in the sense that simple castings can be made up, just as for the S.E. case. But if a lower-end support is to be used, this will involve further machining and drilling of the centre pole, (if rollers are to be used). A base plate will most probably be required to hold the centre pole and lower magnetic ring. It can be made out of some strong but light-weight material like aluminium alloy. This base plate could in fact be quite complex, where machining and casting is concerned.

5.2.4. Choice of Steel and A.C. Coil Construction

The pros and cons for these aspects of shaker construction are common to all three configurations.

Steel Types

A strong magnetic field in the gap with a high flux density is obviously beneficial whatever the compromises are regarding coil diameter but economic considerations must be taken into account. It may be possible to use ordinary magnetic steel for the main shaker body and higher quality magnetic steel for the magnetic ring and centre-pole. This will help to reduce the overall cost of the shaker unit. It may also be conceivable to use steel which has a higher saturation limit for the pole tips and centre-pole, for example Permendur 24. This will mean that higher flux densities can be obtained in the magnetic circuit. It will also mean that the same gap flux, (using ordinary magnetic steel), can be obtained for fewer d.c. ampere-turns. However, the cost of this new steel, (Permendur, etc.), may be prohibitive as a fairly large amount will have to be used, (kilogrammes here instead of the grammes used in small devices like tape heads, magnetic relays etc.). But in cases where it is important to keep the weight of the shaker unit down it may be economically feasible to use the higher grades of steel available.

Adopting a higher grade of steel may be necessary in order to keep the iron losses down, and ideally the magnetic circuit should be built up of laminated steel. But the direction of d.c. flux flow within the magnetic circuit necessitates the use of radial laminations which could be extremely costly and could create manufacturing

problems.

The present range of shakers u e carbon steel ca tings with h'gh magnetic permeability and conform to BS1617 Grade A. The e are clas fied as being suitable for use in the electrical industry, (e.g. m tor cases, y kes, rotors. frames, etc). The magnetisation curve is shown below t gether with the curve for Permendur 24.

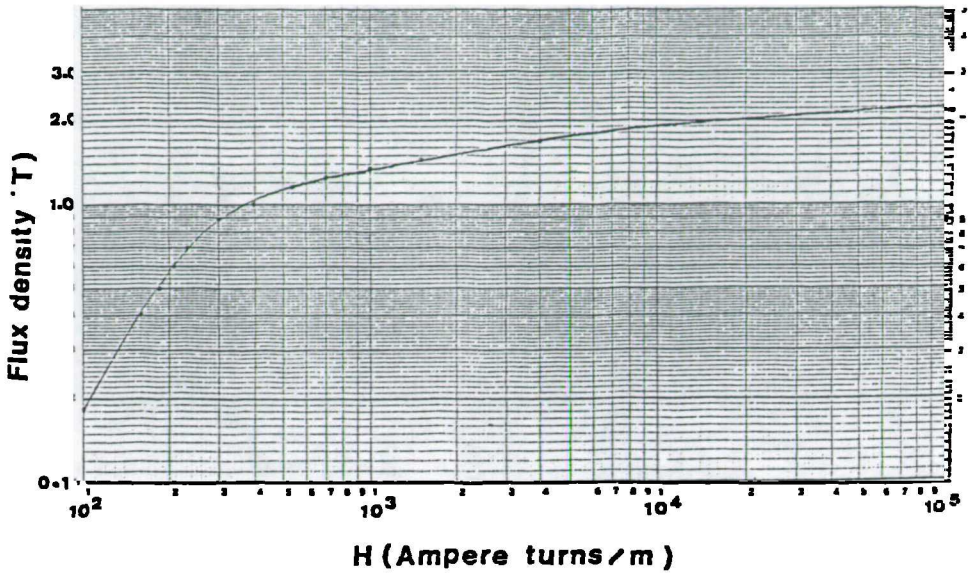


Fig. 5t Present Shaker Steel (BS1617 Grade A)

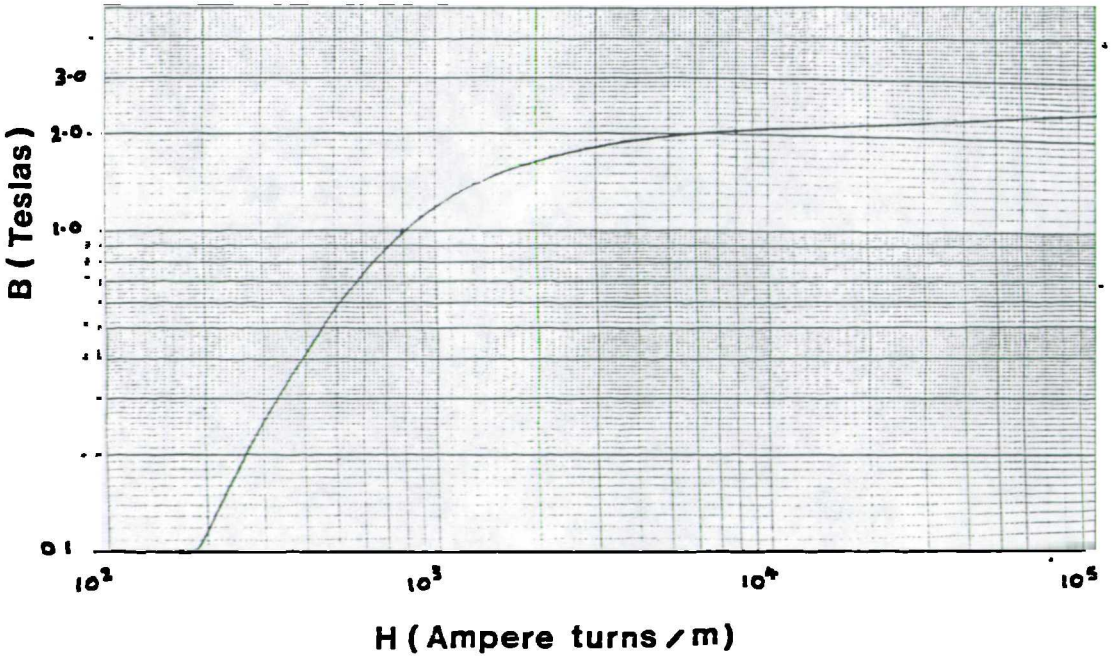


Fig. 5u Permendur 24

Moving Coil Construction

The single-layered a.c. coil may be used for the single-ended shaker but this means that the coil will have to work at higher temperatures, (due to coil resistance being higher, because smaller conductor cross-sections have to be used to get the required number of turns in the axially short air-gap), in order to preserve the thrust. For shakers being driven by the smaller size amplifiers, (e.g. 6, 12 and 18 kVA), air-cooling may still be able to be used. But for the larger amplifier sizes, (24 kVA and above), oil-drenching may be necessary. All this points to the use of the double-layered a.c. coil for such a shaker where only one axially short air-gap is available. However, the use of a double-layered winding also means that higher temperatures will persist in the copper plating, (due to the higher referred plating resistance, proportional to $(2N)^2$, where N is the total number of a.c. coil turns. The a.c. coil itself could suffer from overheating as the heat produced by the inner layer cannot be dissipated readily, unless the coil-former material possesses a high thermal conductivity.

In the case of the double-ended shaker, the same argument applies to the use of the single-layered coil but here the heating problem is alleviated to some extent. This is due to the slightly larger pole face area available, thus allowing larger conductor cross-sections to be used, thus reducing the resistance and heat flux density. Again high heating levels in the copper plating may still be a problem even if a double-layered coil were to be adopted.

The single-layered coil is ideally suited to the c-core machine for which it was originally developed. Heating levels in both the coil and copper plating will be reduced. It should be pointed out that the total heat developed by the two single-layered coils, (one for each gap), might very well be equal to the heat developed by the two cases above, but the heat per square centimetre of coil surface will be halved for the c-core machine.

The presence of the coil former in the single-layered coil alters the reluctance of flux paths and thus affects inductances and skin effect factors, (see equations in Chapter three). There are mechanical and constructional difficulties associated with both types of coil, but in-house expertise and equipment already exist for producing the double-layered coil, whereas construction of the former for the single-layered coil has to be contracted out to another company. In time, the expertise could be developed in-house to cover the single-layered coil too, but financial considerations often play an important part, especially when new ground is being broken.

5.2.5. Effect of Changes in Design Parameters on Comparison

It is possible to obtain improvements in some design and performance features at the expense of others. For instance :

(a) Thrust per pole area F/A can be increased by raising B or J. An increased B requires :

- extra d.c. ampere turns

and/or

- extra iron volume.

An increased J requires :

- two coil layers instead of one

and/or

- an increased gap and moving element thickness

and/or

- an increased a.c. current density (thinner and/or narrower conductors) giving, an increased watts/cm^2 on the a.c. coil and plating surfaces. and hence increased cooling requirements.

(b) Iron cross sections per d.c. flux can be reduced at the expense of d.c. ampere-turns.

(c) B, (i.e. airgap flux density), for a given value of d.c. flux can be increased by decreasing pole area, A, (by decreasing pole height, h, and/or coil diameter, D_m).

This results in a smaller a.c. coil, (or coils). The smaller a.c. coil would have :

- a somewhat smaller resistance and I^2R loss, depending on whether both the length and cross-sectional area are altered
- an unchanged watts/cm^2
- an unchanged motional impedance
- a somewhat lower leakage inductance
- a somewhat smaller magnetising inductance, L_m

The lower resistance would reduce input kVA in the lower frequency range. The lower leakage inductance should lower kVA requirements at higher frequencies.

(d) D.C. slot axial height can be decreased, at constant d.c. slot area, by increasing the d.c. slot radial depth. This makes the shaker height and, (in double-ended and c-core configurations), the moving element height smaller, but leads to an

increased shaker diameter. More importantly, since the d.c. flux leakage across the now narrower d.c. slot is increased, the d.c. flux level in the outer pole ring and elsewhere is raised per useful d.c. flux crossing the airgap. The useful d.c. flux will hence tend to fall unless the iron sections in the outer pole ring, etc. are increased.

General Comment on Trade-offs

Design decisions such as the one to opt for a single coil layer instead of two layers are available whatever the configuration, and result in very similar changes to performance, weight, watts/cm^2, etc..

Conclusions on Comparisons

(a) the single-ended configuration has the lowest d.c. copper weight but the heaviest iron weight.

(b) The c-core configuration has the lowest iron weight. Its d.c. copper weight is equal to that of the double-ended configuration.

(c) For equal thrusts, etc., each configuration's a.c. equivalent circuit will have the same motional impedance. This, plus the equality between the shakers' R_1 and L_1, (and hence for equal plating thicknesses R_2 and L_2), means that the configurations should share very similar a.c. performance figures.

(d) Moving element height is much less for the single-ended configuration. The height comparison between the double-ended and the c-core depends on the design values of h, d_a and d_c.

(e) Single layer coil construction affects all the configurations in a similar way, viz :

(i) need for a larger pole face area if conductor size is unchanged

(ii) lower watts/cm^2 on the plating

CHAPTER SIX
THE PROTOTYPE C-CORE MACHINE

6. The Prototype C-Core Machine

6.1. Evolution of the New C-Core Magnetic Circuit

Before deciding to opt for the c-core magnetic circuit, all three,(single-ended, double-ended and c-core), layouts were examined in some detail using the design procedures described in Chapters 3 and 5. At that stage of the project, emphasis was placed on moving away from the double-layered a.c. coil and its winding and cooling problems. Thus a single-layered winding was adopted and this prompted the evolution of a 'new' magnetic circuit, namely the c-core, incorporating two air-gaps, thus enabling the standard double-layered winding to be split into two identical single-layered windings. This meant that the two separate coils could now be wound onto a preformed coil former, simplifying the coil winding process. The absence of an inner coil also meant reduced heat stress on the overall moving coil and former, and since more copper could now be bared, this facilitated easier cooling. It was discovered in the process that even with the larger amplifier sizes, air-cooling of the moving coil was still possible, where previously oil-drenching had to be used.

A further point in favour of the c-core magnetic circuit, which has also been touched upon in reference 7 is this: because the d.c. field produced by the d.c. coils has opposite directions in the two air-gaps, the current in the two a.c. coils must also flow in opposite directions to be able to produce a resultant force in one direction. The mmfs developed by the a.c. coils therefore largely are hence equal and opposite fields minimising the extent of a.c. fields in the shaker's iron work and possibly reducing iron losses.

In developing the c-core machine, several factors had to be borne in mind :

(i) Simple square and rectangular iron cross-sections throughout the magnetic circuit were to be used wherever possible, to reduce casting and machining costs.

(ii) the total axial length of the moving element had to be as short as possible to preserve the stiffness of the coil former and reduce any axial modes of resonance during shaker operation.

(iii) established d.c. coil current density limits, (approximately 1.62 x 10^6 A/m^2 to 2.0 x 10^6 A/m^2), were to be observed hence fixing the d.c. slot cross-sectional area for a desired ampere-turns.

(iv) established d.c. I^2R loss limit for a certain size of machine were to be observed.

(v) the centre pole diameter should not be excessive in order to avoid excessive moving element weight and size.

(vi) iron weight had to be either less than or equivalent to the existing equivalent shaker to enable direct comparisons to be made.

About 16 major design iterations were carried out in conjunction with technical discussions with the sponsors before freezing the prototype machine design. Figure 6a indicates the evolution of the magnetic circuit of this prototype c-core shaker. The vertical axis of symmetry of the machine is made use of and consequently only half the shaker is shown here. The following development history presents in highly summarised form, a process that occupied several months design work. Finite element computer runs were performed at each stage; full dynamic predictions were made at a majority of the stages.

Design MC6

Design MC6 was a first attempt at producing a shaker with a c-core layout incorporating the single-layered a.c. coil concept. Overhanging pole-tips were used to try and alleviate the flux saturation in the pole tip area immediately adjacent to the air-gap, by presenting a somewhat larger cross-sectional area to the d.c. flux crossing the air-gap, than would otherwise be the case without the overhangs. Design MC6 showed very high flux saturation in the centre pole area and the very narrow outer side limb, thus restricting the d.c. flux flow through the iron, resulting in more leakage flux and thus a relatively low average flux density in the air-gap of about 1.08T.

Design MC6A

MC6A attempted to overcome these problems by having a larger centre pole diameter and thicker side-limbs. This resulted in a higher working air-gap flux density of about 1.31T but required heavier iron cross-sections and also resulted in a larger and heavier moving coil and table.

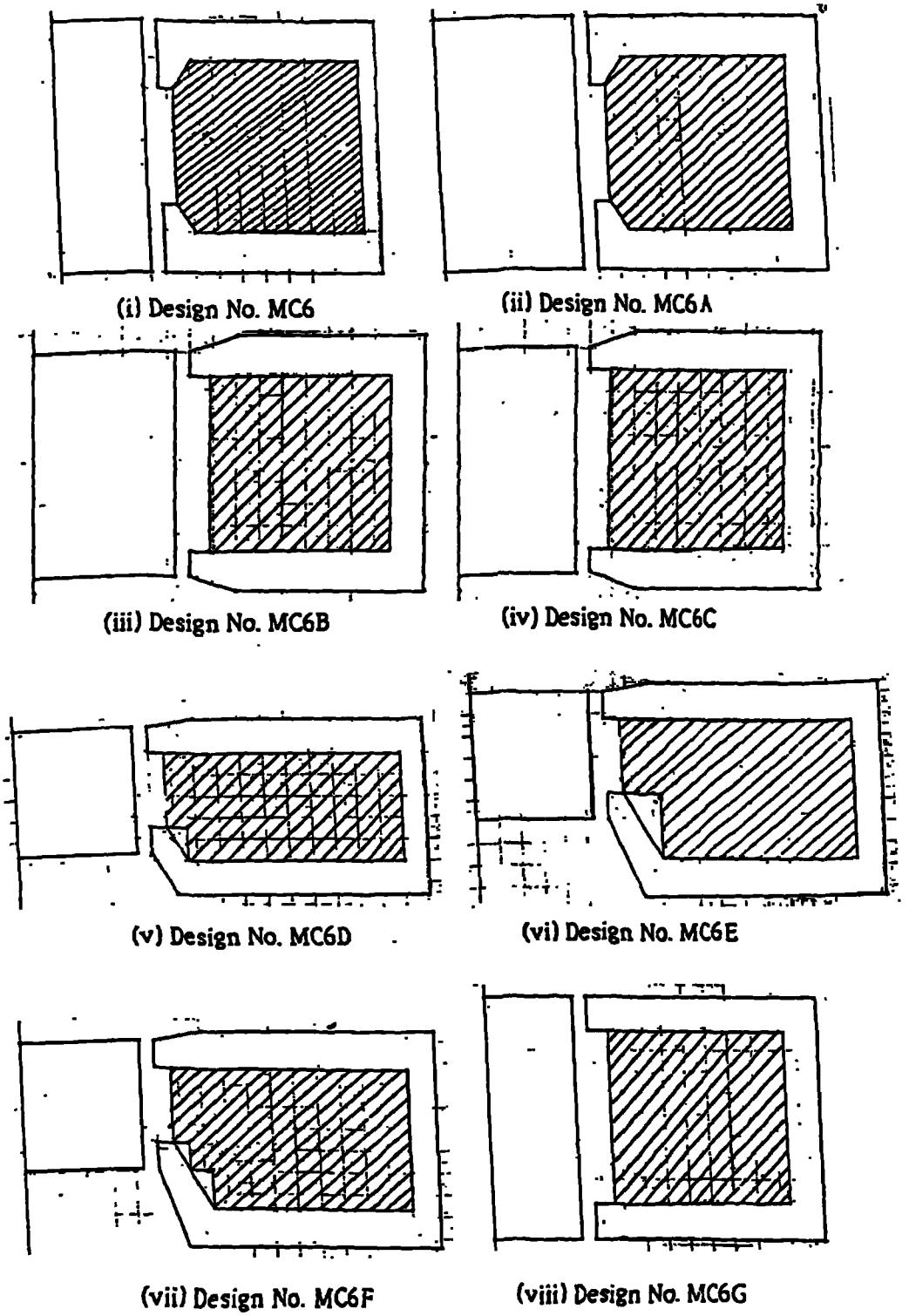
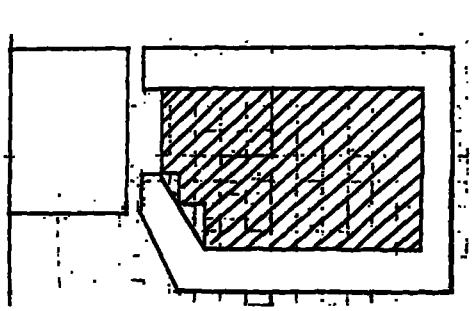
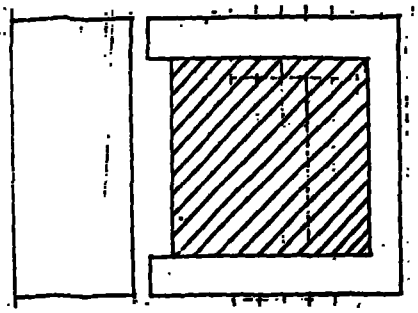


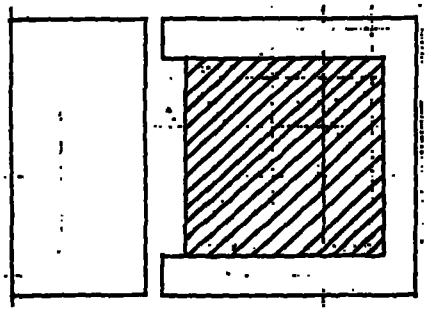
Fig. 6a (i) Development of the C-Core Magnetic Circuit



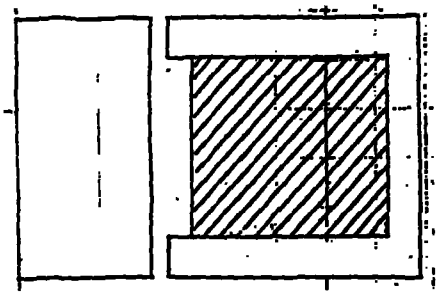
(ix) Design No. MC6H



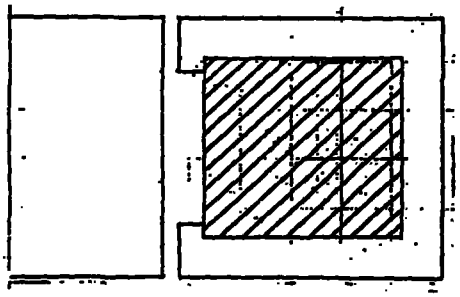
(x) Design No. MC6I



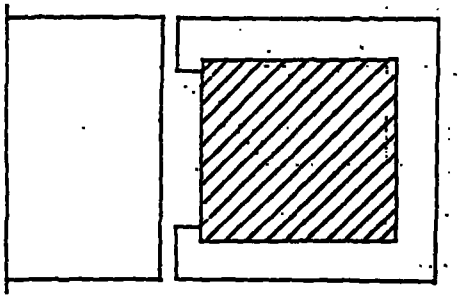
(xi) Design No. MC6J



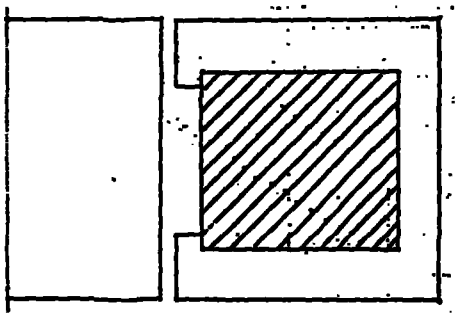
(xii) Design No. MC6K



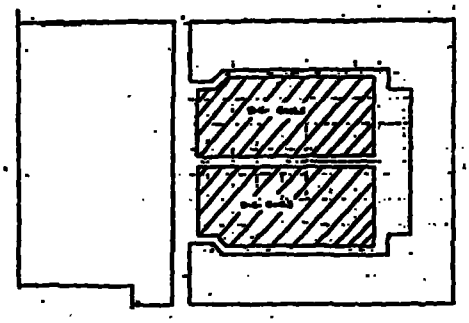
(xiii) Design No. MC7A



(xiv) Design No. MC7B



(xv) Design No. MC7C



(xvi) Design No. DB85

Fig. 6a (ii) Development of the C-Core Magnetic Circuit

Design MC6B

Reducing the centre pole and magnetic ring pole face heights, and tapering the pole tips produced Design MC6B. Tapering the pole tips produced a flux concentration effect in the air-gap, and together with the removal of the pole overhang, raised the average flux density to 1.71T. The shorter centre pole height meant a shorter moving element and hence a shorter shaker axially, which was a step in the right direction. But, on the other hand, the shorter pole face heights necessitated the use of smaller conductor cross-sections for the a.c. coil, (to keep the number of a.c. coil turns and hence thrust the same), and this tended to increase resistances, leading to voltage limiting in the mid to high frequency band, thus reducing the overall working bandwidth of the shaker.

Design MC6C

Here an attempt was made to try and reduce the overall moving element diameter by a reduction in centre pole diameter, while keeping all other main dimensions the same. This had the effect of raising the centre pole saturation level and hence lowering the average air-gap flux density. This meant that the input current had to be increased to maintain thrust and we ended up trading flux density for current, leading to unacceptable heating levels.

Design MC6D

The long moving element of the initial designs was a source of uncertainty and worry as regards the moving element's mechanical performance and pushed the design process into the first of several 'Dog-Leg' designs, so called because of the shape of the lower limb. This alteration to the magnetic circuit greatly reduced the moving element's height from approximately 20.5cm to about 11.8cm. This design made use of a larger d.c. slot and an unchanged centre pole diameter. The main problem associated with this type of magnetic circuit was the different flux leakage fields encountered at the upper and lower limbs, due of course to the unusual shape of the lower limb. This tended to produce significant differences between the d.c. flux densities in the two gaps. This led to worries that the top coil would then experience a different thrust from that experienced by the bottom coil, possibly stressing the two coils and former unnecessarily and maybe even causing distortion in the table top motion. This problem could possibly be alleviated to an extent by winding differing numbers of turns for the two a.c. coils.

Design MC6E

An attempt was made to increase the reluctance of the leakage flux paths in the region of the lower limb's air-gap in order to reduce leakage flux and hopefully push up the working flux density in the lower air-gap, which was rather low for Design MC6D. This seemed to work raising the mean flux density from 1.279T (for Design MC6D) to 1.415T. But the differences in the air-gap flux densities for the two air-gaps still remained.

Designs MC6F & MC6H

These two designs were further attempts to bring the two air-gap flux densities closer into line by making alterations to the lower limb. But it was finally decided that the added complexity of the lower casting and hence the extra costs involved did not justify a 'dog-leg' design, even if the moving element height was reduced.

Design MC6G

MC6G incorporated a simple iron construction using simple rectangular sections, but inevitably led to a longer moving element and larger centre pole diameter. But the working flux density in the two air-gaps averaged out well.

Designs MC6I to MC6K

These three designs were iterations to reduce flux saturation levels in the outer limb, while at the same time trying to reduce the moving element height, by increasing the diameter of the centre pole and hence the overall shaker diameter.

Design MC7A

This design used a longer pole face, so that the required a.c. ampere turns could be accommodated within the region of 'constant' flux density in the air-gap without the need for excessive a.c. current density. This enabled slightly larger conductor sections to be used, thus increasing the available area of bared copper for cooling purposes.

Designs MC7B - MC7C

These two designs were iterations to improve the utilisation of the iron and

to reduce d.c. slot leakage. This led to Design MC7D, also known as the DB85 which was adopted as the prototype c-core shaker after one or two minor modifications.

Design DB85

The prototype was named the DB85 as it had the equivalent rating of a standard VP85 machine and would replace the VP85 if possible. The centre pole was spigotted onto a cast aluminium base plate which held the centre pole to the lower annulus.

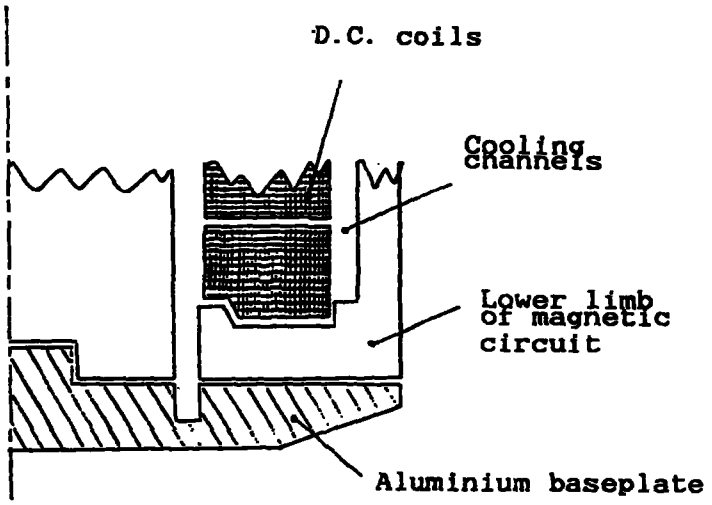


Fig. 6b Lower Half of C-Core Machine Showing Base Plate

The centre pole had four shallow holes drilled radially into it to hold four sets of spring loaded rollers which prevented the moving element from coming into contact with the centre pole.

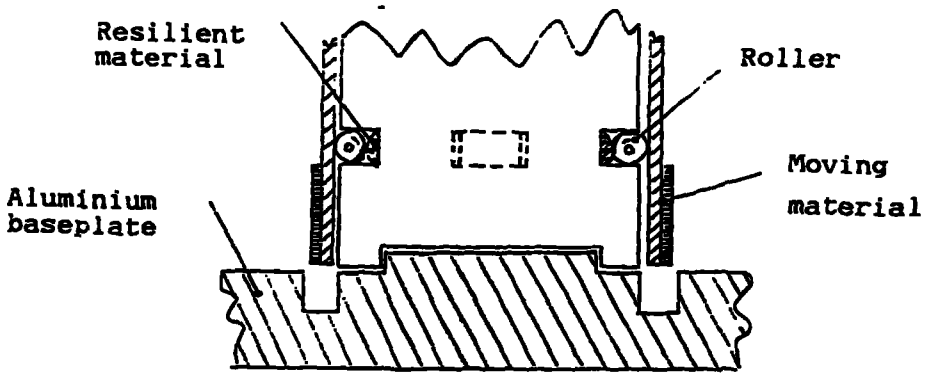
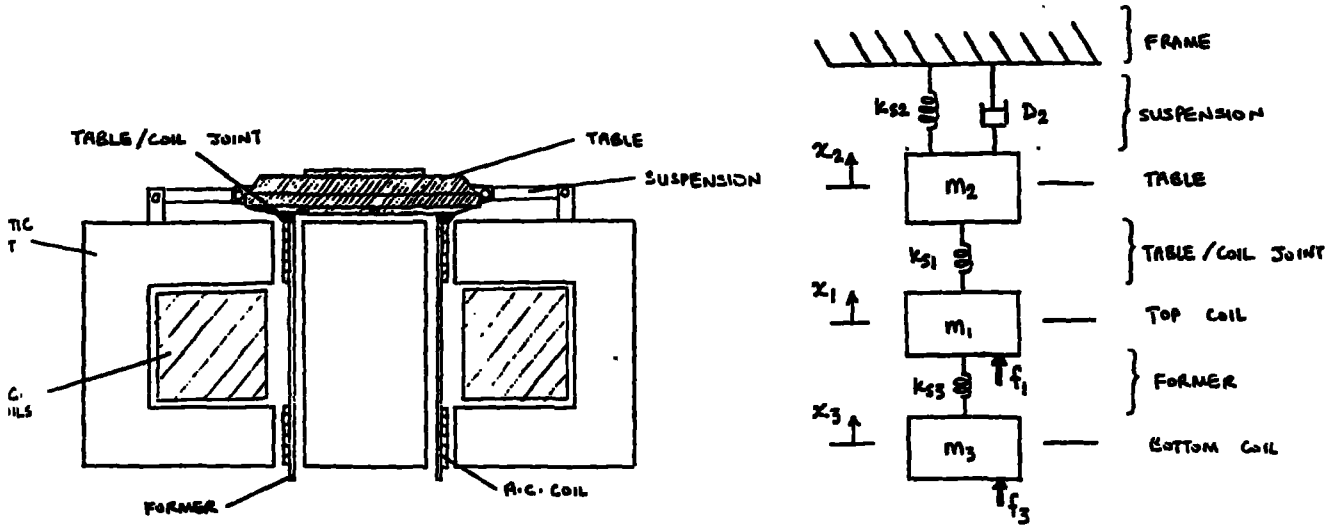


Fig. 6c Moving Element Roller Suspension

6.2. Three-Degree-of-Freedom Representation

A two-degree-of-freedom model was used to describe the mechanical system in the main body of the thesis in order to simplify the equations involved and thus clarify the overall system operation. This representation is adequate for both the single-ended and double-ended shaker configurations, but the c-core shaker requires a three degree of freedom model, as has been done for this project.

Only the derivation of relevant equations and expressions will be dealt with here as much of the theory has already been dealt with. Figure 6d shows how the three mass/ spring system is developed for the c-core shaker.



(i) C-Core Shaker *(ii) Three Mass/Spring System*

***Fig. 6d** Three-Degree-of-Freedom Representation*

This representation is still somewhat simplified but has proved to be sufficiently accurate for our purposes. As assumed earlier in Chapter Three, only motion in the vertical axis is of interest here and any displacement in the horizontal plane is assumed to be very small and has no influence on the vertical motion.

6.2.1. System Equations

Referring to Figure 6d and applying Newton's Second Law of Motion to all three masses;

Mass m_3 ,

$$f_3 = m_3.\ddot{x}_3 + k_{s3}.(x_3 - x_1) \qquad \text{..... (6.1)}$$

Mass m_2 ,

$$0 = m_2.\ddot{x}_2 + k_{s2}.x_2 + D_2.\dot{x}_2 + k_{s1}.(x_2 - x_1) \qquad \text{..... (6.2)}$$

Mass m_1 ,

$$f_1 = m_1.\ddot{x}_1 + k_{s3}.(x_1 - x_3) + (k_{s1}.(x_1 - x_2) \qquad \text{..... (6.3)}$$

where,

m_1 - *mass of top a.c. coil, top portion of coil former and bonding materials.*

m_3 - *mass of bottom a.c. coil, bottom portion of coil former and bonding materials.*

m_2 - *total table mass including any fixtures*

k_{s1} - *armature/table joint stiffness. The joint between the table and the armature, (which consists of bolts and bonding agent), is slightly flexible in the axial direction at certain frequencies.*

k_{s2} - *suspension stiffness.*

k_{s3} - *coil former stiffness (axial direction) between top and bottom coils*

D_2 - *damping coefficient for suspension arms.*

These three linear ordinary differential equations are assumed to possess only constant coefficients and can thus be solved by a 'standard' procedure.

Assuming sinusoidal motion, let,

$$f_1 = F_1.e^{j\omega t}$$

$$f_3 = F_3.e^{j\omega t}$$

and,

$$x_1 = X_1.e^{j\omega t} = \dot{x}_1 = j\omega.X_1.e^{j\omega t} = \ddot{x}_1 = -\omega^2.X_1.e^{j\omega t}$$

$$x_2 = X_2.e^{j\omega t} = \dot{x}_2 = j\omega.X_2.e^{j\omega t} = \ddot{x}_2 = -\omega^2.X_2.e^{j\omega t}$$

$$x_3 = X_3.e^{j\omega t} = \dot{x}_3 = j\omega.X_3.e^{j\omega t} = \ddot{x}_3 = -\omega^2.X_3.e^{j\omega t}$$

Because the performance specifications of displacement, velocity and acceleration relate to the motion of the table, the system equations should be derived in terms of table displacement, X_2, the table velocity, $\dot{X}_2$, and the table acceleration, $\ddot{X}_2$.

Table Displacement, X_2

Substituting the above expressions into equations (6.1), (6.2) and (6.3);
Equation (6.1) becomes;

$$F_3.e^{j\omega t} = -m_3.\omega^2.X_3.e^{j\omega t} + k_{s3}.(X_3.e^{j\omega t} - X_1.e^{j\omega t})$$

$$F_3 = -m_3.\omega^2.X_3. + k_{s3}.(X_3 - X_1)$$

..... *(6.4)*

equation (6.3) becomes;

$$F_1 = -m_1.\omega^2.X_1. + k_{s3}.(X_1 - X_3) + k_{s1}.(X_1 - X_2)$$

..... *(6.5)*

and, equation (6.2) becomes;

$$0 = -m_2.\omega^2.X_2. + k_{s2}.X_2 + j.D_2.\omega X_2 + k_{s1}.(X_2 - X_1)$$

$$0 = X_2.(k_{s2} - m_2.\omega^2 + k_{s1} + j.\omega D_2) - k_{s1}.X_1$$

giving,

$$X_2 = \frac{k_{s1}.X_1}{k_{s2} - m_2.\omega^2 + k_{s1} + j.\omega D_2} \qquad \ldots\ldots\ldots\ (6.6)$$

Check on X_1 / X_3 (Relative displacement of the top and bottom coils)

Using equation (6.4) ;

$$F_3 = X_3.(k_{s3} - m_3.\omega^2) - k_{s3}.X_1$$

$$X_3 = \frac{F_3 + k_{s3}.X_1}{k_{s3} - m_3.\omega^2} \qquad \ldots\ldots\ldots\ (6.7)$$

Substituting equation (6.6) for X_2 into equation (6.5) ;

$$F_1 = -m_1.\omega^2.X_1. + k_{s3}.(X_1 - X_3) + k_{s1}.\left(X_1 - \frac{k_{s1}.X_1}{k_{s2} - m_2.\omega^2 + k_{s1} + j.\omega D_2}\right) \qquad \ldots\ldots\ldots\ (6.8)$$

Note that $F_1 = k_{v1}.I_1'$ & $F_3 = k_{v3}.I_1''$

If the top and bottom coils are connected in series, (as is usually the case), then,

$$k_{v1} = k_{v3} = k_v/2 = B_g.\pi.D_m.N_C$$

where,

N_c = number of a.c. coil turns per end, and
$I_1' = I_1'' = I_1$ = input current.

Therefore,

$$F_1 = (k_v/2).I_1 \quad \text{and} \quad F_3 = (k_v/2).I_1$$

Hence,

$$F_1 = F_3$$

Substituting equation (6.8) into (6.7) we obtain;

$$X_3 = \frac{\left[-m_1.\omega^2.X_1 + k_{s3}.(X_1 - X_3) + k_{s1}.\left(X_1 - \frac{k_{s1}.X_1}{(k_{s2} - m_2.\omega^2 + k_{s1} + j.\omega.D_2)}\right) + k_{s3}.\right.}{k_{s3} - m_3.\omega^2}$$

which finally provides us with the relationship of ;

$$X_3/X_1 = \frac{1}{(2.k_{s3} - m_3.\omega^2)} \cdot \left[2.k_{s3} - m_1.\omega^2 + k_{s1} - \frac{k_{s1}^2.(k_{s2} - m_2.\omega^2 + k_{s1})}{(k_{s2} - m_2.\omega^2 + k_{s1})^2 + (\omega.D_2)^2} - \frac{j.\omega.D_2.k_{s1}^2}{(k_{s2} - m_2.\omega^2 + k_{s1})^2 + (\omega.D_2)^2}\right] \quad \ldots\ldots\ldots (6.9)$$

This allows us to investigate the flexibility of the coil former in the axial direction and thus enables an approximation to be made concerning extra resonances in the moving element. The control of table amplitudes near these frequencies may be made difficult and the resonances should hence be avoided. This may mean using a stiffer coil former

material or incorporating a set of stiffening arms along the length of the former. The stiffness k_{s3} may need to be obtained through testing and hence in most cases has to be approximated for the first few design iterations.

Input Current, I_1

From the relationships for F_1 and F_3 and substituting for X_1 and X_3 The equations for input current in terms of table displacement, velocity and acceleration can be obtained :

For the displacement-limited frequency band,

$$I_1 = \frac{\hat{\hat{X}}_2}{2.\sqrt{2}.k_{s1}.(k_v/2).m_3.\omega^2} \cdot \left[k_{s2} - m_2.\omega^2 + k_{s1} - (k_{s1}^2.A)/B + j.\omega.D_2 \right]$$

the velocity-limited frequency band,

$$I_1 = \frac{\hat{\dot{X}}_2}{\sqrt{2}.k_{s1}.(k_v/2).m_3.\omega^3} \left\{ \omega.D_2 - j.\left[k_{s2} - m_2.\omega^2 + k_{s1} - (k_{s1}^2.A)/B \right] \right\}$$

and, the acceleration-limited frequency band,

$$I_1 = \frac{-9.81\,\hat{\ddot{X}}_2}{\sqrt{2}.k_{s1}.(k_v/2).m_3.\omega^4} \cdot \left[k_{s2} - m_2.\omega^2 + k_{s1} - (k_{s1}^2.A)/B + j.\omega.D_2 \right]$$

where,

$$A = k_{s3} - m_3.\omega^2$$

$$B = -k_{s3}.m_3.\omega^2 - m_1.\omega^2.A + k_{s1}.A$$

$$C = k_{s2} - .m_2.\omega^2 + k_{s1} - (k_{s1}^2.A)/B$$

$$D = \omega.D_2$$

Motional Impedance, Z_m

Using the relationship,

$$Z_m = \frac{E_m}{I_1} = \frac{E_{m1} + E_{m3}}{I_1}$$

where,

$$E_{m1} = \frac{k_v.\dot{x}_1}{2} \qquad \& \qquad E_{m3} = \frac{k_v.\dot{x}_3}{2}$$

the motional impedance is given by,

$$Z_m = \frac{k_v^2.k_{s1}.m_3.\omega^2}{4.B.(C + j.D)} \left\{ \left[\frac{-\omega.D.B}{k_{s1}.m_3.\omega^2.A} \right] - \left[\frac{\omega.D.k_{s3}}{k_{s1}.A} \right] - \left[\frac{\omega.D}{k_{s1}} \right] + j.\omega. \left[\left[\frac{B.C.}{k_{s1}.m_3.\omega^2.A} \right] + \left[\frac{C.k_{s3} + (k_{s3}.k_{s1}^2.A/B)}{k_{s1}.A} \right] + \left[\frac{C + (k_{s1}^2.A/B)}{k_{s1}} \right] \right] \right\}$$

where A, B, C and D are as defined previously.

All other secondary equations can be derived using the equations in this chapter, following the pattern set out in Chapter Three for a two-degree-of-freedom system. The above analysis has been used for the following comparisons.

6.3. Comparison of Predictions and Test Data

At the time of writing only some of the test data on the prototype machine was made available to the author. These were the flux density, current, voltage and impedance measurements carried out at low input levels providing a low constant table acceleration figure of 20 'g'. Nevertheless, the machine parameters, (for the 'as built' machine)', were used to predict the input variables to the a.c. coil. These are shown in Figures 6f, 6g and 6h. First, there is a comparison made between air-gap flux density measured with a Hall probe and MAGNET predicted values.

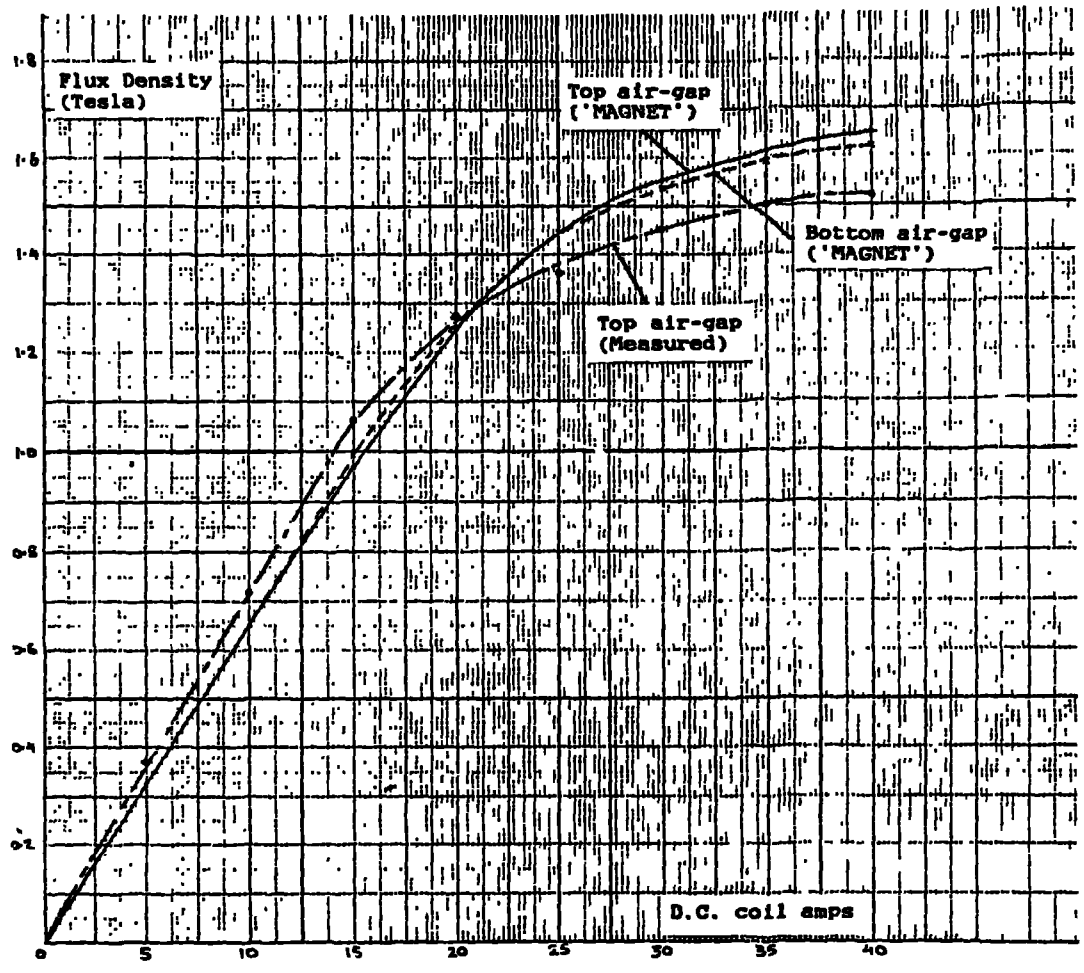


Fig. 6e DB85 - Measured and Predicted Air-Gap Flux Densities

The flux density curves for the top and bottom air-gaps show a great deal of similarity which is encouraging, as there was an initial worry that the average flux density in the bottom air-gap would be significantly different due to the presence of the spigot for locating the support base-plate. This has always been a concern with dual air-gap machines, as differing flux density levels would distort the thrust produced.

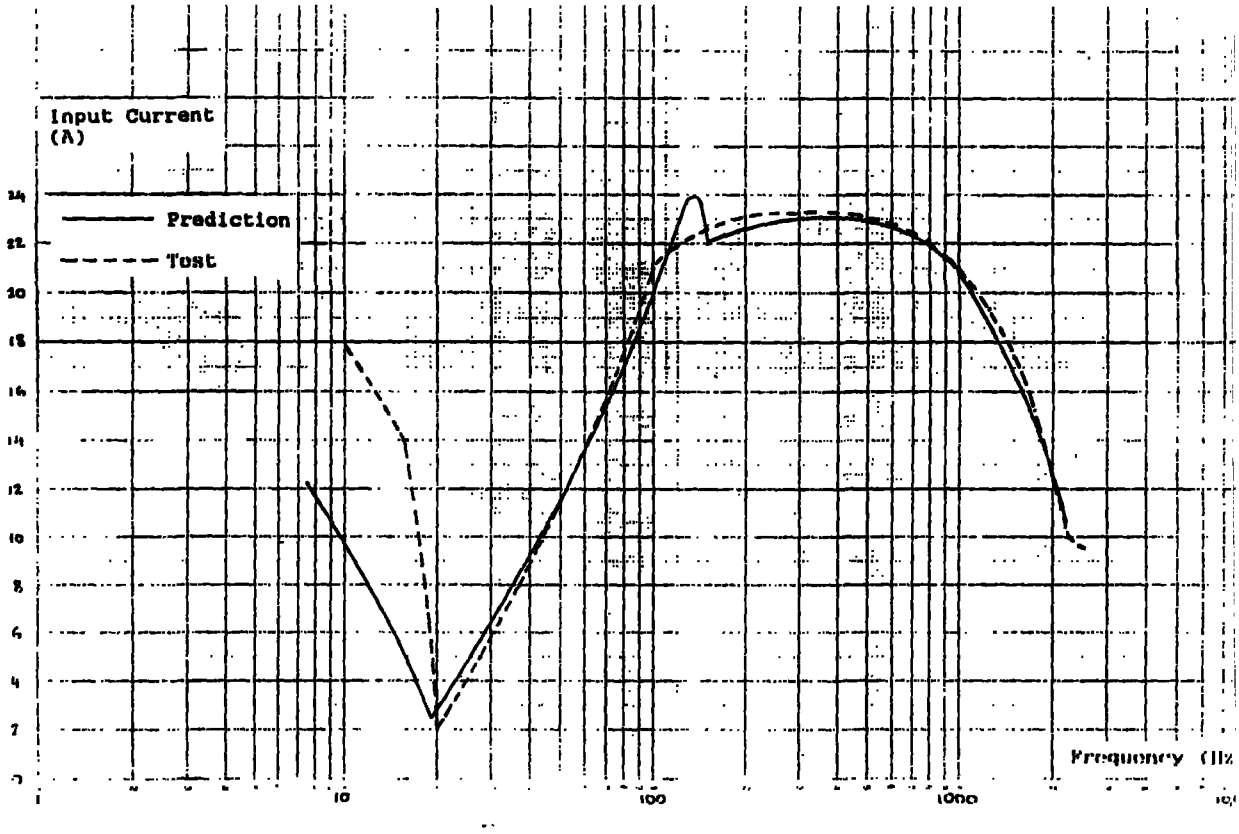


Fig. 6f DB85 - Input Current

As can be seen, the test results for the new DB85 machine indicate clearly the characteristic shape of the input current versus frquency curve which is also common to both the single-ended and double-ended moving coil shakers. The predictions again show a reasonably good tie-up at the mid to high frequencies, the main discrepancies again occuring at low frequencies.

Voltage predictions are seen to be somewhat low at high frequencies, possibly due to inaccuracies in the estimation of leakage inductance.

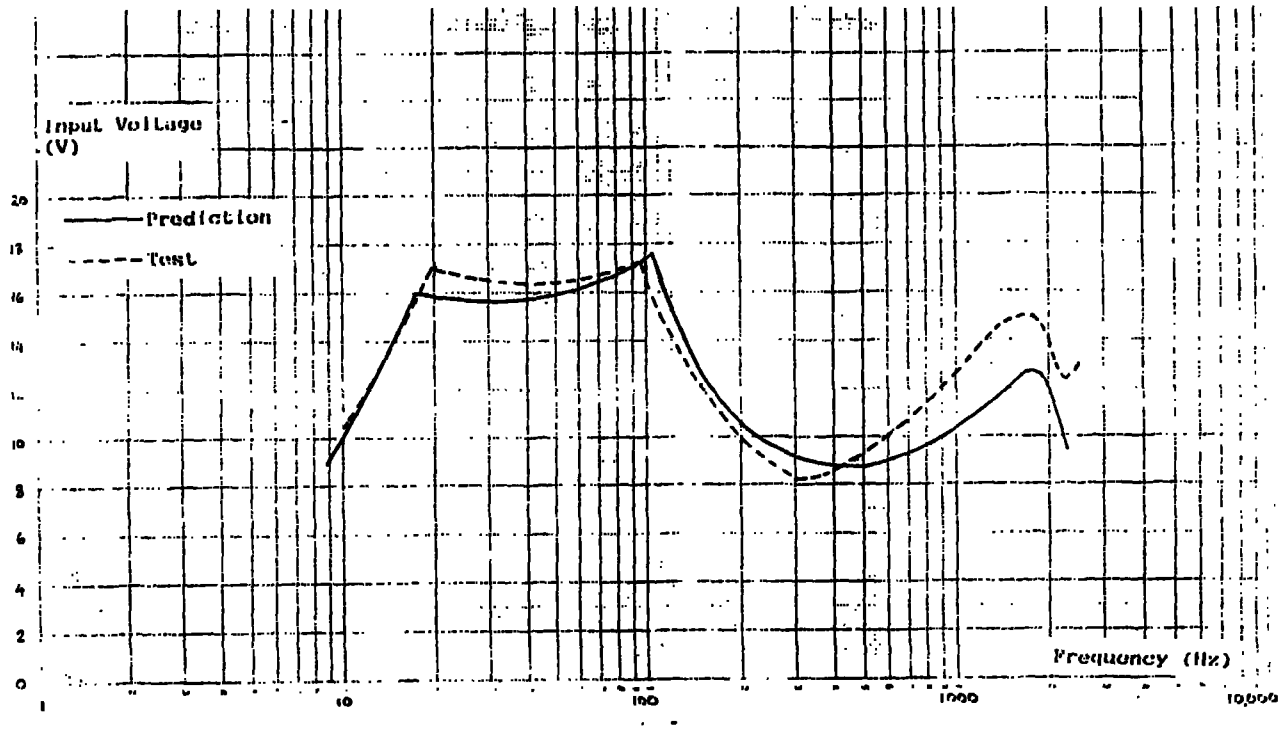


Fig. 6g DB85 - Input Voltage

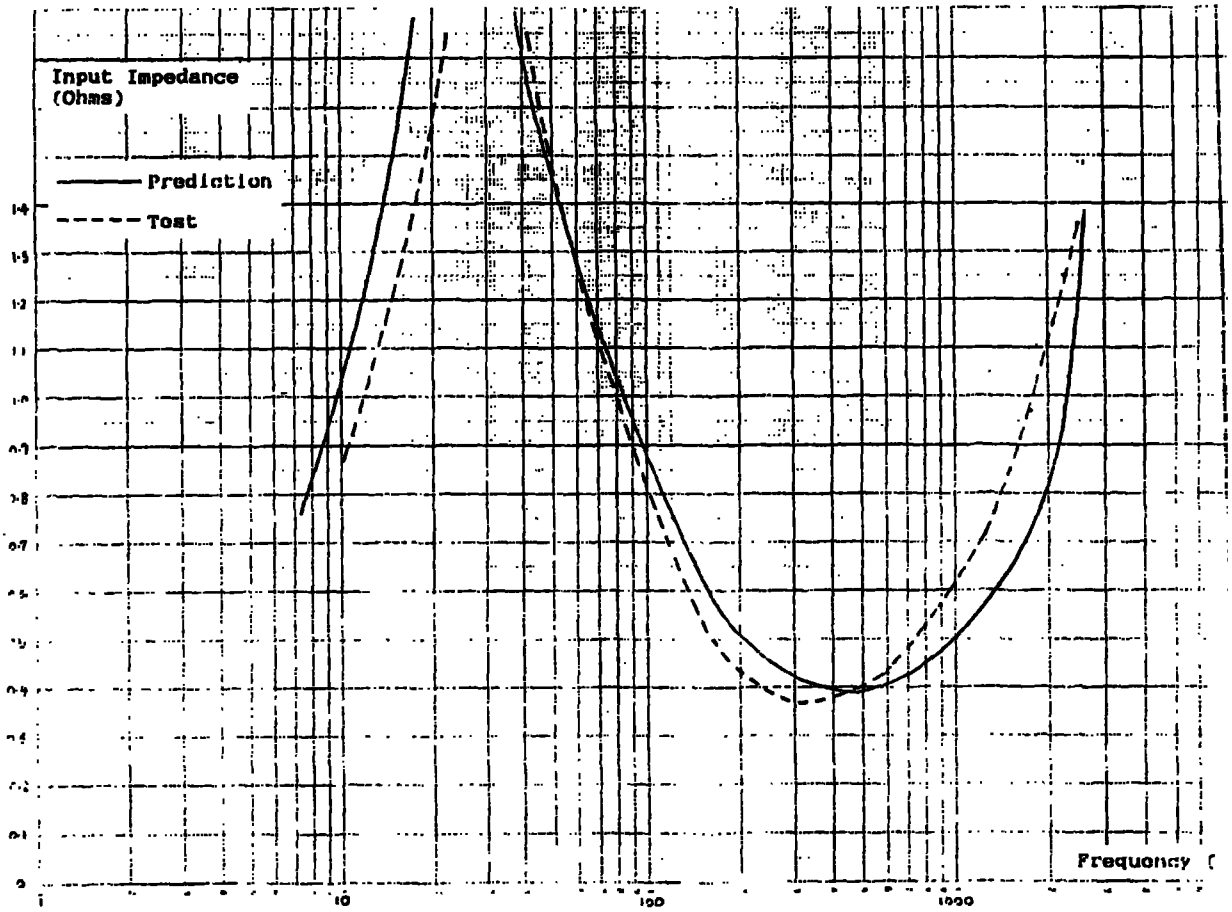


Fig. 6h DB85 - Impedance

The impedance curve serves to demonstrate that the model predicts the overall trend of shaker impedance and thus performance, reasonably well over much of the frequency range of interest.

6.5. Further Work on the C-Core Machine

From an electrical and electromagnetic point of view the c-core shaker was predicted as performing very well. First tests on the prototype built by the sponsor revealed the need for modifications to the mechanical design. In operation it was found that the moving coil armature tended to brush against the outer portion of the magnetic circuit. This caused damage not only to the armature and a.c. coil but also to the pole faces and copper plating layers. This problem was thought to be partly due to the fact that the new armature was somewhat longer than for an equivalent rated single-ended machine, or that axial modes of vibration were being set up at certain frequencies.

The c-core shaker employed a single-layered a.c. coil and initial confidence on the part of the sponsor's workstaff in this new design of coil was not strong. The rigid former had to be produced by a sub-contractor and then brought in-house for the coil winding and curing. All this proved to be relatively expensive and time consuming. Furthermore, experience of winding a single-layered coil onto a preformed former was virtually non-existent within the sponsor's coil shop which provided further cause for worry. As far as the author is aware, the necessary further development to make good these matters was deferred following the departure from the sponsor of the product champion. Other aspects of the c-core shaker for which investigation is desirable include the behaviour of the armature under load conditions, (this may well involve the sub-contractor or a third party carrying out extensive studies on the types of materials used, etc.), and the enhancement of prediction code in order to improve correlation between test results and predictions. Extensions to the mechanical mass-spring model are also desirable. It would also be extremely useful if more testing could be carried out to determine mechanical constants like suspension stiffnesses and damping coefficients with a little more accuracy. The single-ended shaker is known to have a non-linear suspension system and the c-core shaker could suffer from the same problem since the link-arm suspension system is still adopted. The link-arm concept is a reliable one but the author feels that the non-linearity of the rubber bushes used as part of the suspension could possibly be improved upon. Secondly, the 'roller' suspension incorporated in the centre pole, being a new design, should ideally be tested fairly rigorously throughout the usual operating frequency range,

for both the vertical and horizontal shaker orientations.

Above all a paramount need exists for more electrical testing on this prototype machine and more comparisons with the existing single-ended versions.

CHAPTER SEVEN
CONCLUSIONS

7. Conclusions

The aim of this industrially-orientated project was to develop an equivalent circuit to model the behaviour of an industrial electromagnetic moving coil vibration generator, verify the accuracy of the model and then use it to help produce a new cost-competitive shaker of novel design. Comparisons of model predictions with test data from several existing machines and from the prototype machine suggest that this objective has been substantially achieved.

It has also been shown that although the model adopted is quite simplistic in principle, involving some untested assumptions it does appear to predict all the salient points of a shaker's performance with reasonable accuracy. The simplicity of the model enables a whole series of trial and error designs to be attempted with relative ease and with minimal computation time. The examination of impedances and current flows around the circuit can be carried out with ease and provides useful information about the functioning of the shaker at various frequency points, and should be understood to be an integral part of the design process. Although the finite element studies take up a significant part of the overall design time on a completely new design, once the main shaker dimensions have been established, slight modifications to the magnetic circuit are easily executed. Once the full capabilities of the finite element modelling software is realised, meshing and solution times can be dramatically reduced by the use of several short-cuts, of which the use of symmetry within the model is but one example.

It should be stressed that the model presented in the thesis is of course capable of considerable improvement. Firstly, the calculation of the leakage inductances could be based on F.E. plots and could take the a.c. coil position into account. Secondly, non-ideal iron behaviour in respect of a.c. fluxes have not been allowed for. Thirdly, eddy current effects at high frequencies should take into account non-uniformities in the axial distribution of the currents, particularly plating currents. Fourthly, the non-linearity of the suspension system needs some consideration and some allowance has to be made for the variation in its parameters with operating frequency. Finally, the equivalent circuit used at present is only suitable for predicting steady state sinusoidal performance and further development to enable transient studies and shock or random tests to be performed is perhaps desirable.

It is the author's opinion that a little more time should be devoted to improving the accuracy of the mechanical predictions, with regard to the suspension system,

the behaviour of the moving element including some stress and fatigue calculations throughout the operating frequency band, and possibly a more detailed examination of the effect of attaching test loads to the table on the overall shaker performance. This last point has some significance in the matching of a particular vibration system to a customer's specific requirements. It is important that the shaker manufacturer is informed of the test duties that his equipment is likely to undergo together with the possible test loads that need to be handled. The manufacturer should then be able to 'run through' these possible test situations using the model to pinpoint any likely areas of concern, such as additional resonance points, stray flux minimisation etc..

Further testing to isolate and determine the various equivalent circuit components would be desirable and should lead to a greater understanding of the many 'fine-tuning' design options available. There is scope for another research project to address all these items and to develop on them.

As they stand, the prediction techniques developed here provide a clearer insight into the working of a shaker than has previously been available. The recommendations outlined above would be likely to extend the model's capabilities and would usefully build on the ground work presented in this thesis.

APPENDIX A
DERIVATION OF INDUCTANCE RELATIONS

Appendix A provides the full derivation of the inductance relations introduced in Chapter Three. Refer to Reference 6 for the derivations of the primary and secondary internal inductances.

A.1. Primary Main Inductance

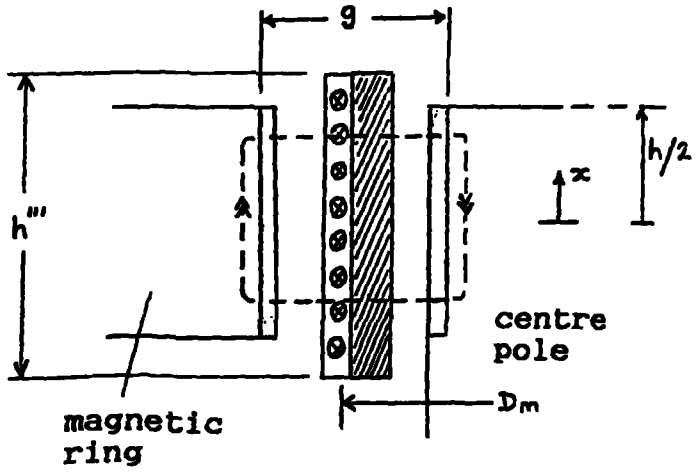


Fig. A1 Main Flux Path

The flux density B_x at x is :

$$B_x = \frac{\mu_o . N . I}{2.g} \cdot \left[\frac{h}{h'''}\right] \cdot \frac{x}{(h/2)} = \frac{\mu_o . N . I}{g} . k_1 . \frac{x}{h}$$

$d\phi$ = flux linkage with coil due to flux between x and $x + \delta x$ is :

$$B_x . \delta x . \pi . D_m \left[k_1 . N . \frac{x}{(h/2)}\right]$$

which gives the flux linkage as,

$$d\phi = \frac{\mu_o}{g} . (k_1 . N)^2 . I . \pi . D_m . \frac{2}{h^2} . x^2 . \delta x$$

$$\text{Total flux linkage} = \int_{x=0}^{x=h/2} d\phi$$

$$= \frac{\mu_o}{g} \cdot (k_1.N)^2.I.\pi.D_m. \frac{2}{h^2} \cdot \frac{h^3}{24}$$

The main inductance is,

$$L_{11c} = \frac{\mu_o.\pi.D_m.h.(k_1.N)^2}{12.g}$$

A.2. Primary Fringing Inductance

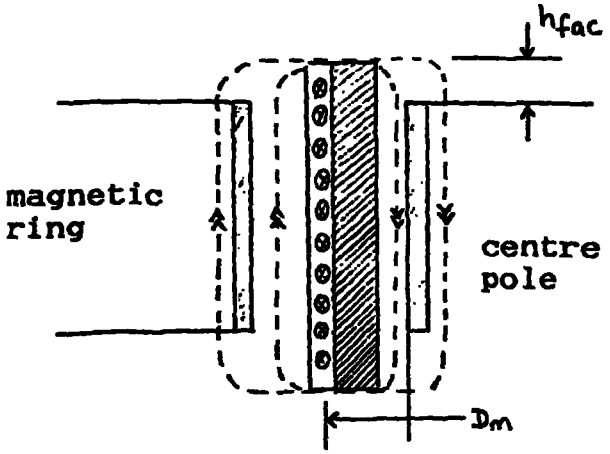


Fig. A2 Fringing Flux Path

With the fringing flux, it is assumed that $k_1.NI$ acts on the overhang gap of axial width h_{frac} at each end of the coil, (assumed that the flux is set up by $k'_1.NI$ and links $k'_1.N$ turns; where $k'_1 = 1/2(1 + k_1)$, the average of the turns within the air-gap and the total coil turns.

Therefore,

$$B_f = \frac{\mu_o}{2.g} .k'_1.N.I$$

and,

$$\phi_f = B_f.\pi .D_m.h_{frac}.k'_1.N$$

Giving the primary fringing inductance as,

$$L_{11F} = \frac{\mu_o.\pi .D_m.h_{frac}.(k'_1.N)^2}{2.g}$$

A.3. Primary Leakage Inductance

Figure A3 shows the primary leakage path and all relevant dimensions. The leakage paths associated with the single-layered a.c. coil are dealt with and correction factors are introduced later for the double-layered coil.

Because of the presence of a rather thick former for the single layered a.c. coil, the left and right hand paths of the leakage path possess different reluctances and have to be evaluated separately.

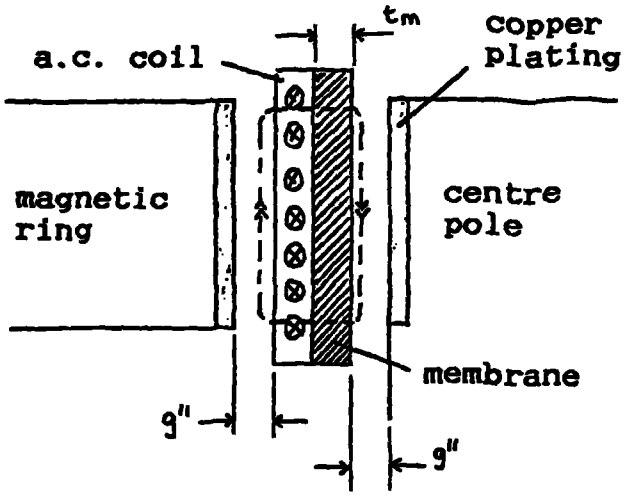


Fig. A3 Primary Leakage Path

Referring to the figure, the reluctance of the left and right hand flux paths are in series and,

$$L_{DL2} \propto \frac{N^2}{R_{EL} + R_{ER}}$$

The reluctance of the right hand path is given by,

$$R_{EL} = \frac{h'''}{\mu_o . A_{EL}}$$

where, A_{EL} = annular area for the right hand flux path and is given by,

$$A_{EL} = \pi \left\{ \left[\frac{D_m}{2} \right]^2 - \left[\frac{D_m - (g'' + t_m)}{2} \right]^2 \right\}$$

$$= \frac{\pi}{4} . \left\{ D_m^2 - D_m^2 + 2.D_m.(g'' + t_m) - \underbrace{(g'' + t_m)^2}_{\text{ignore since very small}} \right\}$$

$$= \frac{\pi}{2} \cdot D_m \cdot (g'' + t_m)$$

$$R_{EL} = \frac{h'''}{\mu_o \cdot (\pi/2) \cdot D_m \cdot (g'' + t_m)}$$

Similarly, for the left hand flux path,

$$R_{ER} = \frac{h'''}{\mu_o \cdot A_{ER}}$$

$$A_{ER} = \pi \cdot \left\{ \left[\frac{D_m + g''}{2} \right]^2 - \left[\frac{D_m}{2} \right]^2 \right\}$$

$$= \frac{\pi}{4} \cdot \left\{ D_m^2 + 2 \cdot D_m \cdot g'' + \underbrace{(g'')^2}_{\text{ignore since very small}} - D_m^2 \right\}$$

$$= \frac{\pi}{2} \cdot D_m \cdot g''$$

Giving the reluctance for the left hand path,

$$R_{ER} = \frac{h'''}{\mu_o \cdot (\pi/2) \cdot D_m \cdot g''}$$

and, the total reluctance, (being in series), is,

$$R_{ET} = R_{EL} + R_{ER}$$

and, in its full form,

$$R_{ET} = \frac{(h'''.g'') + h'''.(g'' + t_m)}{\mu_o.(\pi/2).D_m.g''.(g'' + t_m)}$$

which gives the expression for the primary leakage inductance as,

$$L_{DL1} = \frac{N^2.\mu_o.\pi.D_m.g''.(g'' + t_m)}{2.h'''\ (2.g'' + t_m)}$$

which can also be written as,

$$L_{DL1} = \frac{N^2.\mu_o.\pi.D_m.g''}{4.h'''} \cdot \left[\frac{2\left[1 + (t_m/g'')\right]}{2 + (t_m/g'')}\right]$$

$$L_{DL1} = \frac{N^2.\mu_o.\pi.D_m\ g''}{4.h'''} \cdot C_{F1}$$

where C_{F1} is termed a correction factor and is,

$$C_{F1} = \left[\frac{2\left[1 + (t_m/g'')\right]}{2 + (t_m/g'')}\right]$$

For a double layered a.c. coil, there is no assymmetry in the reluctance paths and hence the correction factor is equal to 1, giving simply,

$$L_{OL1} = \frac{\mu_o . \pi . D_m . g' . N^2}{4 . h'''}$$

A.4. Secondary Main Inductance

The main inductance for the secondary circuit, (copper plating), is evaluated in the same way as for the primary circuit,

$$L_{22C} = \frac{\mu_o . \pi . D_m . h . (k_1 . N)^2}{12 . g}$$

A.5. Secondary Fringing Inductance

The fringing inductance for the secondary circuit is also evaluated as for the primary circuit

$$L_{22F} = \frac{\mu_o . \pi . D_m . h_{rac} . (k_1' . N)^2}{2 . g}$$

A.6. Secondary Leakage Inductance

The derivation of the secondary leakage inductance is dealt with in the same way as for the primary leakage.

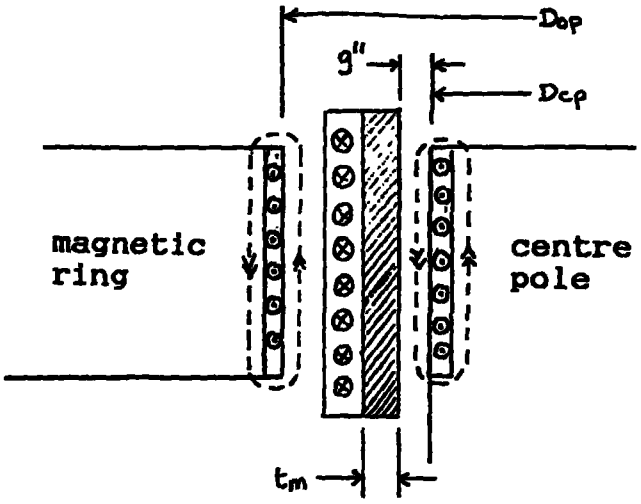


Fig. A4 Secondary Leakage Flux Paths

Here, as before, the reluctances R'_{EL} and R'_{ER} are in series. Note, however that the leakage inductances associated with each layer of plating are in parallel.

The reluctance of the right hand path is,

$$R'_{EL} = \frac{h}{\mu_o . A'_{EL}}$$

where, the annular area is given by,

$$A'_{EL} = \pi \left\{ \left[\frac{D_{cp} + (g'' + t_m)}{2} \right]^2 - \left[\frac{D_{cp}}{2} \right]^2 \right\}$$

$$= \frac{\pi}{4} . \left\{ D_{cp}^2 + 2.D_{cp}.(g'' + t_m) + \underbrace{(g'' + t_m)^2}_{\text{ignore since very small}} - D_{cp}^2 \right\}$$

$$= \frac{\pi}{4}\left\{2.D_{cp}.(g'' + t_m)\right\}$$

giving,

$$R'_{EL} = \frac{2.h}{\mu_o.\pi.D_{cp}.(g'' + t_m)}$$

Similarly, for the left hand path,

$$R'_{ER} = \frac{h}{\mu_o.A'_{ER}}$$

where, the left hand annular area is,

$$A'_{ER} = \left\{\left[\frac{D_{op}}{2}\right]^2 - \left[\frac{D_{op} - g''}{2}\right]^2\right\}$$

$$= \frac{\pi}{4}\left\{D_{op}^2 - D_{op}^2 + 2.D_{op}.g'' - \underbrace{(g'')^2}_{\text{ignore since very small}}\right\}$$

$$= \frac{\pi}{2}.D_{op}.g''$$

which gives the left hand reluctance as,

$$R'_{ER} = \frac{2h}{\mu_o . \pi . D_{op} . g''}$$

This in turn gives the right hand secondary leakage inductance as,

$$L_{EL} = \frac{N^2 . \mu_o . \pi . D_{cp} . (g'' + t_m)}{2.h}$$

and, the left hand inductance as,

$$L_{ER} = \frac{N^2 . \mu_o . \pi . D_{op} . g''}{2.h}$$

As the two inductances are in parallel with each other, i.e.

$L_{22L1} = L_{EL}$ in parallel with L_{ER}

This produces the overall expression for the secondary leakage inductance,

$$L_{22L1} = \frac{N^2 . \mu_o . \pi . D_{op} . D_{cp} . g''}{2.h.(D_{op} + D_{cp})} \cdot \left[\frac{(g'' + t_m).(D_{op} + D_{cp})}{D_{cp}. \quad (g'' + t_m) + D_{op} . g''} \right]$$

$$L_{22L1} = \frac{N^2 . \mu_o . \pi . D_{op} . D_{cp} . g''}{2.h.(D_{op} + D_{cp})} . C_{F2}$$

where,

$$C_{F2} = \left[\frac{(g'' + t_m).(D_{op} + D_{cp})}{D_{cp}.\quad (g'' + t_m) + D_{op}.g''} \right]$$

It should be noted that here N^2 may well be replaced by $(k_1N)^2$ giving,

$$L_{22L1} = \frac{\mu_o.\pi.D_{op}.D_{cp}.g''.(k_1.N)^2}{2.h.(D_{op} + D_{cp})} \;.\; C_{F2}$$

As before, for the double-layered case, the correction factor will be equal to 1, giving the secondary leakage inductance as,

$$L_{22L1} = \frac{N^2.\mu_o.\pi.g''}{2.h} \cdot \frac{D_{op}.D_{cp}}{(D_{op} + D_{cp})}$$

A.7. Mutual Inductance

Figure A5 shows the flux paths used to obtain the mutual inductance expression.

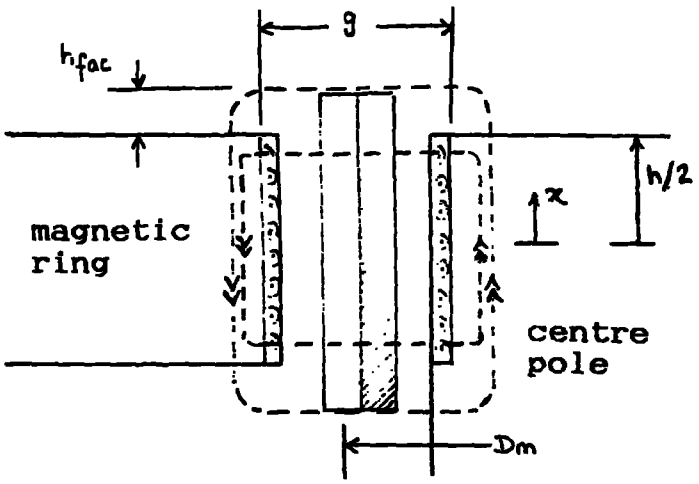


Fig. A5 Main and Fringing Flux Paths

The flux density B_x at x is :

$$B_x = \frac{\mu_o . I_2}{2.g} \cdot \frac{x}{h/2}$$

$d\Phi_{12}$ = flux linkage with coil due to flux between x and $x + \delta x$ is :

$$B_x . \delta x . \pi . D_m . \left[k_1 . N . \frac{x}{(h/2)} \right]$$

which gives the flux linkage as,

$$d\phi_{12} = \frac{\mu_o}{g} . (k_1 . N) . I_2 . \pi . D_m \frac{2}{h^2} x^2 . \delta x$$

$$\text{Total flux linkage} = \int_{x=0}^{x=h/2} d\phi_{12}$$

$$\phi_{12} = \frac{\mu_o}{g} \cdot (k_1.N).I_2.\pi.D_m \cdot \frac{2}{h^2} \cdot \frac{h^3}{24}$$

The main inductance is

$$L_{12C} = \frac{\mu_o.\pi.D_m.h.(k_1.N)}{12.g}$$

The fringe flux is set up by I_2 and is assumed to link k'_1N turns,

$$L_{12F} = \frac{\mu_o.\pi.D_m.h_{frac}.(k'_1.N)}{2.g}$$

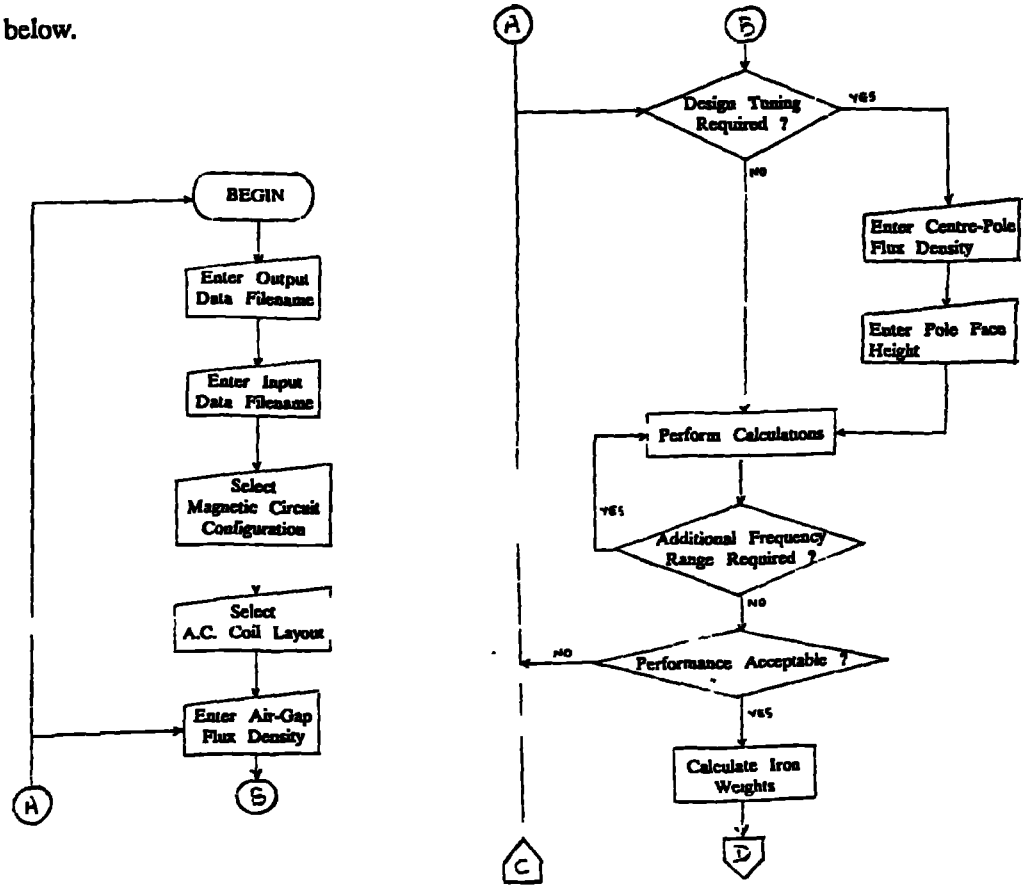
And the total referred to the primary,

$$L_{12} = L_{12C}.(k_1.N) + L_{12F}.(k'_1.N)$$

APPENDIX B
THE DESIGN PROGRAM

B.1. The Design Program

The software package takes the form of a FORTRAN 77 program and is developed to run under MS-DOS, (Microsoft Disk Operating System), on an IBM PC/XT-286 or compatible, desk-top computer. The executable code requires a minimum of 64K bytes of random access memory and has the use of a maths co-processor, though this is not essential. Program run time has been estimated at under a minute, to cover the full operating frequency range of the shaker. The equations presented in Chapter 3 were used to model the electrical and mechanical behaviour of the shaker, and it was relatively easy to convert the set of equations into a FORTRAN 77 program. The final version of the program handles all the three magnetic circuit configurations together with either single-layered or double-layered a.c. coils. The presence of an electrically conducting coil former has also been allowed for. The code also allows the user to insert a fixed inductor into the primary circuit to enhance the low to mid-frequency performance. From the mechanical design point of view, the user is given the choice of solving for either a rigid system, a system with two-degrees-of-freedom or one with three-degrees-of-freedom, (as in the c-core case). Heat flux densities in the a.c. coil and copper plating are also calculated for the whole frequency range. The detailed flowchart indicating all important design steps and branches is shown in Figure B1 below.



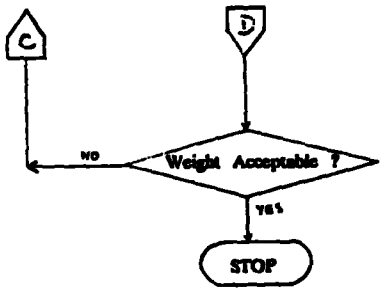


Fig. B1 Detailed Program Flowchart

The user has to prepare three sets of data files prior to running the program :

(a) Frequency Data

The frequency range of interest, together with as many frequency points as is required.

(b) Performance Profile

The displacement, velocity and acceleration required, together with the cross-over frequencies.

(c) Shaker Data

Rough dimensions of the a.c. coil together with all test masses and mechanical constants involved, and amplifier ratings.

The user is prompted for the various data files as required, and is allowed to check and edit any of them when necessary. A very simple 'Design-Tuning' routine is included which provides a rough guide to the mean diameters of the a.c. coil and centre-pole, for values of air-gap and centre-pole flux densities specified by the user. The output from the program can either be displayed on the screen during run time, redirected to a line printer or stored on hard-disk for retrieval later. The amount of output data produced can be controlled by the user at the data input stage. For instance, at very early design stages when the designer is trying out a new shaker design, he may need to calculate and output quite a considerable amount of information, (right down to the real and imaginary parts of certain variables). This also greatly eases

the tracking down of problems and bugs in the coding during program development and upgrading. At later design stages and for further design iterations, only the main characteristics of the shaker need be examined, for example, the output displacement, velocity and acceleration, together with their respective cross-over frequencies and high-frequency roll-offs.

The user is also provided with the option of simply specifying the displacement, velocity and acceleration profile for a certain shaker design and the program will work out the size of amplifier required to do the job, in terms of current and voltage ratings. On the other hand, amplifier ratings can be specified and the performance profile calculated.

A simple routine to evaluate the approximate steel weight of a shaker design has also been made available, enabling the designer to decide whether a particular design is too heavy from a 'force output per shaker size' point of view. This allows him to either discard that design or re-iterate it before going to the finite-element modelling stage to design the details of the steel circuit.

The final product is a reasonably easy to use program which provides the flexibility and accuracy required by the shaker designer. The designer of course has to have some prior knowledge of shaker operation and construction. the code is fairly self-explanatory with sufficient comment statements to enable further additions and modifications to be carried out with ease.

B.2. Further Work

Provision has been made to include further code to enable more complicated mass/spring systems to be modelled. At the present time, the code cannot deal with the mechanical characteristics of loads and their fixtures. The resonant behaviour of certain test loads may seriously affect the overall performance of a particular shaker/amplifier system. This of course need not worry the shaker designer at the design stage, but will certainly be of importance during the day to day activities of the shaker company. Very often customers may require to excite a complex load structure, and it will be extremely useful to be able to predict fairly accurately what the outcome will be, and whether the resulting vibrations, etc. are going to be harmful to the load structure or even to the shaker itself.

One way of implementing this sort of flexibility, whereby different load configurations can be set up and examined with ease, is by using matrix formulations throughout the software. The mechanical system or systems, as the case may be, can be described by

several matrices holding all the relevant mechanical data, such as stiffness and damping coefficients and the various masses. These mass/spring systems, although being very simplified, can still provide useful information to the shaker manufacturer and their customers.

REFERENCES

[1] **BS6140 : Part 1 : 1982**
'Test Equipment for Generating Vibration. Part 1 - Methods of Describing Characteristics of Electrodynamic Test Equipment for Generating Vibration'

[2] **BS6140 : Part 2 : 1982**
'Test Equipment for Generating Vibration. Part 2 - Methods of Describing Characteristics of Auxiliary Tables for Test Equipment for Generating Vibration'

[3] **Camp, L.**
'Underwater Acoustics'
Wiley-Interscience; Division of John Wiley & Sons, 1970.

[4] **Colloms, M.**
'High Performance Loudspeakers'
Second Edition, Pentech Press, 1980.

[5] **Derritron Electronics Shaker Specifications - Data Sheets**
VP30
VP85
VP400
VP400LT/700LT
VP500/700
VP180
VP180L
VP1200
VP1500M
VP2500

[6] **Doepken Jr., H.C.**
'The Minimum A.C. Resistance of Slabs and Tubes'
Proceedings of the IEEE, Volume 57, July 1969.

[7] **Grootenhuis, P. and Gearing, J.W.**
'Design of Electromagnetic Vibration Generators'
Session One, Paper 2, Proceedings of the Institution of Mechanical Engineers 1965 - 1966.

[8] **Oatley, C.**
'Electric and Magnetic Fields - An Introduction'
Cambridge University Press, 1976.

[9] **Timmerman, J.**
'Two Electromagnetic Vibrators'
Philips Technical Review, 33, p249-259, 1973, No. 8/9.

[10] **Tomlinson, M.A.**
'Vibration Testing - An Introductory Guide'
Society of Environmental Engineers - Handbook, 1982/83.

[11] **Tse, F.S., Morse, I.E. and Hinkle, R.T.**
'Mechanical Vibrations - Theory and Applications'
Second Edition, Allyn and Bacon, Inc., 1978.

[12] **Laithwaite, E.R. and Lawrenson, P.J.**
'A Self-Oscillating Induction Motor for Shuttle Propulsion'
IEE Proceedings, 1956, 104A, p93-100

[13] **Smith, A.C. and Appel, L.C.**
'Determining the Maximum Thrust of a Permanent Magnet Linear Actuator'
PhD Project (1985-1988), Department of Electrical Engineering,
Imperial College of Science and Technology, London

[14] **Roubicek, O. and Pejsek, Z.**
'Oscillatory Synchronous Linear Motor with Permanent-Magnet Excitation'
Proceedings of the IEE, Volume 127, Pt. B, No. 1, January 1980.

[15] **Bolton, H.R. Dr.**
'Single-Ended, Double-Ended, C-Core Configuration Comparison for Shakers'
Report for Derritron Group Ltd., Parts 1 and 2, January 1988.

[16] **Bolton, H.R. Dr.**
'Frequency Response of Moving Coil Shakers'
Report for Derritron Group Ltd., July 1987.

[17] **Freris, L.L. and Nunes de Carvalho, J.**
'Electromechanical Filter and its Performance in D.C. Transmission Systems'
Proceedings of the IEE, Volume 122, No. 1, January 1975.

[18] **Saraiva, E.de.S and Freris, L.L.**
'Development of Electromechanical Filter and Performance Evaluation in D.C. Link'
Proceedings of the IEE, Volume 126, No. 12, December 1979.

[19] **Unholtz, K.**
'Vibration Testing Machines'
Shock and Vibration handbook, Second Edition, Edited by Harris, C.M. and Crede, C.E., McGraw-Hill Company, 1976.

BIBLIOGRAPHY

[1] **Adams, G.J.**
'Computer-Aided Loudspeaker System Design.
Part 1 : Synthesis Using Optimisation Techniques,
Part 2 : Determination of System Power Ratings and Some Design Examples Using Optimisation Techniques.'
Journal of the Audio Engineering Society, Volume 26, No. 11, November 1978.

[2] **BS3100 : AM1, AM2**
'Data Sheets on the Properties of Steel Castings - Carbon Steel Castings with High Magnetic Permeability'
Steel Castings Research and Trade Association, 1977

[3] **Eshleman, R.L.**
'Vibration Standards'
Shock and Vibration Handbook, Edited by Harris, C.M. and Crede, C.E., Volume One, McGraw-Hill Book Company, 1961.

[4] **Green, C.W. and Paul, R.J.A.**
'Application of D.C. Linear Machines as Short-Stroke and Static Actuators'
Proceedings of the IEE, Volume 116, No. 4, April 1969.

[5] **Murgatroyd, P.N. and Walker, N.J.**
'Frequency-Dependent Inductance and Resistance of Foil Conductor Loops'
Proceedings of the IEE, Volume 124, No. 5, May 1977.

[6] **Woolley, I.**
'Eddy-Current Losses in Reactor Flux Shields'
Proceedings of the IEE, Volume 117, No. 11, November 1970.

[7] **Derritron Group Limited Company Literature**
'VP400 Vibrator Shorted Turn Optimisation'
Report 78014/TD13, c.1978.

[8] **Pashley, H.C.L. and Thomas, R.C.E.**
'Trends in Electromagnetic Vibrator Design'
Derritron Electronics Limited Company Literature.

[9] **Small, R.H.**
'Direct-Radiator Loudspeaker System Analysis'
Journal of the Audio Engineering Society, Volume 20, No. 5, June 1972.

[10] **Kates, J.M.**
'Analysis of Decoupled-Cone Loudspeakers'
Journal of the Audio Engineering Society, Volume 25, No. 1/2, January/February 1977.

[11] **King, J.**
'Loudspeaker Voice Coils'
Journal of the Audio Engineering Society, Volume 18, No.1, February 1970.

[12] **Klipsch, P.W.**
'A Note on Loudspeaker Impedance and its Effect on Amplifier Distortion'
Journal of the Audio Engineering Society, Volume 26, No. 7/8, July/August 1978.

[13] **Lammeraner, J. and Stafl, M.**
'Eddy Currents'
English Translation edited by Toombs, G.A., ILIFFE Books Ltd., 1966.

[14] **Majmudar, H.**
'Electromechanical Energy Convertors'
Allyn and Bacon Inc., 1965.

[15] **Meisel, J.**
'Principles of Electromechanical Energy Conversion'
McGraw-Hill Book Company, 1966.

2.4. Photographs

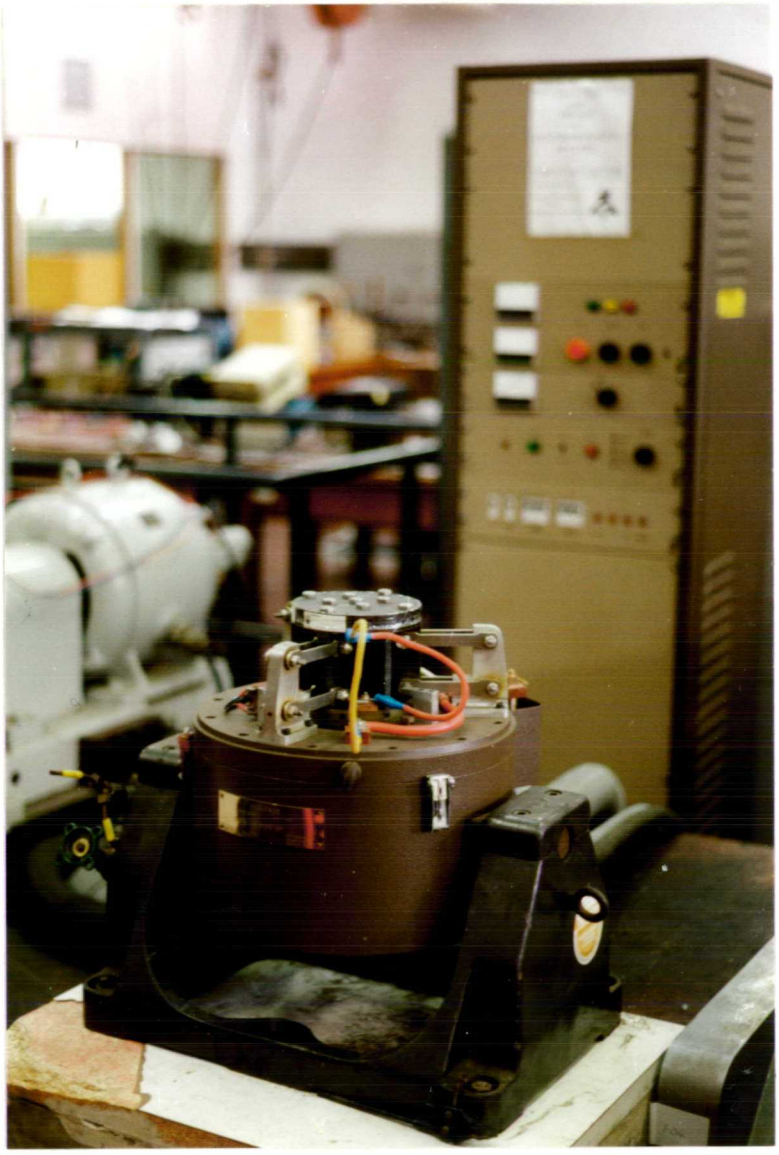


Fig. 2f VP30 Shaker (Power Amplifier in the Background)

The figure above shows the air-cooled VP30 moving coil shaker with its power amplifier in the background (also air-cooled). The top cover has been removed to reveal the moving table and suspension link arms. The shaker is mounted on a large block of pre-stressed concrete which in turn rests upon four isolation pads (not shown). The air-hose and a.c. cable can be seen just behind the shaker.